NASA CR-111933

DEVELOPMENT OF A MINIATURIZED, STERILIZABLE, GAMMA-BACKSCATTER ATMOSPHERE DENSITY SENSOR

By Richard G. Hassenpflug

Prepared under Contract No. NAS1-7791 by

CONRAC CORPORATION
Instrument/Controls Division
Duarte, California

for

NATIONAL AERONAUTICS AND SPACE ADMINISTRATION

ABSTRACT

FOR

DEVELOPMENT OF A MINIATURIZED, STERILIZABLE, GAMMA-BACKSCATTER ATMOSPHERE DENSITY SENSOR

By Richard G. Hassenpflug

A gamma backscatter atmosphere density sensor has been designed and a working model fabricated and tested, demonstrating the density measurement capability with severe size, weight, power, and environmental constraints. Preliminary tests on the working model indicated that further work to improve operation in vacuum environments and weight reduction were necessary. Two prototype gamma backscatter atmosphere density sensors, associated electronics, and a source holder are ready for further tests when facilities become available.

DEVELOPMENT OF A MINIATURIZED, STERILIZABLE, GAMMA-BACKSCATTER ATMOSPHERE DENSITY SENSOR

By Richard G. Hassenpflug

SUMMARY

A gamma backscatter atmosphere density sensor has been designed and a working model fabricated and tested as Phase I of the development program. The program is directed toward demonstrating the density measurement capability within size, weight, power, and environmental constraints. The working model met the size and power goals and identified areas requiring further development. These areas include improvements in methods of detector stabilization, improved operation in vacuum environments, and weight reduction. The Phase II program was directed toward accomplishing these design improvements and fabrication and testing of two engineering prototype gamma backscatter atmosphere density sensors. Further tests will be able to confirm the results obtained in the development laboratory.

TABLE OF CONTENTS

ILLUSTRATIONS

INTRODUCTION

A technique being developed to provide direct measurement of atmospheric density from a high speed entry vehicle involves the scattering of gamma radiation. Some fraction of the gamma flux emerging from a radioisotope source is backscattered by the atmosphere into a radiation detector. The backscatter interaction is linearly dependent upon density in the scattering region. By collimating the source emission and the detector field of view, a measurement can be made of the ambient density in a region outside of the shock wave. No probes or special windows which might affect the integrity of the vehicle skin or heat shield are required. Results of flight tests in the earth's atmosphere of a prototype density sensor employing this technique showed good agreement with existing density data. In addition, a study conducted for Langley Research Center showed the feasibility of applying this technique to measure the ambient mass density of the Martian atmosphere (ref. 1).

The objective of the program reported herein is the development of a miniaturized engineering model atmosphere density sensor employing the gamma backscatter technique. The total program is to:

1. Demonstrate the ability of the device to measure atmospheric density in the region of interest.

2. Demonstrate the size, weight, and power specification of the device.

3. Demonstrate the insensitivity of the device to the anticipated space flight environment including sterilization.

The guidelines of this development are predicated on an eventual space mission culminating in the measurement of the atmosphere density profile of a planet such as Mars. These guidelines define the density profiles, environments, vehicle constraints, etc. The resulting hardware will be proven for application to specific missions as required with only minor adaptation.

The objectives and guidelines of the program are further defined in the next section of this report. These are followed by design details of the various assemblies that make up the sensor. A description of the engineering model is presented along with test data and results. The further development of two prototype sensors and the test data are described along with the problems associated with the development.

This work was sponsored by the National Aeronautics and Space Administration, Langley Research Center, under Contract Number NAS1-7791. The program was under the technical cognizance of Peter J. LeBel, of NASA, Langley Research Center.

SYMBOLS AND UNITS

The International System of Units will be used throughout this report. The symbols are defined below.

A_d	detector area, cm^2
D	dose buildup factor, dimensionless
D	dose rate, mr/hr
E	energy of photons emitted from source, KeV
G	geometry factor, dimensionless
I	count rate, pulses per second
I_{as}	air scattered count rate, pulses/second
I_b	background count rate, pulses/second
I_d	detected count rate, pulses/second
I_o	source strength, photons/second emitted into a 4πsolid angle
I_s	scattered radiation to detector, pulses/second
I_{ws}	wall scattered count rate, pulses/second
K_{as}	air scatter scale factor
K_{ws}	wall scatter scale factor
r	source-detector separation, cm
S	source strength, curies
SA	specific activity
t	thickness, cm
T	decay time, days
V	volume
x	path length, cm
Y	yield, percent

Γ	dose rate constant, $r\text{-}cm^2/mc\text{-}hr$
ϵ_d	detector efficiency, dimensionless
$\mu\alpha$	absorption coefficient, cm^2/gm
ρ	density, gm/cm^3
ρ_α	density of ambient atmosphere, gm/cm^3
σ_{as}	photon scattering coefficient of ambient atmosphere, cm^2/gm
τ	half life, days

PROGRAM OBJECTIVES AND GUIDELINES

This program is one of several steps in the development sequence of a technique to provide a direct measurement of atmospheric density from a high speed entry vehicle. The technique involves the scatter of gamma radiation.

Previous studies and test programs sponsored by NASA - Langley Research Center have demonstrated the feasibility of employing gamma radiation scattering technique for measuring atmospheric density. These included rocket flights attempting measurement of Earth's atmosphere in the 100 to 300 K feet altitude region (ref. 2), a computer analyses of the scatter phenomena and associated auxiliary effects (ref. 3), a feasibility study of applying this technique to the Mars application (ref. 1) and development of sources for specific application to the measurement of atmospheric density.

Objectives

The objective of this program is the development of a miniaturized engineering prototype atmosphere density sensor employing the gamma backscatter technique in order to:

1. Demonstrate the ability of the device to measure atmospheric density in the region of interest.

2. Demonstrate the size, weight, and power specifications of the device.

3. Demonstrate the insensitivity of the device to the anticipated space flight environment including sterilization.

Since this program is not directed toward a specific vehicle or atmosphere, the design requirements are based upon conceptual thinking pertaining to a Mars mission.

The atmosphere profiles considered are the extremes defined by the VM-8 and VM-9 models as described in reference 4. These density profiles are illustrated in Figure 1.

Size, weight, and power constraints are necessarily severe due to the constrained payload capacity of the space vehicles.

The design goals in this regard are:

1. Total sensor weight including shielding - 5.0 lbs.
2. Total sensor volume - 100 in^3
3. Total power from a 28 vdc supply - 5 watts

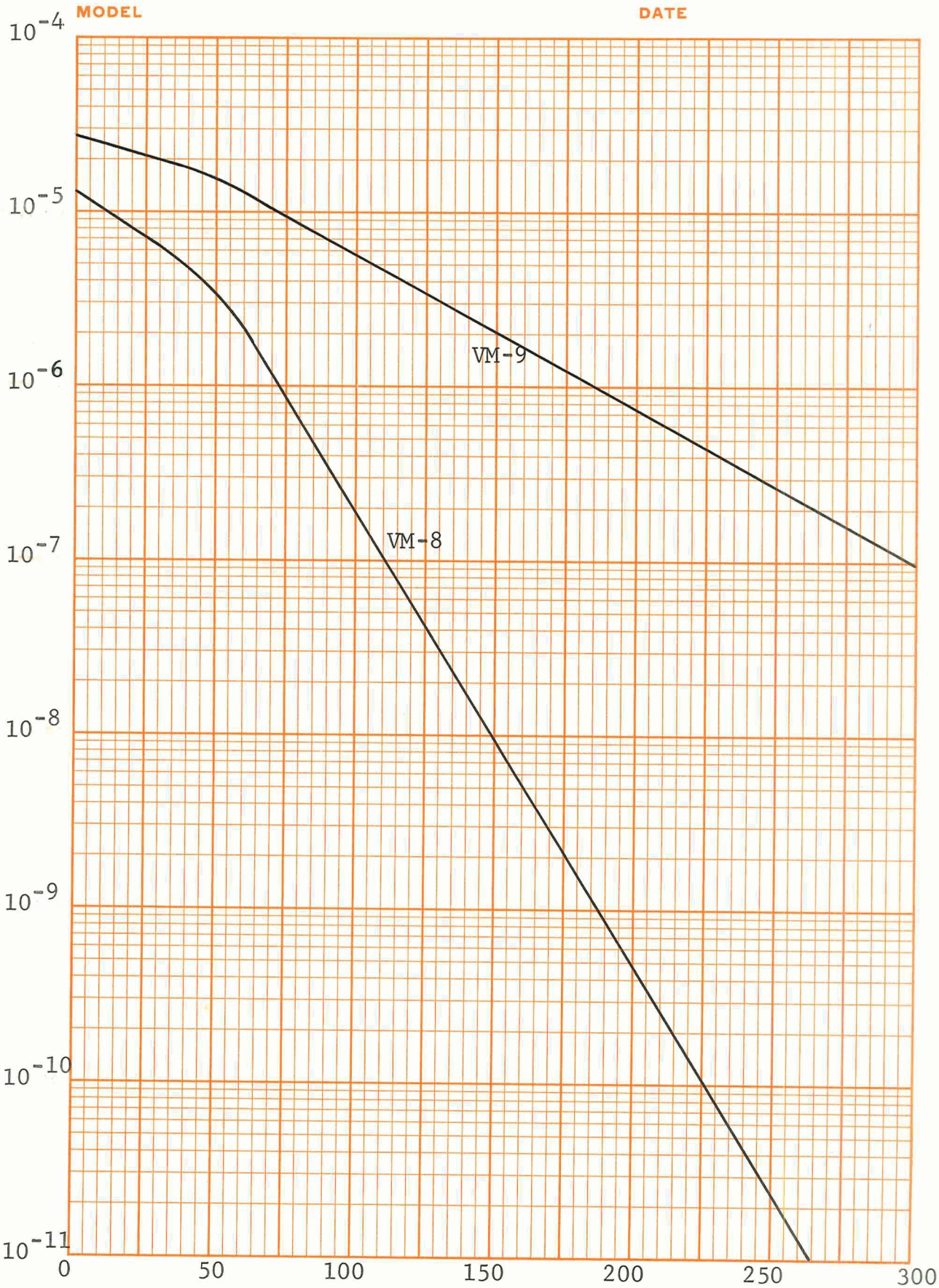

FIGURE 1 - Density as a Function of Altitude for the Extremes of Mars Model Atmospheres, VM-8 and VM-9

One of the primary objectives of this program is to demonstrate with working hardware that these goals can be achieved.

Environments encountered prior to the mission include handling, shipping, and sterilizing. During the mission, environments of vibration, shock, acceleration, temperature, vacuum, electromagnetic radiation, and nuclear radiation will be encountered. The sterilization environment has been summarized in Table I. The other environments used as a guide for this program are listed in Table II.

Design Guidelines

This section presents the design guidelines agreed upon at the start of the program. The primary approach is to carry forward the work performed under Contract NAS1-5341 (ref. 1).

The Mission. A Mars mission is assumed as a guideline. The mission starts with the assembly, testing, calibration, and sterilization of the sensor on Earth, followed by installation into the planetary vehicle. The sensor's gamma radiation source is in a shielded configuration until just prior to launch when it is unshielded via ground command. Once launched, the planetary vehicle passes through the Van Allen radiation belts near Earth and spends eight months in transit to Mars. The trajectory is such that the planetary vehicle is placed in a Mars orbit. The planetary vehicle consists of an orbiting spacecraft and an entry capsule. On command from Earth, the entry capsule separates from the orbiting spacecraft and decelerates aerodynamically, and in the terminal phase by parachute or retromotor, to a soft landing on the Martian surface.

The descent commences at a shallow angle below the horizon, ~20 degrees, and at a maximum velocity of ~5 Km/second. The sensor is activated and the radiation source is shielded for a short period and a measurement of background radiation is made prior to the capsule reaching the Martian atmosphere. As the capsule enters the atmosphere, drag reduces its velocity and shock waves form around the capsule. As the capsule reaches an altitude somewhat above 100,000 feet, the gamma radiation source is exposed and the measurement of free atmosphere density begins. As the capsule further decelerates and descends into the Martian atmosphere, a velocity is reached which is slow enough for heat shield separation. With the heat shield removed, the remainder of the descent is controlled by parachute or retromotor to a soft landing on the Martian surface.

During the descent, data is telemetered from the entry capsule to the orbiting spacecraft and then to Earth.

TABLE I

Sterilization Requirements Summary

ITEM	TEST	CYCLES	TIME-TEMPERATURE
Qualification (Type Approval Tests):			
Parts	Decontamination	6	28 hrs at 50°C
	Heat	6	92 hrs at 135°C
Assemblies	Decontamination	6	26 hrs at 50°C
	Heat	6	64 hrs at 135°C
Flight Acceptance Tests (FAT):			
Parts	None		
Assemblies	Decontamination	1	24 hrs at 40°C
	Heat	1	60 hrs at 125°C

NOTES:

1. In addition to these requirements, the complete Voyager payload will undergo terminal sterilization at levels similar to those specified above for FAT of assemblies.

2. All heat cycles in 100 percent N_2 atmosphere.

3. Decontamination agent is 12 percent ethylene oxide, 88 percent Freon 12.

4. Time quoted does not include time required to raise temperature from ambient and to lower temperature at end of cycle. See JPL VOL-50503-ETS.

TABLE II - Environmental Guidelines

1. Launch Environment - sensor not operating

   a. Sinusoidal Vibration*

      0.6 - 15 g RMS; 5 - 17 cps
      15 g RMS; 17 - 2000 cps

      Single sweep each of three axes; 5 - 2000 cps at 1 octave/minute

   b. Random Vibration (all axes)*

      0.45 g^2 cps, 700 - 1200 cps rolled off at 12 db/octave both sides to 227 and 2000 cps. 0.005 g^2 cps from 20 to 227 cps

      1 g RMS for 80 seconds; 7.5 g RMS for 40 seconds; 15 g RMS for 40 seconds; 20.5 g RMS for 40 seconds

   c. (1) Thrust axis = ±12 g, 5 minutes

      (2) Transverse axes = ±4.5 g, 5 minutes

   d. Shock (all axes)

      35 g, 11 milliseconds

2. Transit to Mars (8 months) - sensor generally not operating except that the device will be activated prior to atmospheric entry for warmup and for background radiation measurements.

   a. Temperature

      -55°C to +40°C

   b. Pressure

      A hard vacuum may be possible

3. Atmospheric Entry - sensor operating

   a. Deceleration

      55 "Mars" g

   b. Pressure

      Increasing from possible hard vacuum prior to entry to ambient at planet's surface (5 - 20 mb)

   c. Temperature

      -30°C to +40°C

*From Atlas-Agena-Lunar Orbiter qualification specification for components.

TABLE II - Environmental Guidelines, Page 2

During the latter stages of entry, the temperature will probably be near the high end of this range. There is the possibility of thermal shock when the heat shield is ejected and the sensor is exposed to ambient atmospheric temperature (-20°C to -100°C at 20,000 feet in Mars' atmosphere).

The Measurement. The measurement of atmospheric density by gamma radiation scattering is illustrated in Figure 2. A radioisotope source of gamma radiation, housed in a shield, emits gamma rays which pass through the vehicle skin, heat shield, and shock layer into the free stream atmosphere. A portion of these gamma rays is scattered by the gas atoms comprising the atmosphere. The portion of gamma rays scattered is directly proportional to the gas density. Some of these scattered gammas reach the detector located within the vehicle, giving a measure of gas density. As the gas density increases, the output of the detector increases proportionately.

Scattering Theory. Before studying the scattering theory, it is useful to examine the significant forms of interaction of γ rays with matter. Of six possible modes of interaction possible, Compton scattering, photoelectric absorption, and pair production dominate so strongly for the γ ray energies to be considered (10 Kev to 10 Mev) that the other processes can be neglected. These three important processes are:

a. Compton Scattering - A γ ray scatters from a single electron which is in an orbit about a nucleus. This electron absorbs some of the γ ray energy and is freed from its orbit. The energy of the scattered γ ray depends upon its original energy, the energy required to free the electron, and the angle of scattering.

b. Photoelectric Absorption - The γ ray energy is completely transferred to an orbiting electron which then leaves its orbit.

c. Pair Production - The γ ray interacts with the electric field about a nucleus or an electron and is converted into a positron and an electron. A minimum γ ray energy of 1.02 Mev is necessary.

Of these three interaction processes, pair production is avoided by using a radiation source of less than 1.02 Mev, and photoelectric absorption results in a high speed electron which travels away from the MP/L and has a negligible chance of producing a count in the detector of the density sensor. Therefore, only the Compton scattering need be considered.

The source and detector are located within the capsule as shown in Figure 2. To avoid measuring the density of the shock wave, both are collimated so that their fields of view intersect only beyond the shock wave. The relationship, describing the number of scattered gammas detected as a function of atmospheric density, is described by the expression:

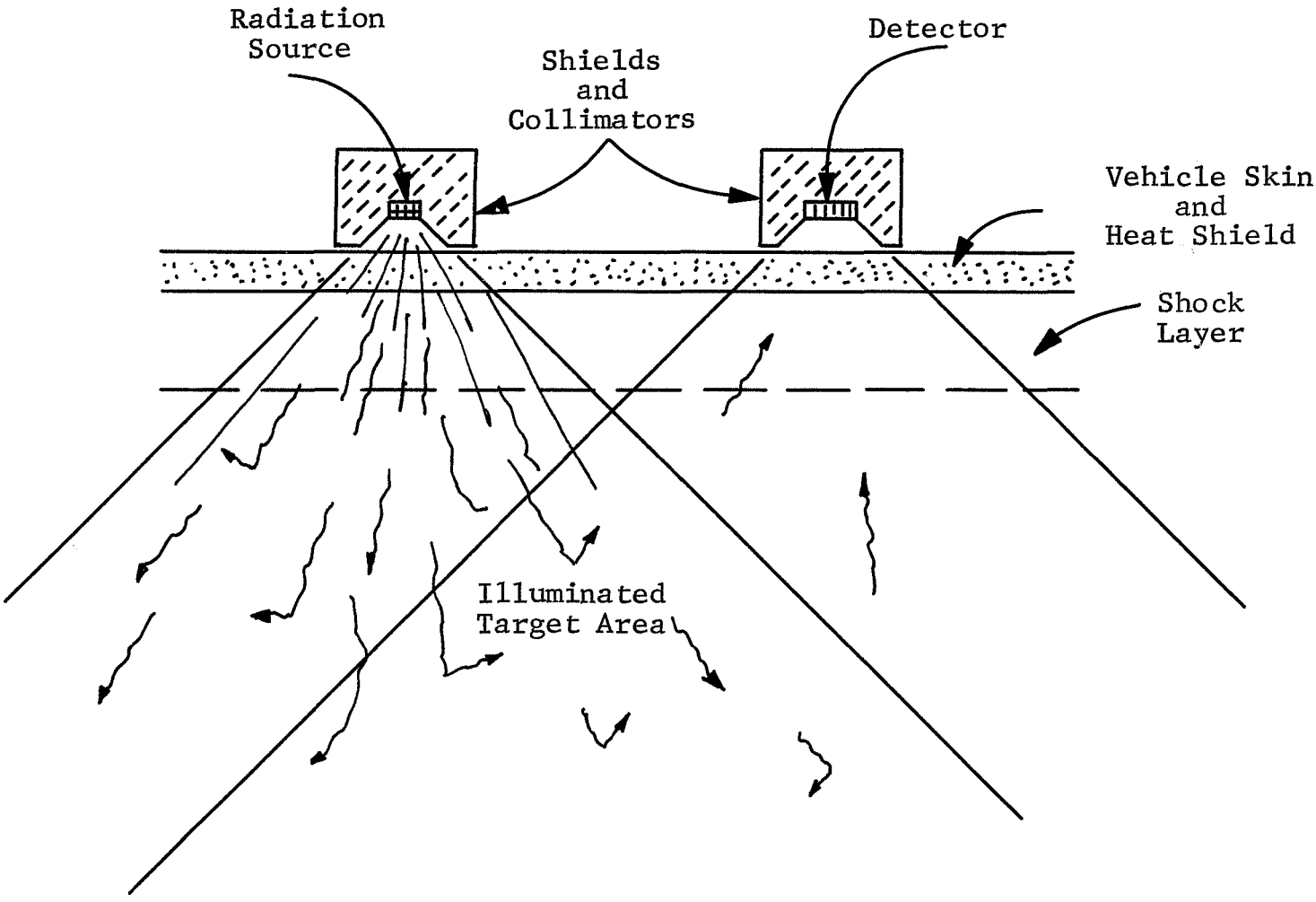

FIGURE 2 - Density Measurement Technique

$$I_s = G\, I_o\, \sigma_{as}\, A_d\, \epsilon_d\, \rho_a \qquad (1)$$

where:

ρ_a is the density of the atmosphere outside the shock wave, in gm/cm^3

ϵ_d is the detector efficiency

A_d is the detector area, in cm^2

σ_{as} is the photon scattering coefficient of the ambient atmosphere, in cm^2/gm

I_o is the source strength in photons/second emitted into 4 π solid angle about the source

G is a constant related to the geometric configuration

I_s is the number of photons per second detected after scattering from the atmosphere

Equation (1) predicts only the count rate resulting from γ rays of energy E_1 which leave the source, reach the region of overlap for the collimated source and detector without further interaction, scatter once in the overlap volume, reach the detector without further interaction, and then are detected. Obviously, counts will be recorded that do not correspond to the above sequence of events. These counts may be divided into two groups -- those which are indicative of the ambient density and those which are not. The first group is useful and its inclusion will benefit the density sensing experiment. They can arise when a source γ ray undergoes a low angle scatter in the heat shield followed by a scatter in the overlap volume and subsequent detection. A brief survey of the possibility of such an event indicates that it (and others of similar types) are not sufficiently numerous to justify the effort needed to accurately predict their effect. Therefore, equation (1) is used as the basis of design even though it gives a pessimistic estimate of the useful count rate I_s.

On the other hand, there are those counts which are definitely not indicative of the ambient atmospheric density. Such counts may arise when a γ ray scatters in the heat shield, proceeds along the heat shield to scatter in the shield over the detector, and is then detected. Cosmic ray counts, etc., are also in this catagory. All such counts cause an error in the indicated atmospheric density.

Design Consideration. The hardware configuration used to sense atmospheric density by gamma radiation scattering must include the following elements:

1. A radioisotope source is needed to emit gamma photons of the proper energy to provide good scatter in the atmosphere, be able to penetrate the vehicle skin easily, be easily shielded and collimated, and have a long half life.

2. A detector is needed which can efficiently detect the scattered gamma photons, retain calibration after a long mission, and withstand the environments encountered.

3. Shields are needed around the source and detector to prevent direct transmission from the source and internal scatter within the vehicle from reaching the detector. The source radiation pattern and detector viewing pattern are shaped so that the scatter signal reaching the detector is from a volume of atmosphere which is beyond the effects of vehicle interaction, thus providing a direct measure of the free stream atmospheric density.

4. A source shuuter provides means of shielding the sources just prior to entry into the atmosphere so that an accurate background measurement may be made.

5. Background noise limits the accuracy of the sensor at the high altitude-low density end of the measurement range. Therefore, it is necessary to minimize this noise by means of electronic rejection.

Baseline Design. Since the vehicle configuration and mission have not been defined, many of the specifics of design must be selected somewhat arbitrarily. The configuration resulting from Contract NAS1-5341 is used as the basis for the selected configuration with some geometric changes to improve the response. The basic guidelines are listed below.

1. Source - The source design provides shutter capability so that there need be no unusual precautions required during vehicle assembly and so that a measure of background noise can be made prior to entry into the atmosphere. The source mechanism also provides suitable protection in the event of a launch pad explosion. The source configuration is updated to include results of recent ORNL investigations (ref. 5).

Specific characteristics are:

Source material - Gadolinium 153
Emission - 100 Kev gammas
Half Life - 242 days
Useful strength at the time of measurement - 20 gamma curies

Collimation efficiency factor - 3
Time decay factor - 2.42
Self absorption factor - 1.33
Abundance factor - 2.18

Strength when delivered from manufacturer - 480 curies

2. Detector - The detector characteristics on which the design is based are:

Type - Scintillation crystal/photomultiplier tube
Scintillation material - NaI(Tl) or equivalent
Diameter - 2 inches
Thickness - 0.25 inch
AGC reference - Source to provide minimum background noise - under 32 Hz

3. Geometry - The geometric configuration is based on the following:

Source - Detector separation - 100 cm
Source collimation - 30° to 150°
Detector collimation - 30° to 150°

4. Shielding - That necessary to reduce direct transmission to less than 1 Hz with shield open and to provide a maximum dose rate of 2 mr per hour at one meter with shield closed.

5. Heat Shield - Assumed as follows:

Thickness - 0.5 cm
Density - 0.5 gm/cm^3

6. Electronics - Based on the following:

Response - 100 Hz to 40,000 Hz
Window discriminator - 60-100 Kev
AGC - Necessary to maintain calibration through sterilization, transit time, and environment

7. Ablation Gages - None

8. Accuracy - ±10%

9. System Size, Weight, and Power:

Size - 100 in^3
Weight - 5 lbs.
Power - 5 watts

10. Sterilization - The design is based upon maximum utilization of sterilization proven parts.

11. Reliability - The design is based upon maximum utilization of proven, high reliability parts.

DESIGN

This section presents the design approaches, tradeoffs, considerations, and design details which have resulted in the present design configuration for the working model.

Mathematical Model

The mathematical model is derived in Appendix A showing the basic design relationships. The atmosphere scattered signal as detected is expressed as:

$$I_s = G\, I_o\, \sigma_{as}\, A_d\, \rho_a \qquad (2)$$

The geometry factor, G, is seen to be a function of basic variables pertinent to the basic design configuration. These are the radiation pattern of the source, the sensitivity pattern of the detector, and the source to detector separation. The source and detector patterns and their effect on sensitivity are not separable and must therefore be considered together. One obvious conclusion is that the broader the collimation is, particularly the region between source and detector, the greater the sensitivity. However, as this collimation is broadened to include volumes close to the vehicle between the source and detector, more scatter occurs within the shock layer and the accuracy is degraded. In lieu of a detailed analysis of this effect since actual vehicle and shock layer constraints are unknown, an arbitrary source and detector collimation of from 30 degrees to 150 degrees was selected. Subsequent analysis by Whittaker et al (ref. 3) has shown that significant error can be expected from shock layer effects using these collimation angles, and, in fact, even narrowing the collimation from +60 degrees did not show a marked improvement.

Source Assembly

As has been reported previously (ref. 1), the source material should emit low energy gammas for a high scattering probability, but high enough in energy to minimize absorption in the vehicle structure. The reasonable compromise is in the region of 100 Kev. A second important consideration is a minimum content of high energy gammas which must be shielded from direct transmission. Several sources have been considered in a study by ORNL (ref. 5) which included in order of preference:

1. Gadolinium-153 from natural europium
2. Europium-155 from enriched ^{154}Sm
3. Cobalt-57, cyclotron produced
4. Gadolinium-153 fron enriched ^{152}Gd

The Gadolinium-153 was selected for this program having properties as listed below.

Half life - 242 days
Types of decay - Electron capture - 100%
Emissions:

Gamma Energies (Kev)	Percent Yield	Relative Percent Abundance
70	3.1	5.6
97	30	54
103	22	40

Specific Activity - 78 curies per gram of Gadolinium maximum
Density - 3 gm/cm^3
Purity - 10^{-6} percent yield of gammas of energy greater than 150 Kev

The optimum configuration of the source capsule is dependent upon several tradeoffs. First, the source must be thin to minimize self-absorption. Second, the source must be close to a point source to minimize shielding and collimation weight. Third, the source must have a volume consistent with the source strength desired and specific activity achievable. Fourth, the configuration must be such that remote shielding is practical. Evaluation of these four constraints have resulted in the selection of a line source configuration as shown in Figure 3. This source has a length of 10 cm, a width of 1 cm, and a thickness of 0.24 cm. The source capsule is a welded, stainless steel container having a wall thickness of 0.015 cm.

For a 20 gamma curie effective source, the required source strength is computed as follows:

Self Absorption

$$\frac{1}{\mu\rho t}\left[1 - e^{-\mu\rho t}\right] = 0.35 \qquad (3)$$

where:

$\mu = 4\ cm^2/gm$

$\rho = 3\ gm/cm^3$

$t = 0.24\ cm$

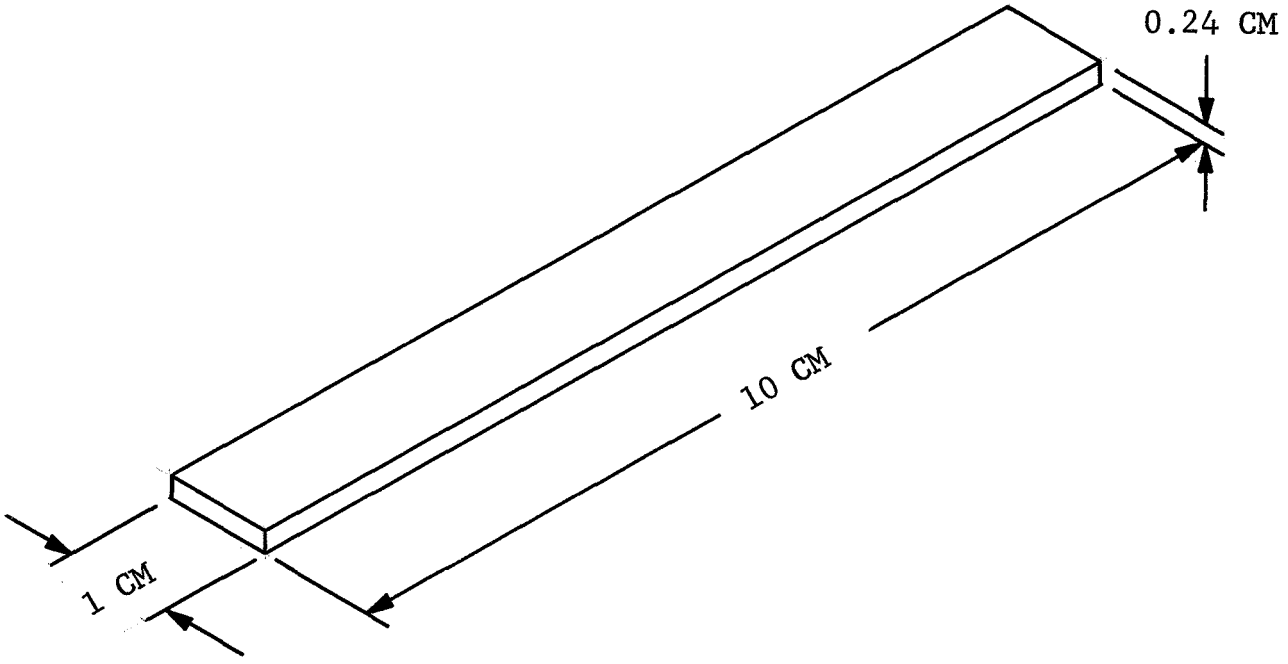

FIGURE 3 - Source Configuration

Half-Life Correction

$$e^{-.69\frac{T}{\tau}} = 0.55 \qquad (4)$$

where

T = 270 days for mission

τ = 242 days half-life

Yield

0.52

Absorption in Capsule Skin (stainless steel)

$$e^{-\mu\rho t} = 0.945 \qquad (5)$$

where

μ = 0.37 cm^2/gm

ρ = 10 gm/cm^3

t = 0.15 cm

The required source strength is thus

$$S = \frac{20 \text{ gamma curies}}{0.35 \times 0.55 \times 0.52 \times 0.945} = 210 \text{ curies} \qquad (6)$$

The required specific activity to package 210 curies in the capsule volume is calculated as

$$SA = \frac{S}{V\rho} = \frac{210}{10 \times 1.0 \times 0.24 \times 3.0} = 29.1 \text{ curies per gram} \qquad (7)$$

This is well below the possible 78 curies per gram, indicating adequate margin. The capsule thickness was selected based upon an existing thin wall tubing extrusion. If the source was reduced to 0.1 cm thickness, the required strength would be 128 curies and the specific activity 43 curies per gram.

Purity - The source purity must be such that no high energy gammas are emitted such that they reach the detector and contribute a significant background level. This background can be computed as follows, assuming no absorption.

$$I_B = \frac{Y}{100} \frac{S A_D}{4\pi r^2} 3.7 \times 10^{10} \qquad (8)$$

letting

I_B = 1.0 pulse per second background due to impurities

Y = Percent yield of impurities of high energy

S = Source strength = $\frac{20}{.52}$ = 38.5 curies

A_D= Exposed detector area = 3.25 cm^2

r = Source-detector separation = 100 cm

results in a percent yield of

$$Y = \frac{100\ 4\pi\ 100^2}{1.0 \times 38.5 \times 3.25 \times 3.7 \times 10^{10}} \qquad (9)$$

Thus, a 2.7×10^{-6} percent yield or less of high energy gammas is required. Effects of absorption, dose buildup, scattering, and detector response would tend to modify this somewhat, but it is not felt that a significant change would result if these effects were considered since they would be self-compensating.

Source Shielding - The source shielding must perform three functions. First, it must attenuate the direct transmission of gammas to the detector such that a negligible background noise is produced. Second, it must provide the desired collimation to the source. Third, it must, when in the closed position, attenuate the radiation to a safe level for working personnel in the vicinity. The thickness of shielding required is calculated as follows. The direct transmission is expressed as

$$I = \frac{I_o\ A_D}{4\pi\ r^2} De^{-\mu\rho x} \qquad (10)$$

for the design being considered.

$I_o = 20 \times 3.7 \times 10^{10} \times 0.52 = 3.84 \times 10^{11}$ pps

$A_D = 3.25\ cm^2$

r = 100 cm

μ = 4.2 cm^2/gm for tungsten and 100 Kev gammas

ρ = 17 gm/cm^3 for tungsten

I = 1 pps, the maximum allowable count rate

D = 3.0, dose buildup factor from ref. 6, page 45

The required shielding thickness is thus

$$t = -\frac{1}{\mu\rho} \; n \; \frac{I \; 4\pi \; r^2}{I_o \; A_D} = 0.24 \text{ cm} \qquad (11)$$

Since the source configuration is a line source, effective collimation can be achieved only in one direction, about the major axis. The line source is thus oriented with the major axis perpendicular to the direction to the detector. Collimation about the minor axis is not necessary for elimination of shock layer effects. The inherent collimation due to absorption is sufficient. The source cross section illustrated in Figure 4 shows the collimation configuration. The actual pattern achieved, including both geometrical and absorption effects, is also shown. Figure 5 illustrates the pattern about the minor axis, primarily the result of self-absorption effects.

The shielding required for safety considerations is calculated as follows:

$$D = \frac{S \; r}{4\pi \; r^2} \; De^{-\mu\rho t} \qquad (12)$$

where

D = 2 mr/hr dose rate

S = 210 curie source strength

$\Gamma = 0.22 \; \frac{r - cm^2}{mc - hr}$ or $0.22 \times 10^6 \; \frac{mr\text{-}cm^2}{curie\text{-}hr}$ dose rate constant

r = 100 cm

D = 3.0 dose buildup factor

μ = 4.2 cm^2/gm for tungsten and 100 Kev gammas

ρ = 17 gm/cm^3 for tungsten

t = thickness in cm

The required shielding thickness is then:

$$t = \frac{1}{\mu\rho} \; n \; \frac{S \; \Gamma \; D}{D \; 4\pi \; r^2} = 0.077 \text{ cm} \qquad (13)$$

Source Mechanism - The completed source assembly is illustrated in Figure 6. The design of the shield mechanism is to provide proper shield positions for the following:

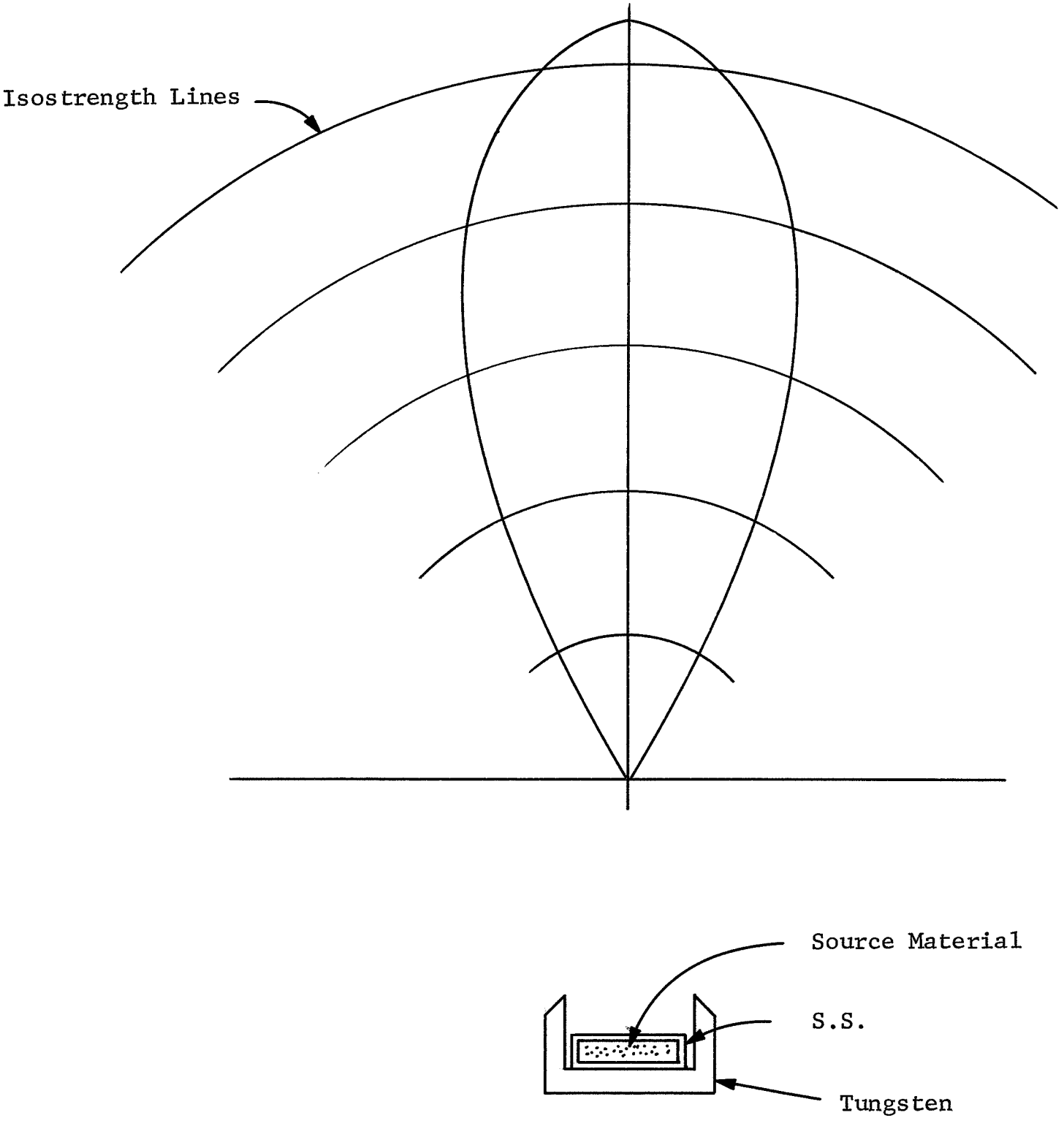

FIGURE 4 - Source Cross Section and Pattern

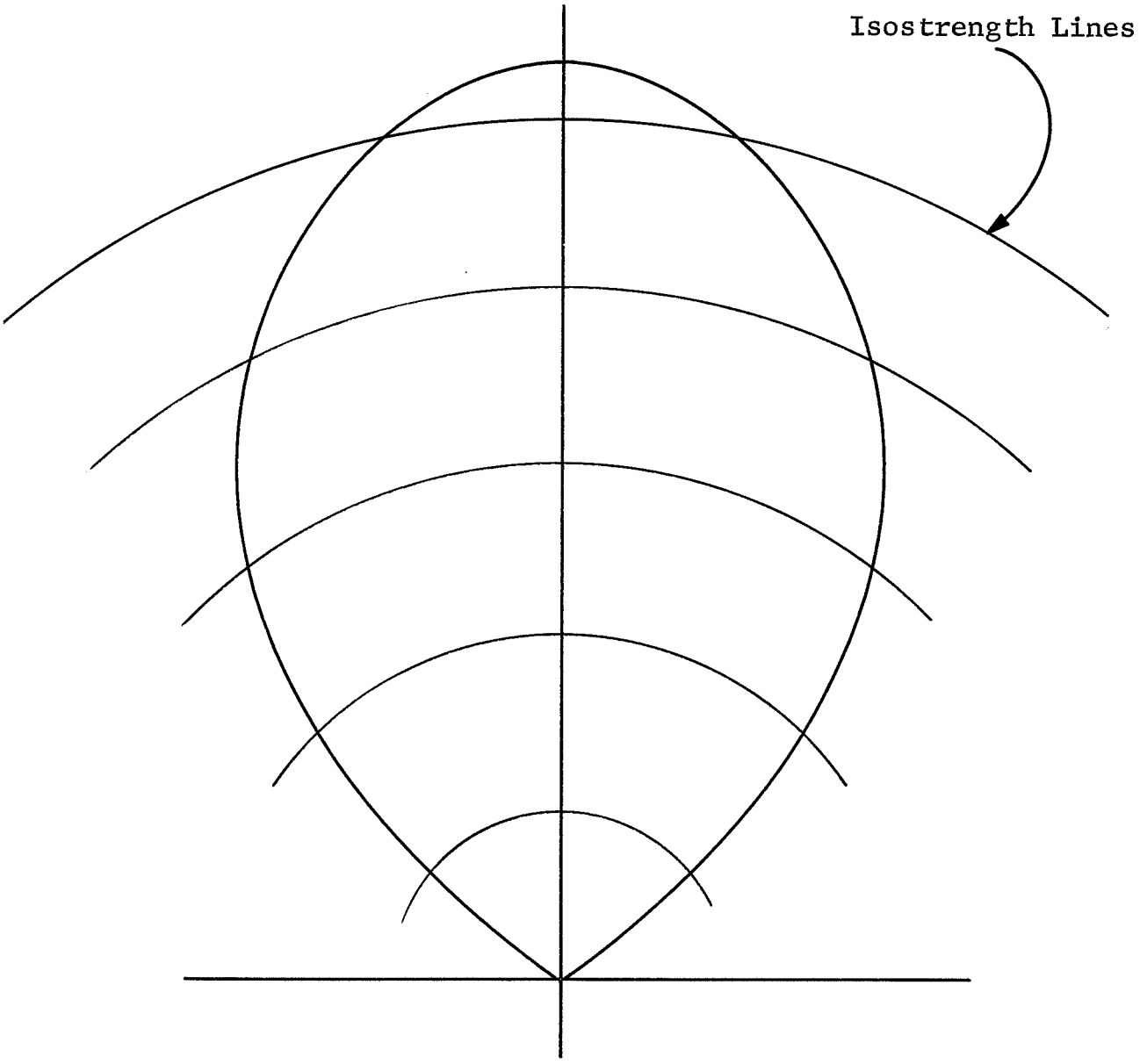

FIGURE 5 - Source Pattern, Minor Axis

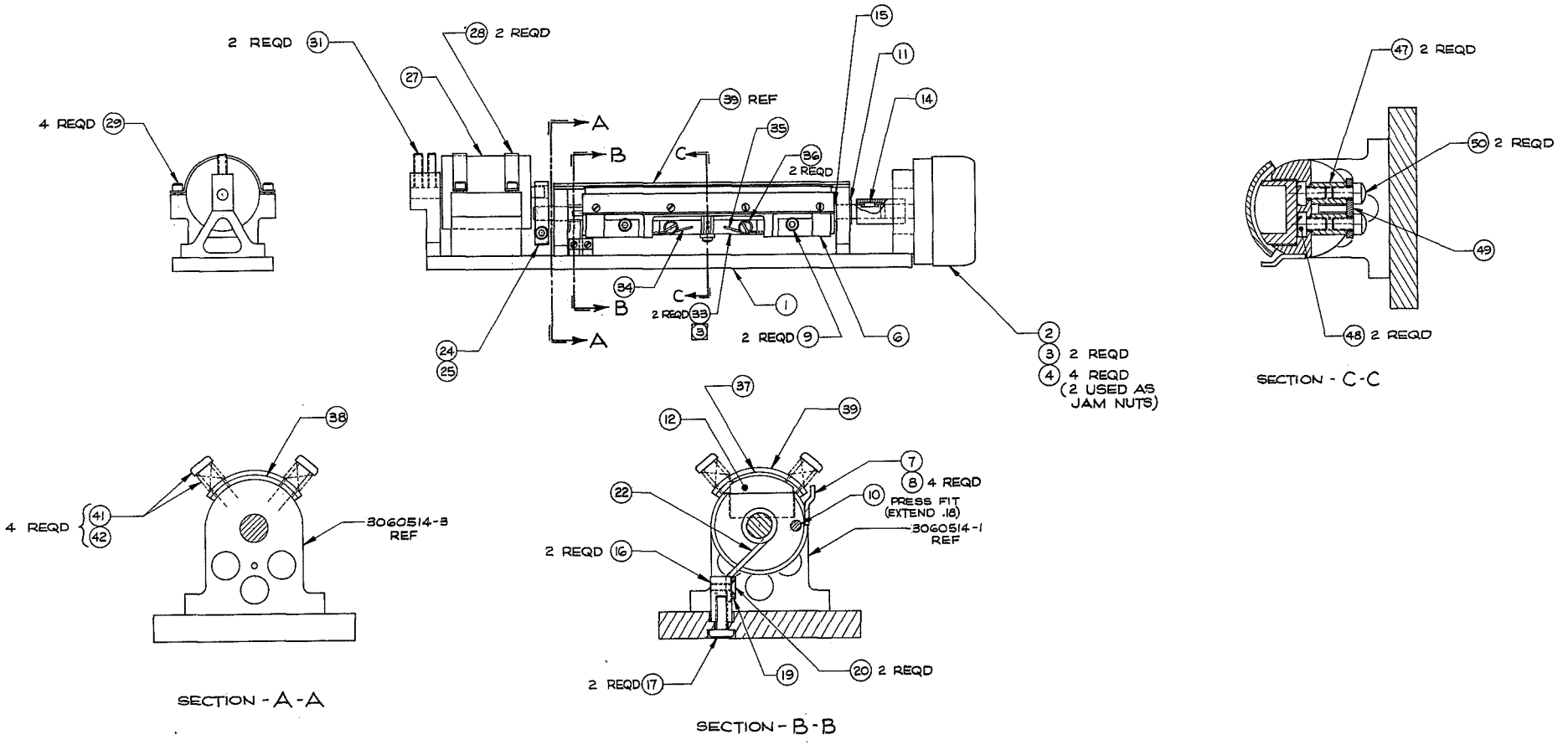

FIGURE 6 - Source Assembly

a. Pre-launch activities
b. Launch accident and fire
c. Fail-safe operation during the mission

The following sequence was used to establish the shield performance criteria:

a. During the pre-launch activities, the shield should be closed with no power applied.

b. Just prior to launch, the shield should be remotely opened for preliminary test and possible calibration check on the system.

c. During the measurement phase, the shield should fail-open to permit completion of the measurement phase of the mission; however, normal operation permits a choice of remotely selecting either open or closed positions for background radiation correlation.

Referring to Figure 6, the various elements of the shield assembly are identified. The source capsule is housed in the source holder. This holder is tungsten and provides the shielding necessary to permit direct transmission and properly collimate the source. The source holder is installed in the source mechanism and is closed by rotating 90 degrees to face the safety shield (item 39, Figure 6). The source holder is secured by tightening the screws (item 9). The shield housing is motivated to the closed position by activating the rotary solenoid (item 2). To retain the shield housing in the closed position, the bidirectional linear solenoid (item 27) is activated. Pins (item 31) fall into detents in the linear solenoid shaft to insure positive positioning. The shield housing is shown in the closed-retained position in Figure 6.

To open the shield housing, the retaining shaft is withdrawn by activating the linear solenoid in the reverse direction. A spring integral with the rotary solenoid opens the mechanism rotating the shield housing 90 degrees counterclockwise. To perform a mid-mission radiation background measurement, the rotary solenoid is activated to the closed position. The linear solenoid is not activated. In this manner should there be an electrical failure, the housing will remain in the open position, as the rotary solenoid is spring loaded open.

In case of a launch pad explosion or fire, the following features provide safe containment of the radioactive source.

The radioactive material is contained in a stainless steel capsule having a melting point of 2500°F. The mounting plate, bearing blocks, and main housing are fabricated of titanium which has a melting point of 3270°F. The source housing and shield are of tungsten which has a melting point of 6090°F. When the source is in the shielded position, the above parts provide a secure housing for the radioactive material up to 2500°F. At this temperature, the stainless steel capsule will melt, but the source housing, shield and mounting plate will last to 3270°F.

The sequence of operations during a fire is as follows: (assume the source is in open position)

The tin spring retainer (item 19) melts at 449°F. This releases the spring (item 22) which drives the shield housing via the pin (item 10) into the closed position.

At 620°F the lead retainer (item 49) melts and allows the positive arm locks (item 33) to be wedged into the mounting plate. This secures the housing in the closed position during the fire. At this same temperature, the tungsten shield (item 39) is spring driven (item 42) into the bearing blocks (3060514). These parts are solder coated and they will be fused together during cooling. The three functional springs are so constructed that they will retain a sufficient amount of temper to satisfactorily operate at 620°F.

Detector Assembly

General Requirements. The requirements of the detector assembly of the atmosphere density sensor are that it is sensitive to 100 Kev gamma radiation, that it be stable, and that it be insensitive to adverse environments. The detector must present a large area since the basic sensitivity scale factor, which determines the overall sensitivity of the instrument, is based upon the maximum counting rate. The larger the area of the detector for a corresponding source size, the more sensitive the unit will be. The detector assembly must be rugged enough to withstand the environments associated with the vehicle launch and the temperature extremes experienced during a sterilization cycle. The unit also must be of small size and light weight.

Several types of radiation detectors can be considered for this application. These include the solid state detector, Geiger Mueller tubes, proportional counters, and scintillation detectors. The scintillation detector was chosen for this application for its availability with large sensitive areas, high efficiency, good sensitivity to 100 Kev gammas, and proven ability for use in applications such as this.

Common crystal materials available for use in a scintillation detector include thallium activated sodium iodide, thallium

activated cesium iodide and sodium activated cesium iodide. Table III shows the various properties of these three crystal materials. Thallium activated sodium iodide is the material which is typically used for scintillation counting of gamma photons. However, sodium iodide is relatively fragile and care must be taken in packaging such a crystal. Sodium iodide crystals are also quite sensitive to thermal shock. Cesium iodide crystals on the other hand are very rugged. They can stand extreme shocks and rapid temperature changes. The light output from a cesium iodide crystal, as seen in Table III, is less than that of sodium iodide. Also, the pulse decay time is significantly longer. This tends to limit the high count rate response of such a detector.

A more recently developed crystal, which seems to have the desired properties of both of the two crystals, is sodium activated cesium iodide. This crystal material is rugged, will withstand severe shocks, both thermal and mechanical, and has almost as high a light output as sodium iodide. The pulsewidth is somewhat longer than sodium iodide crystal, but still within an acceptable limit.

The size and shape of the detector crystal are determined by packaging considerations. It is desirable to have as large a detector area exposed as possible, limited by the weight and size of the total package.

A 2-inch diameter, thin cylindrical-shape was selected for this application. The 2-inch diameter gives 200 square inches of detector surface area. The thickness of the crystal is kept as small as possible such that the sensitivity or the exposed area to gammas coming directly from the source is minimized. Also, the amount of shielding that is necessary to attenuate direct transmission is minimized. The crystal must be thick enough to totally absorb the 100 Kev gammas. The crystal thickness may be determined from the following equation for 90 percent absorption:

$$0.9 = 1-e^{-\mu\rho t} \tag{14}$$

where

$\mu = 1.5 \frac{cm^2}{gm}$, absorption coefficient of crystal for 100 Kev gammas

$\rho = 3.67 \frac{gm}{cm^3}$, density of crystal

t = thickness of crystal to provide 90 percent absorption

TABLE III - Crystal Properties

Scintillator	NaI(Tl)	CsI(Tl)	CsI(Na)
Density gm/cm^3	3.67	4.51	4.5
Wave Length of Emission Å	4,100	4,100	4,100
Refractive Index	1.7	1.79	1.79
Light Output Related to CsI(Tl)	2.0	1.0	2.0
Hygroscopic	Yes	No	Slightly
Decay Time, μsec	0.25	>1	1.0
Absorption Coefficient:			
100 Kev gammas cm^2/gm	1.5	1.2	1.2

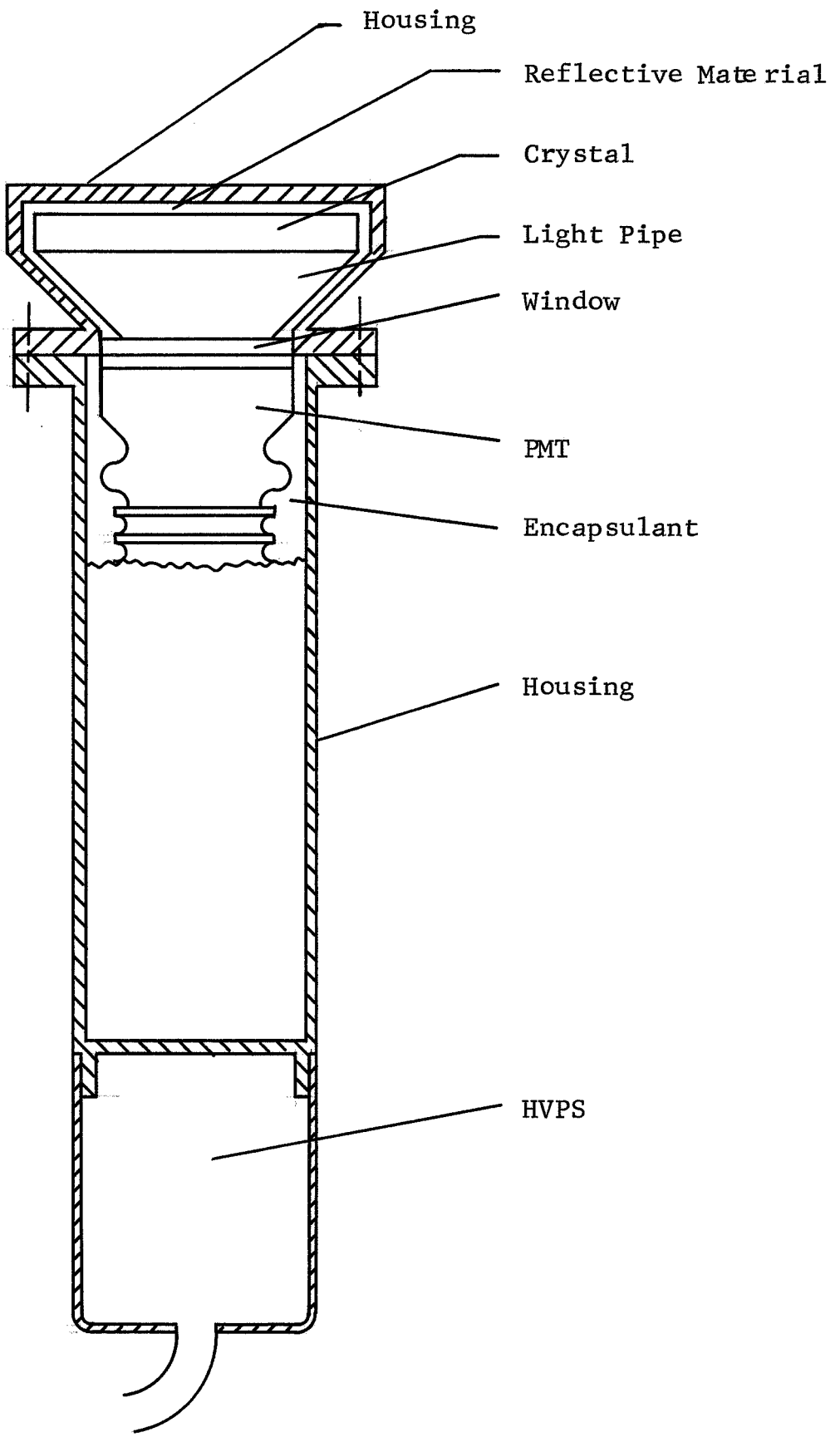

FIGURE 7 - Detector Configuration

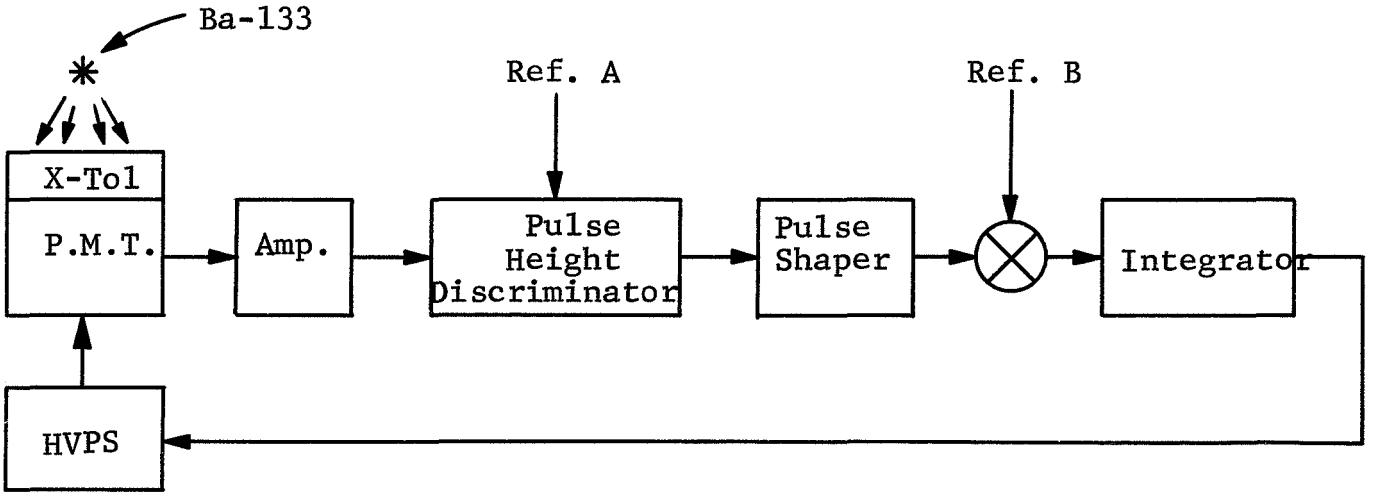

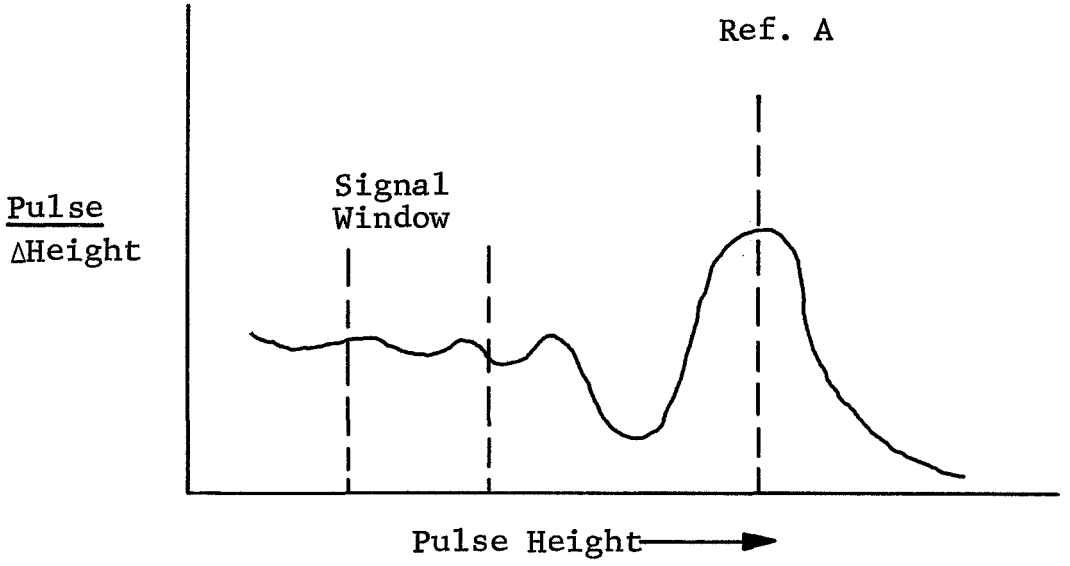

FIGURE 8 - Block Diagram, Automatic Gain Control

Solving for t gives a minimum required thickness of 0.42 cm. Thus, the selected thickness of 0.25 inch is adequate to absorb the 100 Kev gammas.

The photomultiplier tube chosen has a 1-inch diameter photo cathode. The 2-inch area output from the crystal must be reduced via an optical coupling to a 1-inch diameter face mating with the photomultiplier tube. A quartz glass material is used to provide this optical coupling. As illustrated in Figure 7, the optical coupling is seen to be a truncated cone with a 45° slope. The crystal manufacturers recommend this as the optimum geometry for maximum light collection. The entire crystal assembly is sealed in a stainless steel container. A reflective material surrounds the crystal to enhance the light reflection.

This crystal assembly is mated to the photomultiplier tube high voltage power supply combination. Several photomultiplier tubes were investigated for this application. The photomultiplier tube must have an S11 photo cathode in order to match the 4100 Å spectral output characteristics of the scintillation material. A 14-dynode venetion blind type dynode structure tube was selected for its ruggedness and small size. The particular tube was selected primarily because of its stability after sterilization cycling. A special photocathode material was developed in a program sponsored by the Jet Propulsion Laboratory. This work is discussed in reference 9. The characteristics of this photomultiplier tube are shown in Table IV.

The high voltage power supply required to power this photomultiplier tube must be small in size and light in weight. The most critical portion of the environment for this photomultiplier tube assembly is the ability to contain the 2,000 to 3,000 volts of high voltage in the vacuum environment without leakage or corona. The optimum method of providing this corona protection, and yet maintain a package of small size and weight, is to internally package the high voltage power supply and photomultiplier tube. The entire assembly can thus be sealed, providing complete protection from the vacuum environment. Only low voltage is required to drive the integrated photoelectric assembly.

Automatic Gain Control. Typical detector assemblies are noted for their lack of long term stability through rigors of environmental change. One particularly severe environment is that of sterilization. The long periods of high temperature soak tend to change the photocathode output and overall photomultiplier tube gain. Also, during a six month period in transit, the photomultiplier tube and power supply may tend to change their operating characteristics in terms of gain. During reentry, changing environment also causes shifts in the detector response. In order to compensate for these gain changes, some type of automatic gain control (AGC) is required.

TABLE IV - Photomultiplier Tube Characteristics

Quantum Efficiency at 4100 Å	21.5%
Cathode Luminance Sensitivity	72.0 μamps/lm
Voltage Required for 10^6 Current Amplification	2950 volts
Dark Current at 10^6 current Amplification	2.5×10^{-11} amps
Pulse Height Resolution (FW HM) for Cs 137, NaI(Tl)	8%
Shock	100 g, 11 ms
Vibration	30g, 20-300 cps
Temperature	-55° to +100°C
Number of Dynodes	14
Effective Cathode Diameter	1 inch

Several methods of AGC were studied in this program and are discussed in Appendix A. The method of gain stabilization employed is to place a small reference source near the detector and monitor the resultant detector output. The detector gain is then controlled to maintain the output pulse height constant from this reference. Some of the important requirements for the AGC are: the reference source must have a long half-life; the reference source pulse height must track the signal pulse height; and the reference source must not contribute significantly to the background noise level in the signal energy region.

A number of possible sources and scintillation detectors were considered for this automatic gain control technique. Some of the sources considered were Americium 241, alphas; Americium 241, 60 E Kev gammas; Barium 133, 335 Kev gammas; and Gadolinium 153, 100 Kev gammas. The signal in all cases is the Gadolinium 153, 100 Kev gammas, as backscattered by the atmosphere. The detector crystals considered were thallium activated cesium iodide, or combinations thereof.

The combinations of scintillators and AGC are illustrated in Table V, with their various advantages and disadvantages listed. The method selected for application in the first phase is Method 5, which employs the sodium activated cesium iodide crystal and the 355 gammas from a barium 133 gammas source. There is no shutter. The unit is simple, rugged, and not temperature sensitive. The disadvantage of the method is that there will be a small noise contribution in the region of signal. For the phase II a cesium iodide crystal and an americium 241 source was used because of the interference that was observed from the barium source during the testing of the Phase I system. The interference observed during temperature was greater than could be tolerated. The temperature compensation required by using americium 241 with a cesium iodide crystal were made in the electronics.

The operation of the AGC is illustrated in the block diagram Figure 8. The operation is essentially the same for both phase I and phase II. The 355 Kev gammas from the Barium 133 entered the scintillation crystal and result in output pulses following the spectrum shown. There is the fairly broad photo peak and extensive Compton continuum. These pulses out of the detector are amplified and are fed into a single level pulse-height discriminator. Those pulses of amplitude greater than the reference level are passed and those lower than the reference level are rejected. The pulses that are passed are integrated and compared with a reference such that the output of the integrator is equal to the integral of the difference between the reference level and the AGC count rate. The output of this integrator then drives the gain control input to the photomultiplier tube high voltage power supply. This gain input controls the high voltage output of the supply, thereby increasing and decreasing the total photomultiplier tube gain as required. If the

TABLE V - Comparison of Various AGC Techniques

	Signal Crystal	Ref. Crystal	Ref. Source	Shutter	Advantages	Disadvantages
1	CsI(Na)	CsI(Na)	Am-241 Alpha	None	Rugged Simple	Very temperature sensitive. Some noise at 60 Kev.
2	NaI(Tl)	CsI(Tl)	Am-241 Alpha	None	Simple No noise contribution	Somewhat temperature sensitive. Not rugged. Susceptible to thermal shock.
3	CsI(Na)	CsI(Tl)	Am-241 Alpha	None	Simple No noise contribution Rugged	Somewhat temperature sensitive.
4	CsI(Na)	CsI(Na)	Am-241 Gamma	None	No noise contribution Rugged Not temperature sensitive	Complicated electronics. Limited dynamic range (high rate).
5	CsI(Na)	CsI(Na)	Ba-133 Gamma	None	Simple Rugged Not temperature sensitive	Small noise contribution.
6	CsI(Na)	CsI(Na)	Gd-153 Back-scatter Gamma	None	Rugged Not temperature sensitive No noise contribution	Complicated electronics. Limited dynamic range (low rate).
7	CsI(Na)	CsI(Na)	Ba-133 Gamma	Yes	Rugged Not temperature sensitive No noise contribution	Complicated mechanically. Less than 100% duty cycle.

detector gain is lower than its desired value, the pulses out of the detector from the AGC reference source are lower in amplitude. Therefore, fewer of them pass through the level discriminator to drive the integrator. The countrate is thus lower than the AGC reference and the integrator output thus increases. As the integrator output increases, the high voltage power supply output increases, causing the photomultiplier tube gain to increase, thuse causing the AGC reference pulses to increase in amplitude until they reach an amplitude such that the count rate passing through the level discriminator is equal to the desired count rate as established by the gain reference.

Referring to the AGC count rate spectrum (Figure 8), it can be seen that a large percentage of the AGC countrate is included in the signal window. Therefore, a very low AGC count rate is required. Also, a very long averaging time is required in order to minimize the statistical fluctuation of a low count rate average. It is desired to keep the noise contribution below 30 pulses per second. With a 60 pulse per second count rate, a very long averaging time is fine for stabilizing long term drifts of the photomultiplier tubes such as encountered in a recovery from sterilization cycling and a long transient to a planet, but would not correct for rapid changes that might be encountered during atmospheric entry. Therefore, the detector and electronics must be inherently stable over short term changes.

Electronics Assembly

Signal Conditioning Electronics. The signal conditioning electronics is illustrated in block diagram, Figure 9, and the schematic drawing, Figure 10.

The gamma rays emitted by the source are absorbed by the scintillator. The resulting light photons are transmitted to the PM tube and are converted into electrical pulses. The output of the PM tube is amplified and fed to the AGC and window discriminator. The output pulse of the window discriminator goes to conversion electronics which transform the pulse data into a dc analog signal and a pulse delay signal.

To stabilize the gain of the PM tube, an AGC is used. The AGC uses as reference a calibration source output. A single level discriminator splits the calibration source spectrum in half. If the gain changes, the calibration peak shifts and the number of counts seen by the single level discriminator changes. The AGC circuit senses this change and adjusts the PM tube high voltage power supply to a new high voltage and adjusts to keep the gain constant.

Preamplifier. The preamplifier consists of a high gain dc amplifier μA702 with appropriate input impedance and feedback resistance to control the gain and the linearity of the signal.

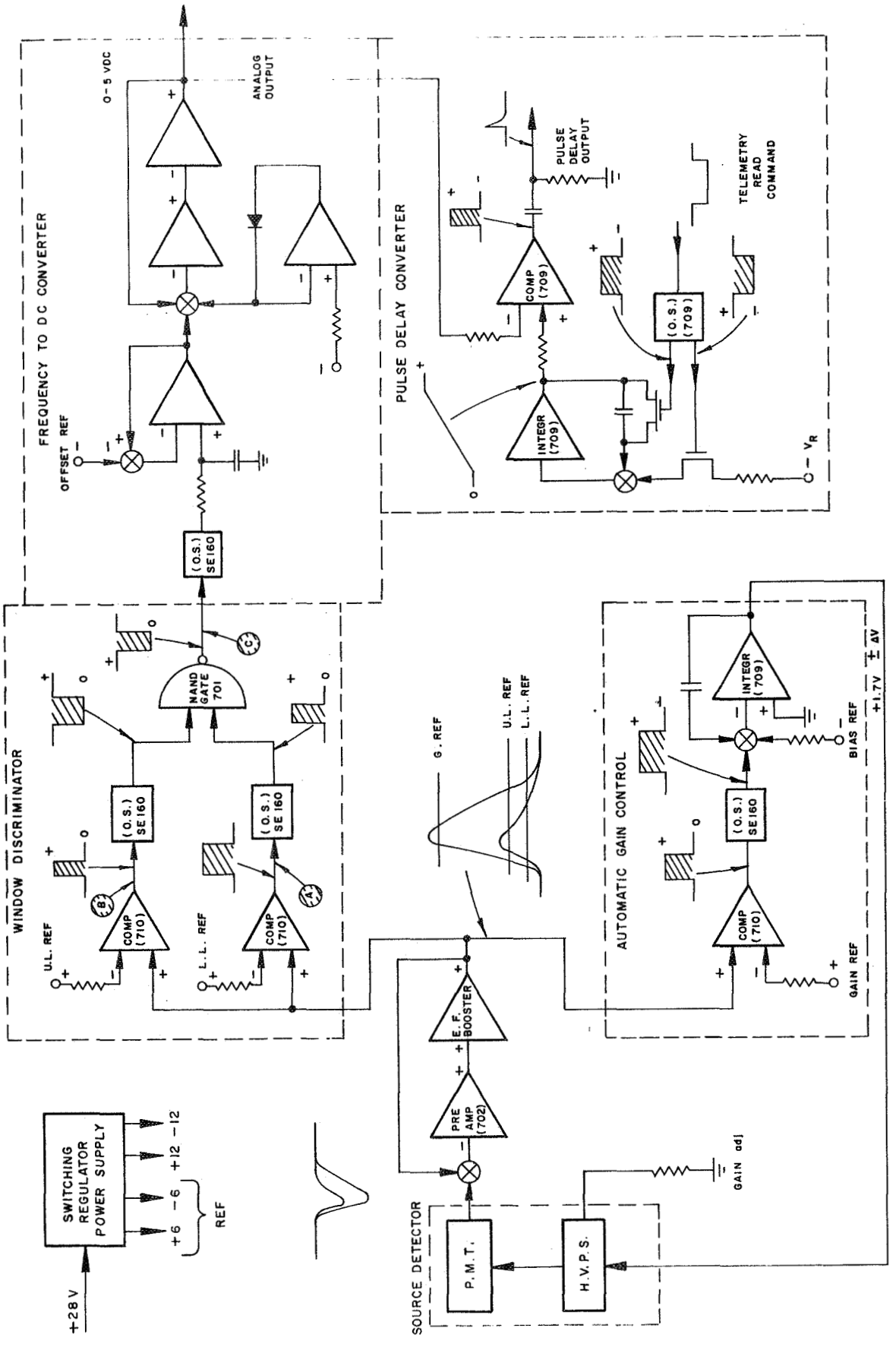

FIGURE 9 - SCHEMATIC BLOCK DIAGRAM, ATMOSPHERE DENSITY SENSOR

The emitter follower is necessary to minimize the instability due to the interstage loading effect, and gives a low source impedance to drive the window discriminator and AGC circuit.

Discriminator. The window discriminator, as shown in Figure 9, consists of two integrated level detectors (μA710), two pulse reformation circuits (SE-160), and a NAND Gate (701) which provide the anticoincidence necessary to obtain the window.

A reference voltage is inserted at the inverting input. The positive input pulses are applied at the non-inverting input, if:

$$V_{in} \leq V_{Ref}, \quad V_o \text{ is zero} \tag{15}$$

$$V_{in} > V_{Ref}, \quad V_o \text{ is positive} \tag{16}$$

The trailing edge of the output of the UL and LL comparators is used to trigger the monostable multivibrators (SE 160).

The signals from the two comparators do not occur at the same time. The trailing edge of the lower comparator waveform delays the input of the anticoincidence circuit.

The anticoincidence circuit produces an output signal if the signal from the lower comparator is not accomplished by one from the upper comparator.

The NAND logic is expressed as:

$$A \cdot \overline{B} = C \tag{17}$$

where:

A = low level signal exists

$\overline{B}$ = high level signal does not exist

C = output signal exists

Figure 11 shows the logic pulse formation on the window discriminator.

Automatic Gain Control (AGC). A single level comparator detects the variations in the system gain and applies a correction signal to the high voltage power supply. This causes the gain of the system to return back to the original value.

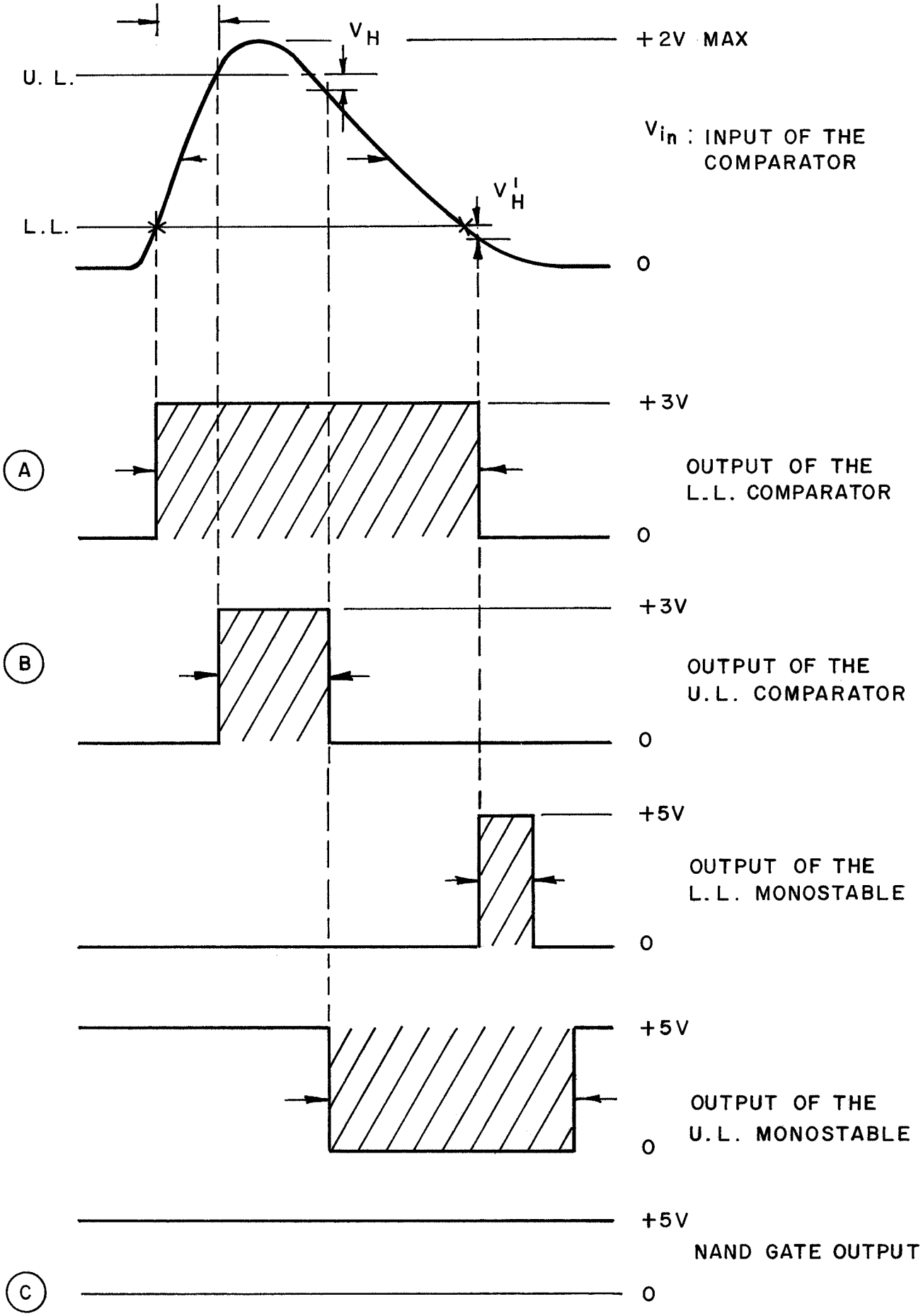

FIGURE 11 - Window Discriminator Pulse Formation

Gain variations are detected by the high speed comparator (μA710). A monostable multivibrator (SE-160) shapes the pulse and the integrator (709) provides a feedback voltage to control the high voltage power supply.

Gain reference voltage and bias reference adjustments are used to establish what point on the calibration spectrum the system will operate.

Analog Output. The output required of the sensor is a 0-5 volt signal to drive a telemetry system. In order to minimize the error induced by the telemetry system, a scale change is necessary. The output voltage nominally would be a dc level proportional to the pulse count rate from the signal conditioning electronics. Obviously at very low pulse rates, it would be a very low dc signal. For a linear 0-5 volt output, equivalent to a 0 to 40,000 pulses per second full scale range, the minimum 100 pulse per second signal would appear as a 12.5 millivolt output signal. Typical telemetry systems have a 1% error band which is equivalent to 50 millivolts in a 0-5 volt system. Obviously, the 12.5 millivolt signal would be lost in this 50 millivolt error band. Thus, scale changing is required. Various methods of scale changing were studied in this program. The majority of them requires the switching of amplifier gains as a function of selected count rates, or providing dual outputs, one for high level outputs and one for low level outputs. All of these methods add to the complexity of the overall system.

The approach finally selected is to provide a single output, but with a two slope scale arrangement. This scale change is illustrated in Figure 12. The 0-2.5 volt output is the equivalent to a 0 to 2,500 pulses per second signal. Then the 2.5 to 5 volt output range provides information proportional to the 2,500 to 40,000 pulses per second count rate. This shaped dc output is provided as follows:

Frequency to DC Converter. The output frequency of the window discriminator is shaped and inverted to monostable SE-160 (Figure 9). This output is then averaged and amplified. The output of the amplifier is then inverted by the voltage inverter (709) and used to produce an analog signal output.

The gain of the frequency to dc converter is controlled by a sharp active limiter. The limiter determines the optimum count rate at which to affect the automatic scale change and select the proper gain of the output amplifier.

Digital Output. An investigation was performed directed toward providing a digital output from the sensor. This appears desirable since the information started with is digital in format as pulses or pulse rate. This study showed that the pulses could be directed to counters, shift registers, etc., which could provide a serial or parallel output on command. The electronics

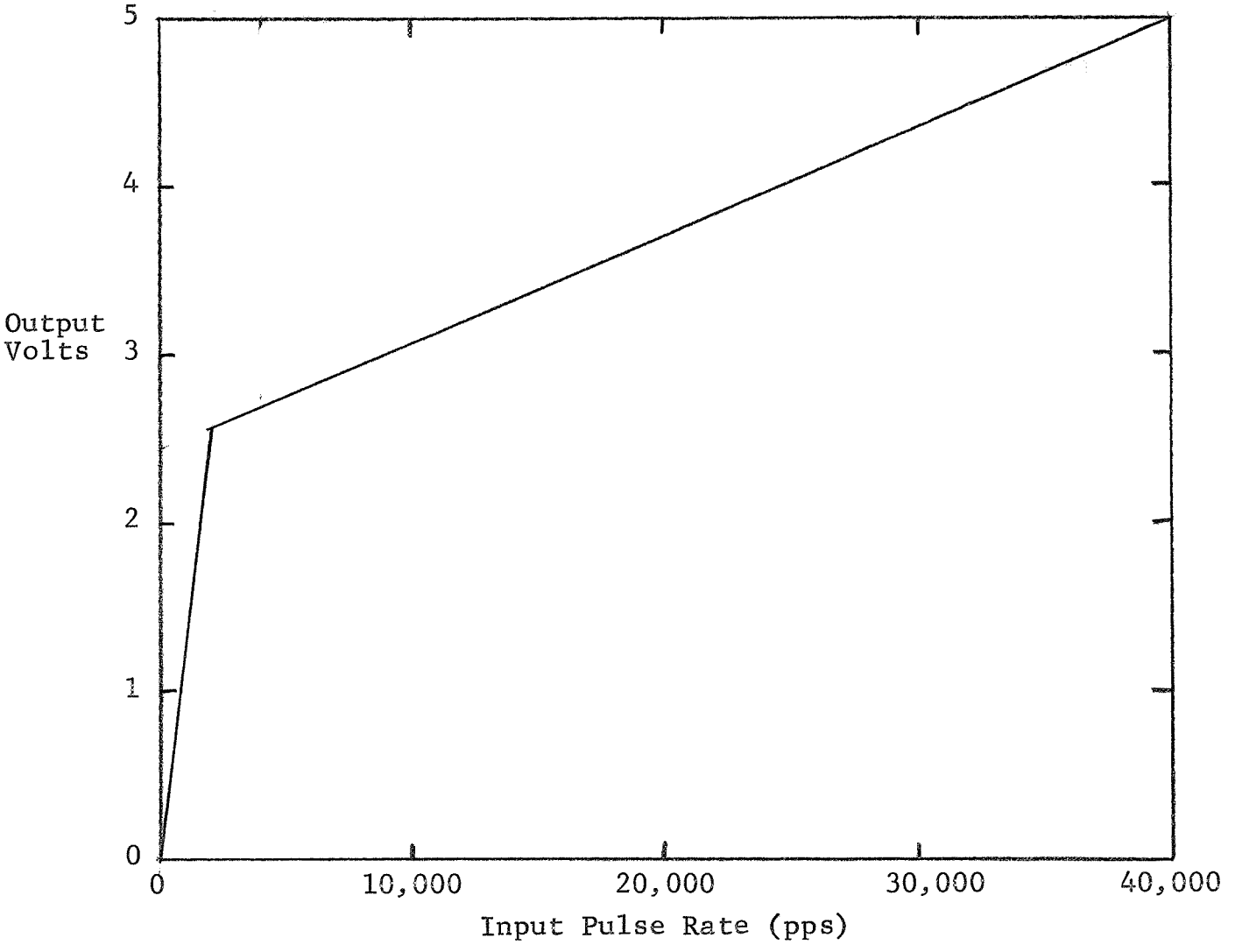

FIGURE 12 - Pulse to DC Converter Calibration

required for digital signal conditioning added to the complexity of the overall system. An investigation of existing data transmission techniques for planetary probes showed that most often a pulse delay type output was used. This was due to limited bandwidth and a limited number of telemetry channels available for such information. A pulse delay output is one in which an interrogation pulse is directed to the sensor and the sensor generates an output pulse at some time interval later. This time interval is proportional to the information desired. In other words, a pulse delay of 1 second could be equivalent to an input signal of 1 volt, or a count rate of 1,000 pulses per second. The conversion from a pulse rate in counts per second to the pulse delay information is most easily done by converting count rate to an analog signal and then converting from analog to pulse delay. This requires less electronics than performing the entire function in a digital fashion.

Pulse Delay Converter. The pulse delay (refer to Figure 9) output is generated in the following manner. The controller initiates a read command pulse. The leading edge of the command pulse triggers the one-shot multivibrator. The output of the one shot controls a gate which applies a reference voltage to a linear integrator. The output of the linear integrator and the analog output are fed to a comparator which turns on when the linear integrator output is slightly greater than the analog output. The comparator output is differentiated to produce the delay pulse. The time delay of the delay pulse with respect to the leading edge of the telemetry read command signal is directly proportional to the analog output as compared to the linear portion of the integrator output. Figure 13 shows the pulse formation delays.

Packaging. The electronics are packaged as shown in Figure 14. The circuit components are mounted on two printed circuit boards which are mounted into the electronics chassis via standoffs. The interconnection between the two printed circuit boards and connectors is provided by hard wiring. This results in a low weight unit that can be easily modified and reworked in a development program.

Size, Weight, and Power Summary

Table VI summarizes the size, weight, and power goals along with those that were achieved by Phase I of this development.

The size goals were met in all cases. The weight goal was missed by 6 ounces, primarily due to an overweight detector assembly. This overweight detector was not anticipated and it is felt that a significant weight reduction still could be effected in this area. The power summary shows that the power goal was achieved during normal operation of the sensor. This power does

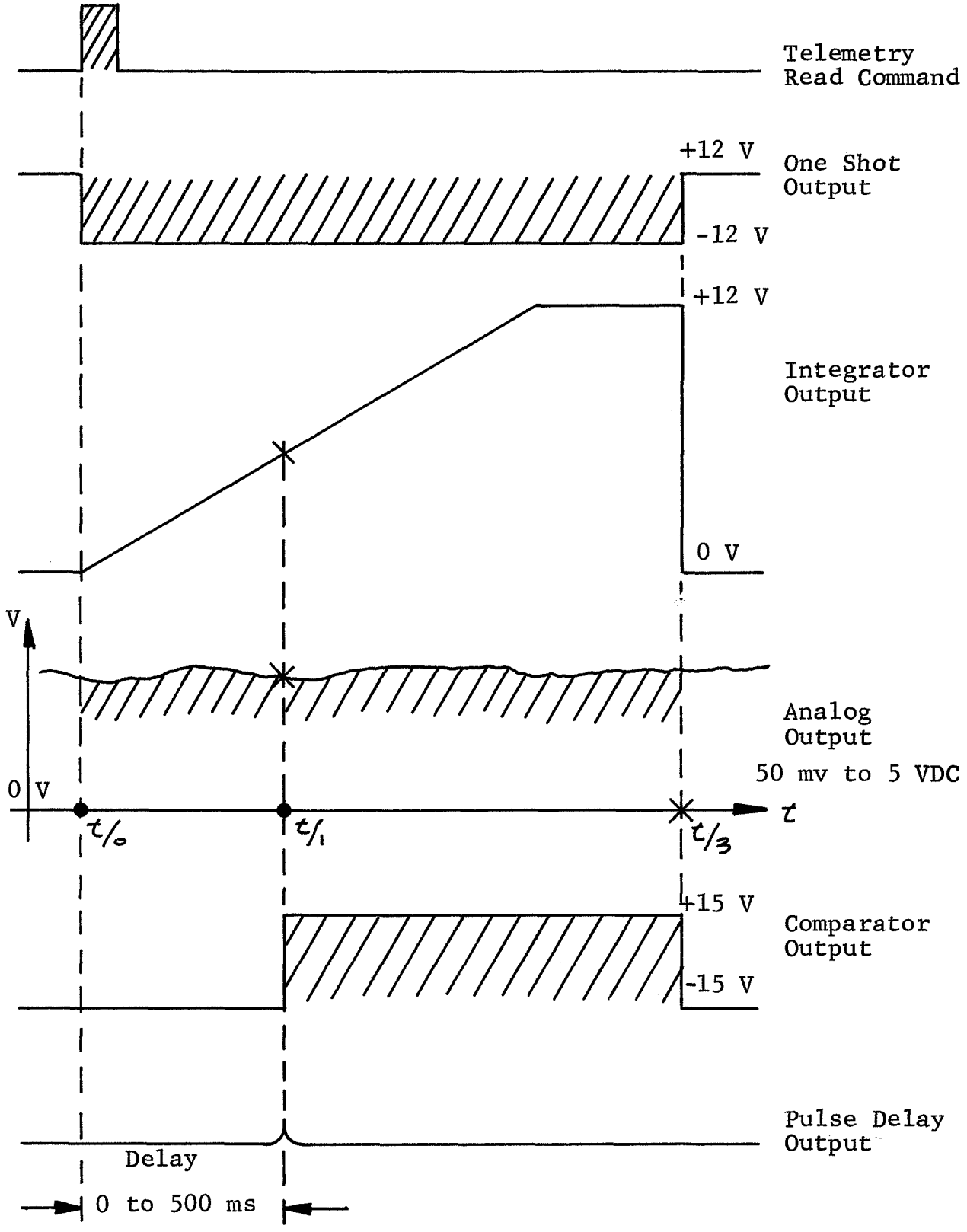

FIGURE 13 - PULSE DELAY FORMATION

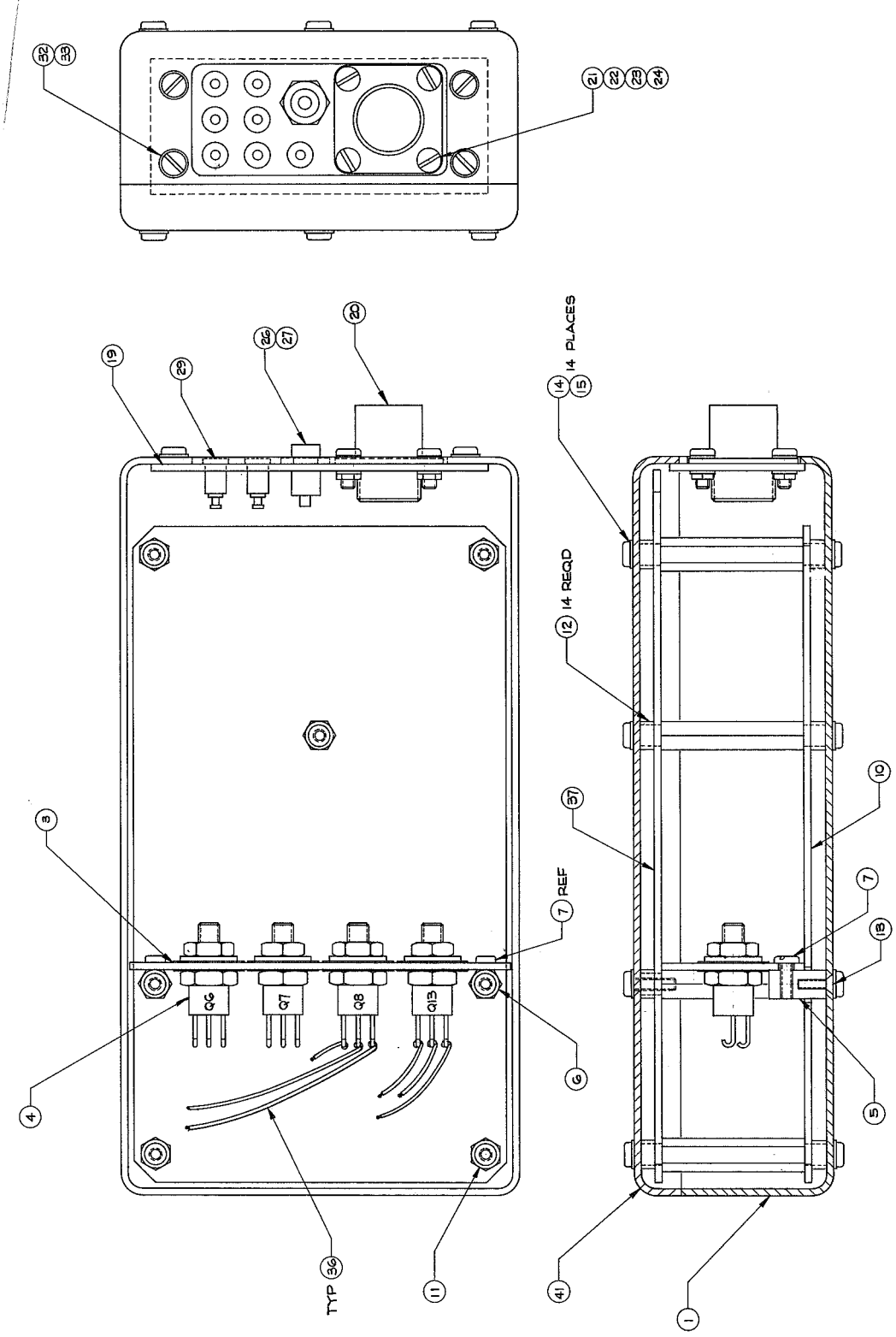

FIGURE 14 - Electronics Package

TABLE VI - Size, Weight, and Power Summary
PHASE II

	Size ($In.^3$)		Weight (lbs.)		Power (Watts)	
	Goal	Actual	Goal	Actual	Goal	Actual
Source Assembly	15	31.6	1.3	2.51		
Detector Assembly	35	18.9	1.0	1.75	1.5	.2
Electronics Assembly	45	39.8	2.7	1.24	3.5	4.6
TOTAL	95	90.3	5.0	5.50	5.0	4.8

not include that required to operate the shield motivating solenoids. This additional power will be available before launch via external sources. During the background measurement period, external power will not be available.

Alternate methods of operating this solenoid were considered, but they all involve latching or motivating the shield to a closed position and the condition could exist that if power was lost at that point in time, the shield could not be opened again. This is unsatisfactory since such a failure would completely void the mission.

RELIABILITY

A complete reliability analysis was performed on this sensor and is included in Appendix B. The results of this reliability analysis are illustrated in Table VII. The sensor is divided into six subassemblies, the first being the PM Tube and high voltage power supply; second, the amplifier and the discriminator electronics; third, the AGC electronics; fourth, the analog electronics; fifth, the pulse delay converter electronics; and sixth, the low voltage power supply.

The sensor mission is divided into four operating conditions; the launch period, the transit period, the orbit period, and the descent period. The application factors were then applied corresponding to sensor operation or non-operation, the environment during these various periods, and a complete summary of the reliability was formed. The results of this show a total mission probability of success of 89%. This probability is almost completely contingent upon the transit period operating condition. There is a 53,000 hour MTBF during this 5,760 hour period. In reviewing the various contributors, it is apparent that the PM Tube high voltage power supply is the element that if improved would result in the most significant overall system improvement.

Appendix B shows all of the electronic components, their values, their part numbers, the reliability level, and qualifying document. In almost all cases, the electronic components were selected from a JPL ZZP document which categorizes the parts in terms of their ability to withstand the sterilization environment as well as provide high reliability (ref. 8).

TABLE VII - RELIABILITY ANALYSIS SUMMARY

(1)	(2) Subassembly	Failure Rate x 10^{-6} (3) Launch	(4) Transit	(5) Orbit	(6) Descend	(7) Remarks
1 2	PMT Assy. & HVPS	180.75	9.84	27.03	376.75	Actual Part Calculation
3	Amp. & Disc.	20.37	1.72	3.46	27.83	Actual Part Calculation
4	AGC	7.90	1.95	3.59	10.20	Actual Part Calculation
5	Analog Conv.	13.07	2.19	4.23	15.96	Actual Part Calculation
6	Pulse Conv.	18.57	1.47	2.17	23.60	Actual Part Calculation
7	LVPS	40.27	1.47	3.44	86.51	Actual Part Calculation
	Total F.R.	240.93	18.64	43.92	540.85	
	MTBF (Hrs)	4151	53,648	22,769	1,849	
	PROBABILITY OF SUCCESS	99.98%	89.85%	99.78%	99.97%	TOTAL MISSION P_T = 89.61%

Column Description:

(1) Block identification from the reliability block diagram.
(2) Block (Subassembly) Description
(3) (4) (5) (6) Assumed mission regimes

	Launch	Transit	Orbit	Descent
a. Duration (t)	0.5 hr	5/60 hr	50.0 hr	0.5 hr
b. Power Applied	No	No	Yes	Yes
c. Component Temperature (T)	+85°C	+40°C	+85°C	+85°C
d. Application Factor (K_A)	Missile	Orbit	Missile	Missile

(7) Conditions for determining predicted values.

STERILIZATION

A study was conducted to determine the sterilization status of the Gamma Backscatter Atmosphere Density Sensor. Reference is made to the Reliability Analysis, Appendix B, which includes a detail listing of all parts used in the sensor design and their qualification status. Maximum use is made of previously qualified parts appearing in JPL Specification ZPP-2010-SPL-D Sterilization Parts List for Spacecraft Application dated 20 October 1967 (ref. 8).

Referring to the Reliability Analysis, the Qualification Document is specified for all components. Those referring to a ZPP document indicate their selection from the JPL Sterilization Parts List.

Other components are shown as being on the QPL, indicating qualification to the referenced MIL-Spec. The remaining components have not been qualified, but have been selected for some unique operational characteristics.

Table VIII summarizes the electronic parts not appearing on the JPL Sterilization Parts List for Spacecraft Application and the reason for their selection. This list covers 30 of the 280 parts used. Thus, 89.3 percent of the parts are sterilization proven. This list shows 14 generic part types. In most cases, a size constraint or particular performance characteristic made selection of these from the Sterilization Parts List impractical. The following paragraphs describe the approach recommended for the remaining parts.

PMT-HVPS Assembly

The Photomultiplier Tube-High Voltage Power Supply Assembly is a totally encapsulated unit. The components used in this assembly that have not been tested to the sterilization environment are all similar to types that have been subjected to the heat sterilization cycle. By virtue of the steel housing and encapsulents, these electronic components will not be subjected to the decontamination agent. It is recommended, therefore, that the entire assembly be tested to the sterilization environment rather than the individual components.

Electronic Assembly

The remaining parts consist of a capacitor, two transistors, a diode, and a transformer. The 2 μf capacitor can be replaced by a 1 μf from ZPP-2744-2508 with a minor design change. The 2N1132 transistor is similar to the 2N2907A except that it is in a TO-5 rather than a TO-18 case. It is anticipated that a suitable

TABLE VIII - Electronic Parts Not On JPL Sterilization Parts List

SECTION	COMPONENT	DESCRIPTION OR P/N	SPECIFICATION	COMMENTS
$\lambda_1 + \lambda_2$ PMT Circuitry & HVPS	Resistors (Dynode)	6-8 M Ω		Micronox Film - No equivalent on Sterilization Parts List
	Sensistor	TG 1/8	MIL-T-23648A	
	Capacitor	109D825x0060C0	Similar to MIL-C-25	No equivalent on Sterilization Parts List that can meet small packaging constraings
	Capacitor	MKW102K30	Similar to MIL-C-25	" " " " " " " " " "
	Capacitor	MKW102K50	Similar to MIL-C-25	" " " " " " " " " "
	Transformer	TF6QX40ZZ	MIL-T-27	Special to this application
	PMT	EMR-591N-01-14	MIL-E-1	Selected based on JPL Sterilization test results - development continuing.
	Transistor	2N718A	MIL-S-19500	Selected based on use history in application
	Diode	1N3284	MIL-S-195100	Special high voltage diode - No equivalent on Sterilization Parts List.
λ_3 Amp & Windo Discriminator	None			All parts from Sterilization Parts List
λ_4 AGC	None			All parts from Sterilization Parts List
λ_5 Analog Converter	None			All parts from Sterilization Parts List
λ_6 Pulse Delay Converter	Capacitor M	2 μf CTM	MIL-C-27278	Similar to ZPP-2744-2508
	Transistor	2N1132	MK-S-19500/177	Also used in LVPS - Selected for special performance (Power and Size) - No equivalent on Sterilizatim Parts List.
	Transistor	MEM550		Selected for special performance (FET) - No equivalent on Sterilization Parts List.
λ_7 Low Voltage Power Supply	Diode	1N4942	MIL-S-19500/359	Selected for special performance (High Speed) - No equivalent on Sterilization Parts List.
	Transformer		MIL-T-27	Special to this application - Can be manufactured to JPL Specification ZPP-2737-1300.

PNP silicon transistor in a TO-5 case will become available as the JPL sterilization test program continues. The MEM550 is a MOS-FET used for switching. This device is gaining wide application and it is anticipated that an equivalent device will become available as the JPL sterilization test program continues. Both the above transistors can be stored at 135°C and are hermetically sealed. The 1N4942 diode is selected for its high speed. It is packaged in a glass subminiature case size similar to the 1N916 (ZPP-2746-3001) and can be stored at 135°C. It is anticipated that this diode or one of equivalent characteristics will be added to the Sterilization Parts List as the sterilization program continues. The transformer is a toroidal type capable of being manufactured by an approved vendor in accordance with JPL Specification ZPP-2737-1300. Similar transformers are included on the Sterilization Parts List.

It is felt that special testing of the above devices is unnecessary since equivalents will become available as existing sterilization programs continue and sufficient confidence in their suitability is already established based upon similarity.

WORKING MODEL

The working model was assembled and tested to verify the design described previously. This working model verified the size, weight, and power goals of this program and verified performance through limited environmental testing and operation in the altitude sphere to simulate the actual measurement of density. The working model is shown in photographs in Figures 15, 16, and 17.

Before this working model was assembled, a detector and its electronics were breadboarded and tested. Problems were encountered with temperature shifts of the AGC. This first AGC method utilized alpha particles from an Americium 241 source as reference and a sodium iodide crystal detector. The problem encountered was that as the temperature of the crystal changed, the detector response to alpha particles did not track the response to gamma photons. The AGC was designed to accurately control the pulse height of the alpha particles, but through temperature the relative height of the backscattered gammas would change. This produced significantly large errors in the gamma output. This effect was also verified using the sodium activated cesium iodide crystal and thallium activated cesium iodide crystal.

It became evident that one means of getting the AGC Reference Source pulse height to track the backscattered gamma radiation pulse height was to use gammas as the reference source. The 350 Kev gamma of cesium 135 was selected. The disadvantage of a cesium 137 gamma source as a reference was that the Compton continuum from this higher energy gamma plus the 80 Kev gamma would produce a significant background in the region of back-scattered gamma radiation. In order to minimize this background, the AGC source strength had to be made as small as possible, shielding added, and the AGC made to operate on as few counts per second as possible.

In this regard, a very small cesium 137 source was placed against the crystal assembly and the output spectrum measured. Lead shielding was introduced between the source and the detector in thin layers. The shielding first attenuated the cesium 137 low energy gammas. Shielding was added until the 80 Kev gammas were totally absorbed and the ratio of AGC source to background noise reached a constant ratio. In this way, the thickness of shielding required was determined. The background then consisted primarily of the Compton continuum from the 355 Kev gammas.

The electronics breadboard was investigated and temperature tested. Several improvements were made through this program in order to arrive at an electronics design for minimum power, particularly in the area of power supply, efficiency, and transformer design.

FIGURE 15 - Source Assembly

FIGURE 16 - Detector Assembly

FIGURE 17 - Electronics Assembly

After breadboard testing was completed, the assembly of the working model was begun. The source mechanism was fabricated from the original design drawings and a few problems were encountered. Most of these problems were minor in nature and solutions effected with ease. One problem, however, became quite significant. This was in regard to the springs which are used to force the shield assembly closed in the event of a fire or launch pad explosion. It was found that springs could not be obtained which would retain their temper and provide a positive return force at high temperature within space that was available for them in the original design. This problem was left unresolved since it would require a complete refabrication of the assembly with an increased overall length dimension to allow a slightly longer spring to be used for this purpose. All other functions of the source assembly proved the proper design.

The working model electronics was assembled without problem. The detector assembly, although plagued by delays in delivery of the photomultiplier tube assembly, was finally assembled by the crystal manufacturer who used a proprietary optical coupling material to attach the crystal assembly to the photomultiplier tube assembly. Upon completion of this, all the parts of the working model were integrated into a unit and a series of calibrations and tests performed.

The source assembly was tested through temperature and vacuum environments. The unit was soaked at -50° and +100°C and operated at those temperature extremes without problem. The unit was put in a vacuum chamber and soaked in a vacuum and operated with no problem. The source material was received from the manufacturer and found to fit the source mechanism without problem. This source assembly, with a 1 curie source and a 5 curie source installed, was mapped in the open and closed positions, providing the radiation patterns for determination of the adequacy of shielding and collimation.

Integration of the working model detector with its electronics uncovered one particularly severe problem. The sodium activated cesium iodide crystal had a characteristic that was not anticipated in the electronics design, this being a longer than anticipated decay period. A change in the discriminator pulsewidth was required to insure blanking of the low level pulse by the high level pulse. Also, some differentiation circuitry was added to the output of the detector to shorten the pulses.

In calibrating the AGC circuitry, attempts were made to achieve very low AGC count rates and very low background. The final sensor operated at an AGC pulse rate of approximately 50 pulses per second. Working with this low count rates required working with a very low level signal in the AGC loop, and zero offsets of the one-shot pulse generator and its variation with

a very low level signal in the AGC loop, and zero offsets of the one-shot pulse generator and its variation with temperature became significant. A following transistor stage was added with low offsets to minimize the drift of the AGC with temperature. Also, with the low count rate, a long averaging time is required in order to minimize the random fluctuation of the AGC. This was accomplished by reducing the loop gain of the AGC loop to provide the desired slow response. This created a turn-on problem in that a long time was required from initial turn-on to final establishment of the desired AGC level. In order to shorten this turn-on time, an initial offset to the AGC control voltage was added so that it was much closer to its final state at turn-on.

Some modification of the drive capabilities of the output circuits was required to insure adequate operation with long cables in the altitude sphere.

During this period of system integration, a series of temperature tests were performed on the detector and its electronics. Temperature drifts were seen in these tests and improvements were effected. At the conclusion of this test program, the unit showed slight drift, but it was felt acceptable since it could be seen by variations in the AGC countrate and thus, if necessary, compensation could be provided.

The detector and the electronics were subjected to a vacuum test and performed satisfactorily.

The calibration of the discriminator levels was established by measuring the backscatter spectrum from the 100 Kev, 1 and 5 curie sources, and setting the window levels to encompass this peak. The backscatter spectrum and the relative positions of the window discriminators are illustrated in Figure 18.

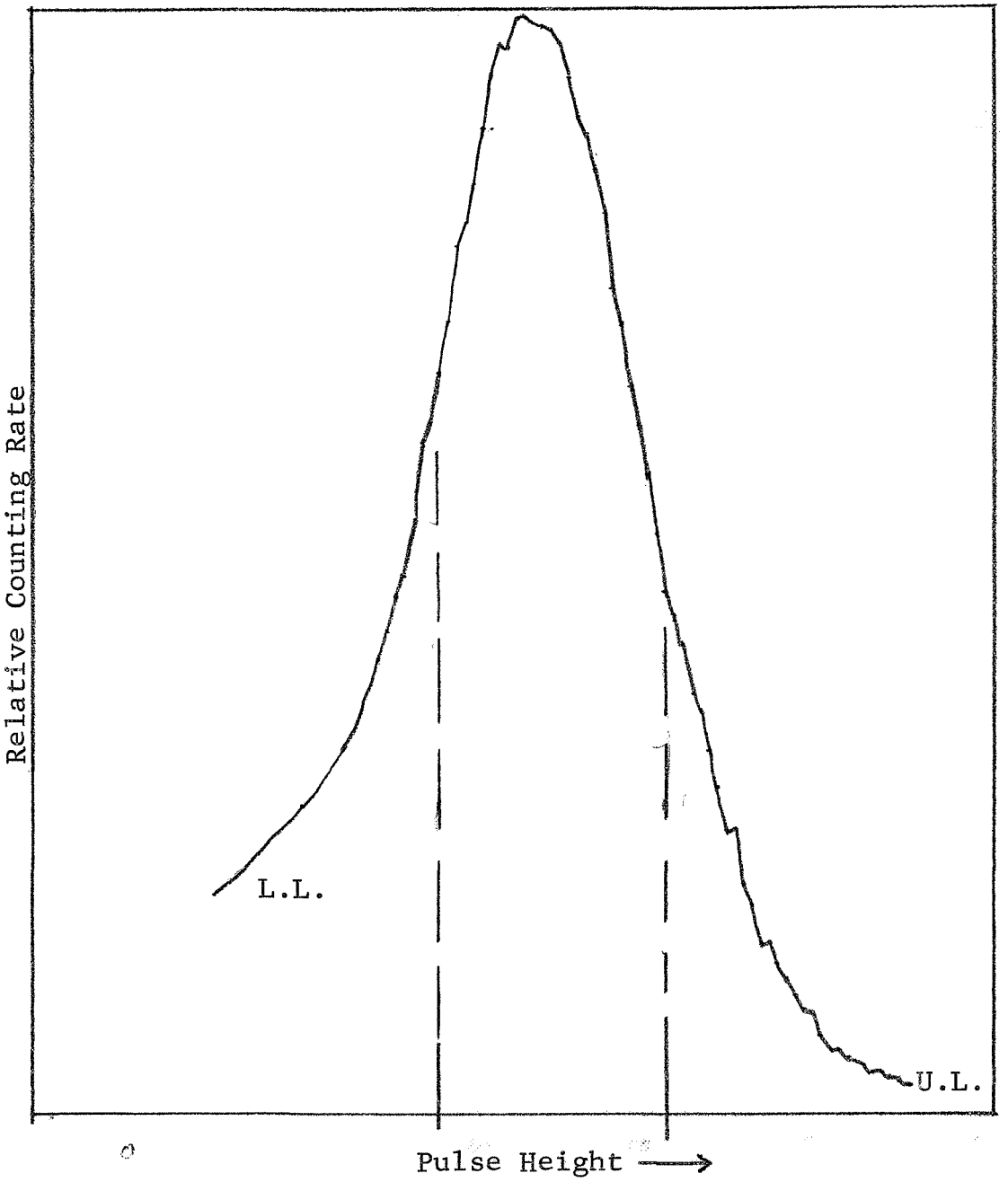

FIGURE 18 - Backscatter Pulse Height Spectrum

DEMONSTRATION TESTING

The working model, along with a test box and a simulated vehicle structure, were packaged and shipped to Langley Research Center for demonstration testing in the 60 foot diameter altitude sphere. The purpose of the testing was to demonstrate the response of the sensor to the variations in density and provide a measurement of the calibration constants and determine proper operation of the unit. Also, during periods other than density runs, the equipment was checked for stability. The actual sequence of tests is outlined in Table IV.

The unit was first placed in the chamber, cabling attached, and a checkout of the unit operation performed. This checkout included a stability run in which the unit was allowed to operate overnight and the output count rates continuously recorded. The results of this stability run indicated that there were some temperature instabilities requiring improvement. Also, the fluctuation of the AGC caused lack of short term stability.

Minor changes were effected to reduce the loop gain of the detector electronics in order to stabilize the AGC and reduce the effect of AGC source statistical fluctuation. Also, by reducing this loop gain, the temperature stability was improved.

The checkout continued with density run No. 1. This run involved the installation of the 1-curie source and evacuating the chamber to the equivalent of 100 millimeters and returning to 760 millimeters of mercury. The various data points were reviewed to verify proper operation. This checkout showed a significantly higher wall scatter than anticipated. Modifications to the test setup were made which added shielding around the detector to minimize scattering from the chamber walls near the bottom of the chamber. Also, a portion of the vehicle skin was removed to minimize possible multiple skin scatter.

Stability test No. 2 was then run, showing a significant improvement.

Density test No. 2 was then run, with the 1-curie source. The sphere was evacuated to 1 millimeter of mercury and data points were taken on the way down. The unit was then soaked overnight in this 1 millimeter vacuum and the run continued the next day by bringing the unit while operating back to one atmosphere, taking data points on the way.

The next test No. 3 was run with the 5-curie source installed. The sphere was evacuated to 1 millimeter and data points taken during this run. The unit was then turned off and allowed to soak in this vacuum over a weekend, and upon return it was turned on and found to operate properly and the sphere returned to one atmosphere and data points taken on the return.

TABLE IX Operation Log - Atmosphere Density Sensor - ADS-104

Test Date	Test Description	Input Voltage	Control Voltage	Operating Time (Hrs)	Sensor Temperature °F	Pressure mm Hg
1/8	AGC Calibration	28	1.8	8	75	760
1/9-1/11	Sensor Calibration	28	1.8	24	75	760
1/13-1/14	Sensor Calibration	28	2.05	16	75	760
1/15	Temperature Test	28	2.05	8	-22 to +122	760
1/16	Vacuum Test	28	2.05	4	+70 to +100	25 to 760
1/16	Temperature Test	28	2.05	4	-22 tp +122	760
1/17	Final Checkout	28	2.05	8	75	760
1/21	Checkout in chamber	28	2.05	4	40	760
1/21	Stability Run #1	28	2.05	14	40	760
1/22	Density Run #1	28	2.05	6	40 to 70	100-710
1/22	Stability Run #2	28	2.05	14	40	760
1/23	Density Run #2a	28	2.05	8	40 to 70	760 to 1
1/23	Vacuum Soak (non-operating)	0	0		40	1 to 3
1/24	Density Run #2b	28	2.05	4	40	1 to 760
1/24	Density Run #3a	28	2.05	4	40	760 to 1
1/25-1/26	Vacuum Soak (non-operating)					
1/27	Density Run #3b	28	2.05	4	40	3 to 760
1/27	Density Run #4	28	2.05	4	40	760 to 1
1/27	Vacuum Soak (operating)	28	2.05	14	40	1 to 3
	Failure Replaced Detector Assembly			148		
1/30	Sensor Checkout	28	2.05	1	40 to 70	760
1/30	Density Run #5	28	2.05	1	40	760 to 100
	Failure			2		

In Density Test No. 4, the sphere was again evacuated, with a 5-curie source installed, and data points taken down to 1 millimeter of mercury. In this fourth run, argon gas was then to be introduced in order to provide a measure of the unit operation with a gas of different molecular weight. Unfortunately, as the unit was vacuum soaked, a failure of the detector assembly occurred. The detector assembly was replaced with a second unit and sensor checkout performed again.

Density test No. 5 was then initiated and the second detector failed when a pressure of 100 millimeters of mercury was reached.

The failures encountered were similar in nature. A large increase in operating current was noticed, along with a reduction in detector output. Upon investigation of the failed units, it was determined that the failure of the high voltage power supply was caused by voltage breakdown of the encapsulants.

The sphere data that was obtained before the detector failures provided enough information to form several conclusions. These will be discussed later in the report. The sphere data was reduced by computing the actual density in the chamber from measured temperature and pressure data. This actual density is plotted with respect to the detector countrates, and are shown in the following Figures 19, 20, 21, and 22. The solid line shown in these figures is a least square curve fit of a second order equation to these data points. The actual data points and data are contained in Appendix D.

Demonstration Test Data Analysis

The detected countrate as a function of gas density in the altitude sphere can be expressed by the following equation:

$$I_D = I_{AS} + I_{WS} + I_B \tag{16}$$

where:

I_D = detected count rate

I_{AS} = air scatter count rate

I_{WS} = wall scatter count rate

I_B = background count rate

The air scattered count rate is related to air density ρ, source strength S, and a scale factor K_{AS}.

$$I_{AS} = K_{AS}\ S\ \rho \tag{17}$$

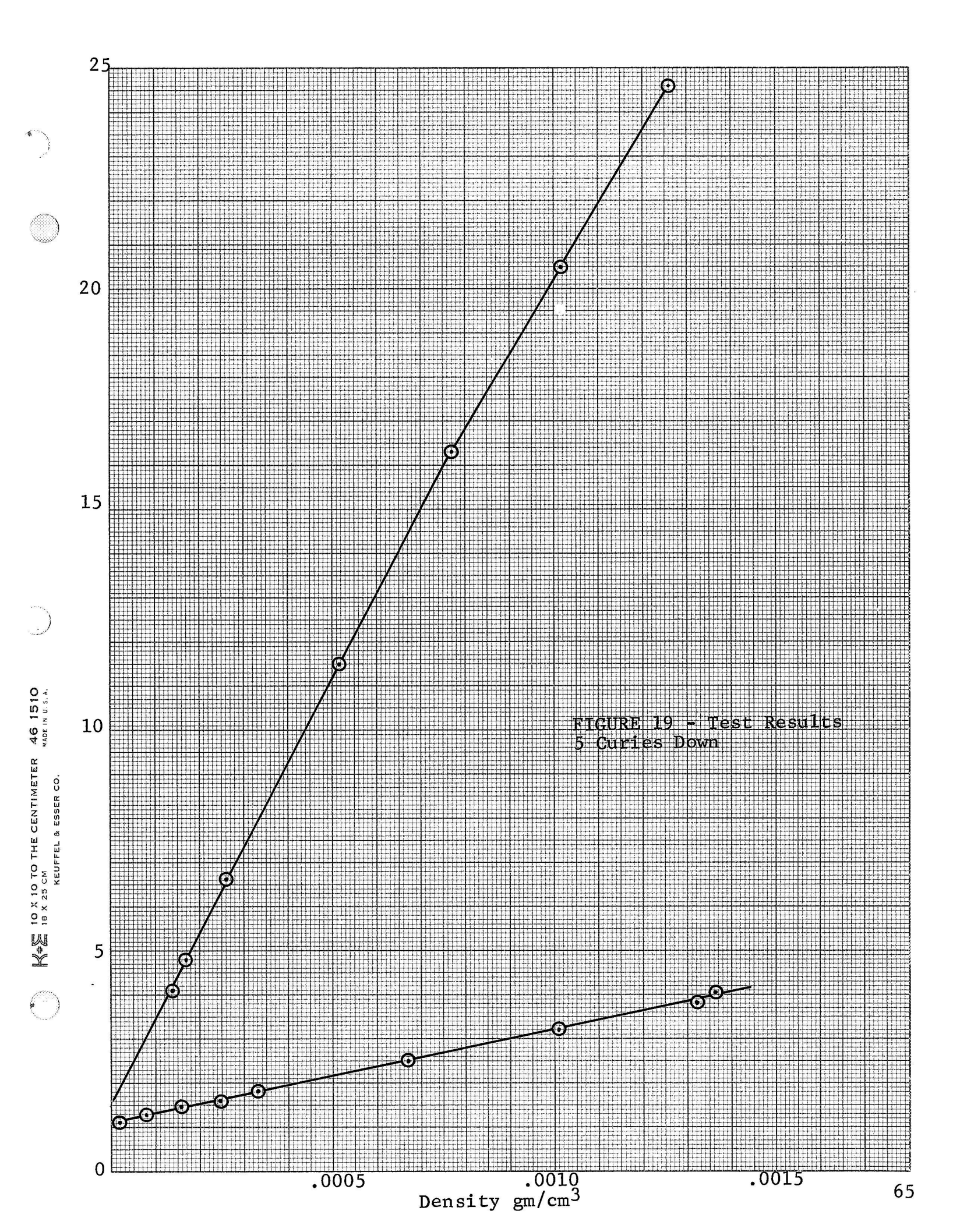

FIGURE 19 - Test Results
5 Curies Down

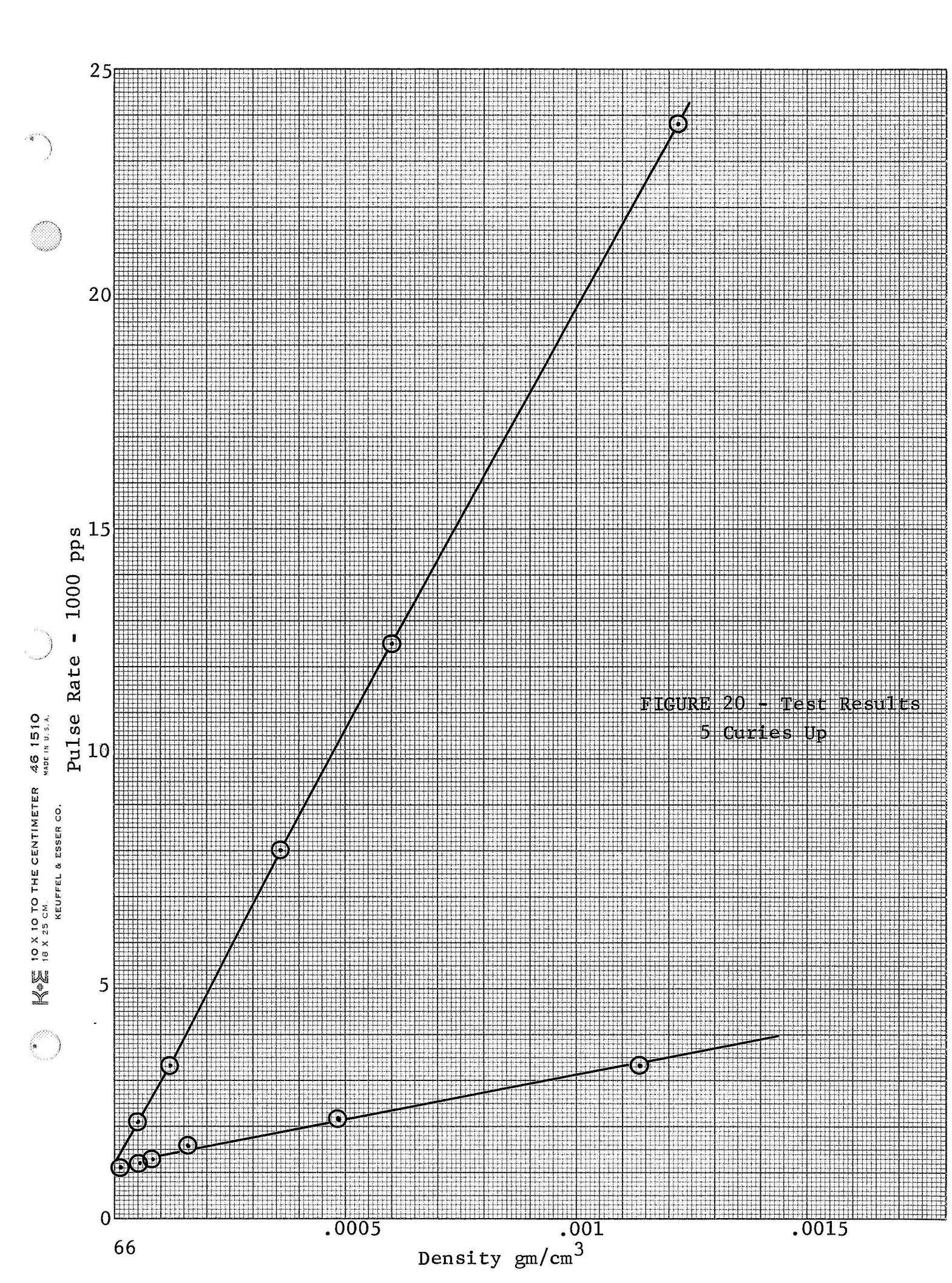

FIGURE 20 - Test Results
5 Curies Up

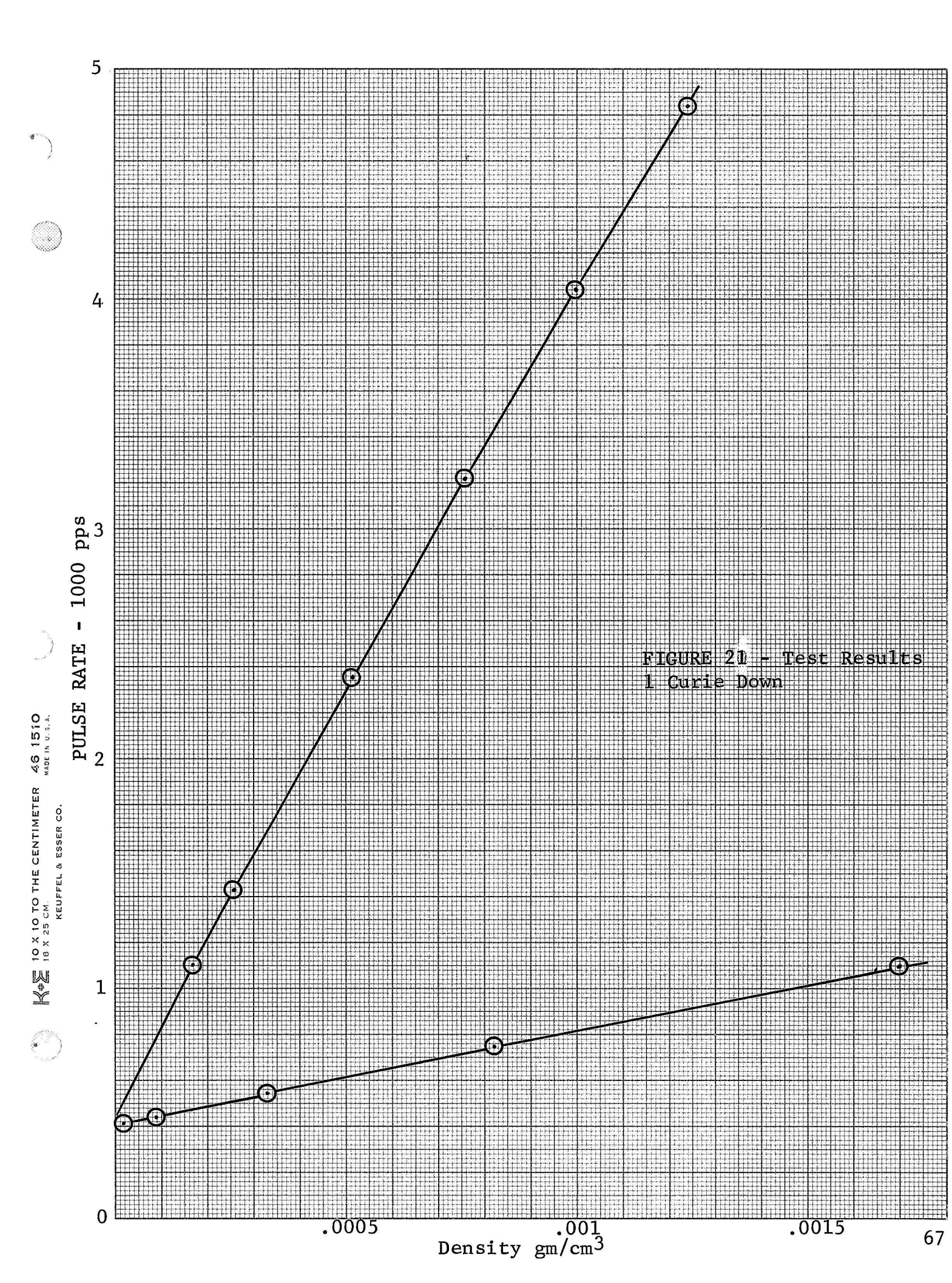
5
4
3
2
1
0
PULSE RATE - 1000 pps
.0005
.001
.0015
Density gm/cm3
FIGURE 21 - Test Results
1 Curie Down
10 X 10 TO THE CENTIMETER 46 1510
18 X 25 CM
KEUFFEL & ESSER CO.
MADE IN U.S.A.

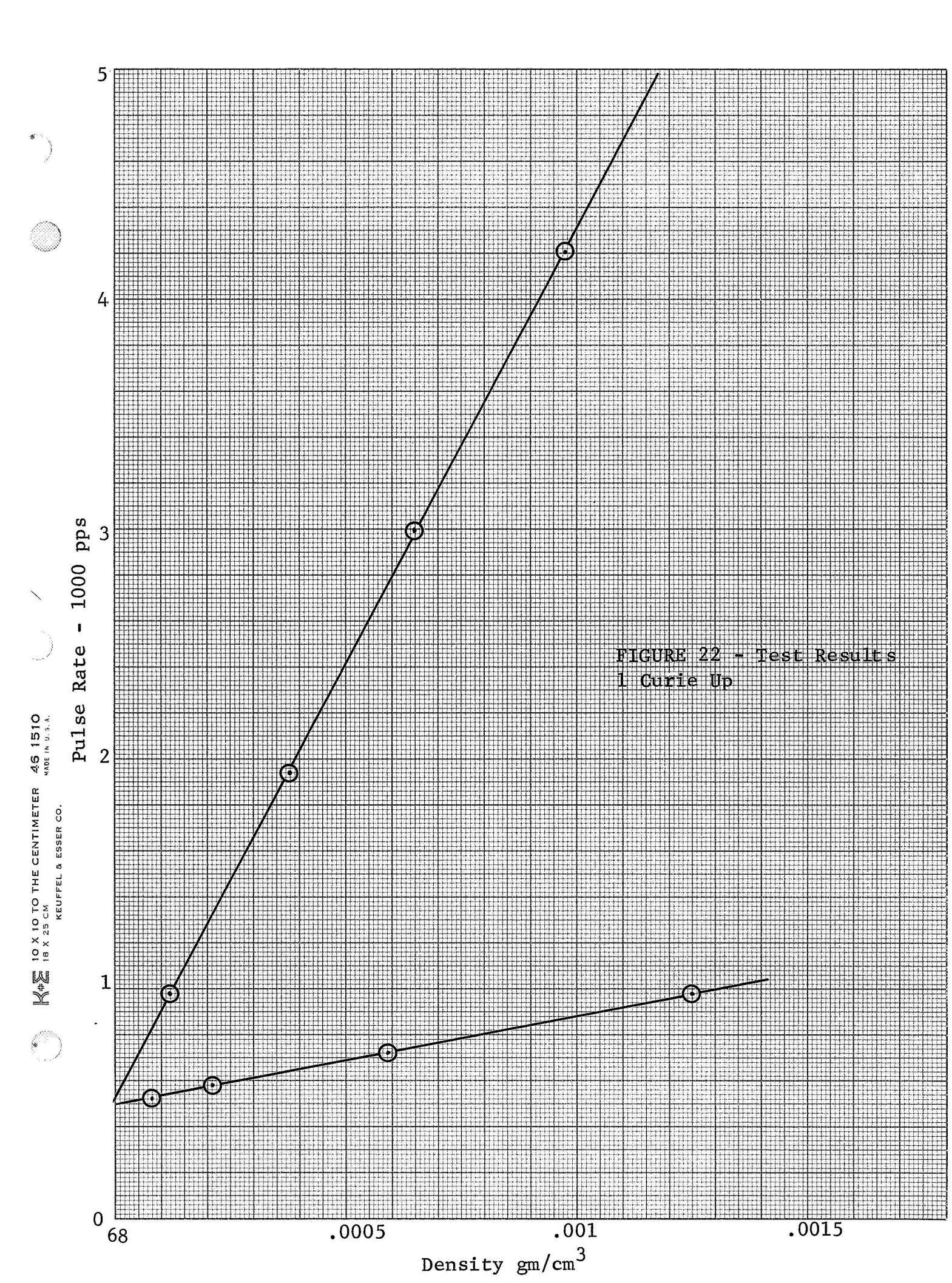
5
4
3
2
1
0
Pulse Rate - 1000 pps
68
.0005
.001
.0015
Density gm/cm3
FIGURE 22 - Test Results
1 Curie Up
10 X 10 TO THE CENTIMETER 46 1510
18 X 25 CM
MADE IN U.S.A.
KEUFFEL & ESSER CO.

The wall scatter countrate is related to source strength and a scale factor K_{WS}.

$$I_{WS} = K_{WS}S \tag{18}$$

Referring to the test data, Figures 18 through 21, the factor $K_{AS}S$ can be determined as the slope of the count rate vs density plot. The extrapolation of this plot to zero density provides the sum $I_{WS} + I_B$. Thus, each of the elements of equation (1) can be found from the experimental data. In order to provide a consistent method of obtaining this data, a least squares curve fit program was applied to the data points, the results be being presented in Appendix D. Since there was some non-linearity in the data, a second order equation, rather than a linear expression, was used for this curve fit as below.

$$I_D = A + B\rho + C(\rho)^2 \tag{19}$$

The data points are shown encircled and the fitted curve shown as the solid line of Figures 18, 19, 20, and 21. The resultant parameters for each test run are shown in Table X. Notice in Appendix C that with few exceptions, the data points fall within ±5% of reading of the fitted curves.

Discussion

Scale Factor. The parameter of interest is the scale factor. This is Item B of equation 19 and Table X. For the five-curie source, the scale factors vary from 1.94×10^7 to 2.16×10^7 pulses per second per unit density. The one curie scale factor was seen to be from $.387 \times 10^7$ to 3.93×10^7 pulses per second per unit density. The ratio of scale factors thus ranged from

$$\frac{1.94 \times 10^7}{.393 \times 10^7} = 4.93 \text{ to } \frac{2.16 \times 10^7}{.387 \times 10^7} = 5.55 \tag{20}$$

The ratio of source strengths as measured by the manufacturer were 5.09. Thus, there is experimental agreement of the scale factors between various runs and the predicted value of within ±6%.

The background measured with the source mechanism closed is shown in columns D and E of Table X. This background varied from 213 pulses per second to 271 pulses per second. The background was always high with the chamber at low density and low with the chamber at high density. It is concluded that some portion of the background is a result of secondary radiation being generated as the natural background interacts with the chamber walls. This is easily demonstrated by the fact that the background level in the low energy region of interest outside the

TABLE X - Data Parameters

Test Run	A Zero Density Count Rate (pps)	B Slope pps/gm/cm^2	C Non-Linearity pps/(gm/cm^3)^2	D Background pps High ρ	E Low ρ	F Wall Scatter pps
5 Curies Down	1083	2.16×10^7	-2.34×10^9	214	253	830
5 Curies Up	1111	1.94×10^7	$-.658 \times 10^9$	224	271	840
1 Curie Down	420	$.387 \times 10^7$	$-.259 \times 10^9$	213	234	186
1 Curie Up	474	$.393 \times 10^7$	$-.0846 \times 10^9$	223	260	214

chamber is lower than in the chamber. The air in the chamber then attenuates this background giving the noticed change in count rate with density.

The wall scatter plus background is given as the extrapolation of the fitted curves to zero density which is listed in column A of Table X. Subtracting the associated backgrounds at low density gives the wall scatter of column F of Table X.

Linearity. The data is seen to become non-linear at the high density, high count rate regions. This non-linearity is caused primarily by AGC sensitivity to detected count rate and secondarily to detector coincidence loss and air absorption of wall scatter. The air absorption wall scatter can be approximately estimated using the attenuation expression

$$e^{-\mu\rho x} \tag{21}$$

where:

x = two way path length = 100 feet = 3050 cm

ρ = density at 1 atmosphere = .00127 gm/cm^3

μ = absorption coefficient for air at 100 Kev

= 0.13 cm^2/gm

giving:

$$e^{-0.13 \times .00129 \times 3050} = 0.6 \tag{22}$$

Thus, the wall scatter at 1 atmosphere density is about 60% of that at zero density. Since the wall scatter at zero density is about 3% of the 1 atmosphere air scatter, the non-linearity due to this effect would account for a 1.8% drop in count rate.

The sensor response is approximately 10^6 pulses per second. Coincidence loss at 25 KHz count rate would account for a 2.5% drop in count rate at 1 atmosphere. These two non-linear effects are of minor significance.

The major contribution to non-linearity is the interaction of the 100 Kev scattered gammas with AGC circuitry. At the high backscatter countrate, a small portion of these counts reach the AGC discriminator level and are detected as part of the AGC reference gammas. This results in an erroneous reduction in gain to compensate for the increase in count rate. This gain reduction decreases the sensor scale factor as a function of the density. This effect was seen to contribute the major sensor non-linearity.

Stability. The stability of the sensor was sampled by sampling 10 second count rate averages over a period of 16 hours without changing test conditions other than natural ambient temperature swings of approximately ±10°F. The data points are shown plotted in Figure 23. Referring to the AGC count rates, the average of 20 points varied by ±0.8%. The 2 σ statistical variation to be expected for 200 second averages is 1.88%. This test showed negligible drift of the AGC within the measurement accuracy. The spread of 10 second averages was seen to be ±6.4%. The expected 2 σ statistical variation for 10 second averages is computed as 8.5% again showing the variations to be within the expected 2 σ measurement tolerance.

The 10 second average output count rates are seen to fall within the 2 σ expected statistical fluctuation of ±1%. The overall drift is seen to be approximately ±1.3%.

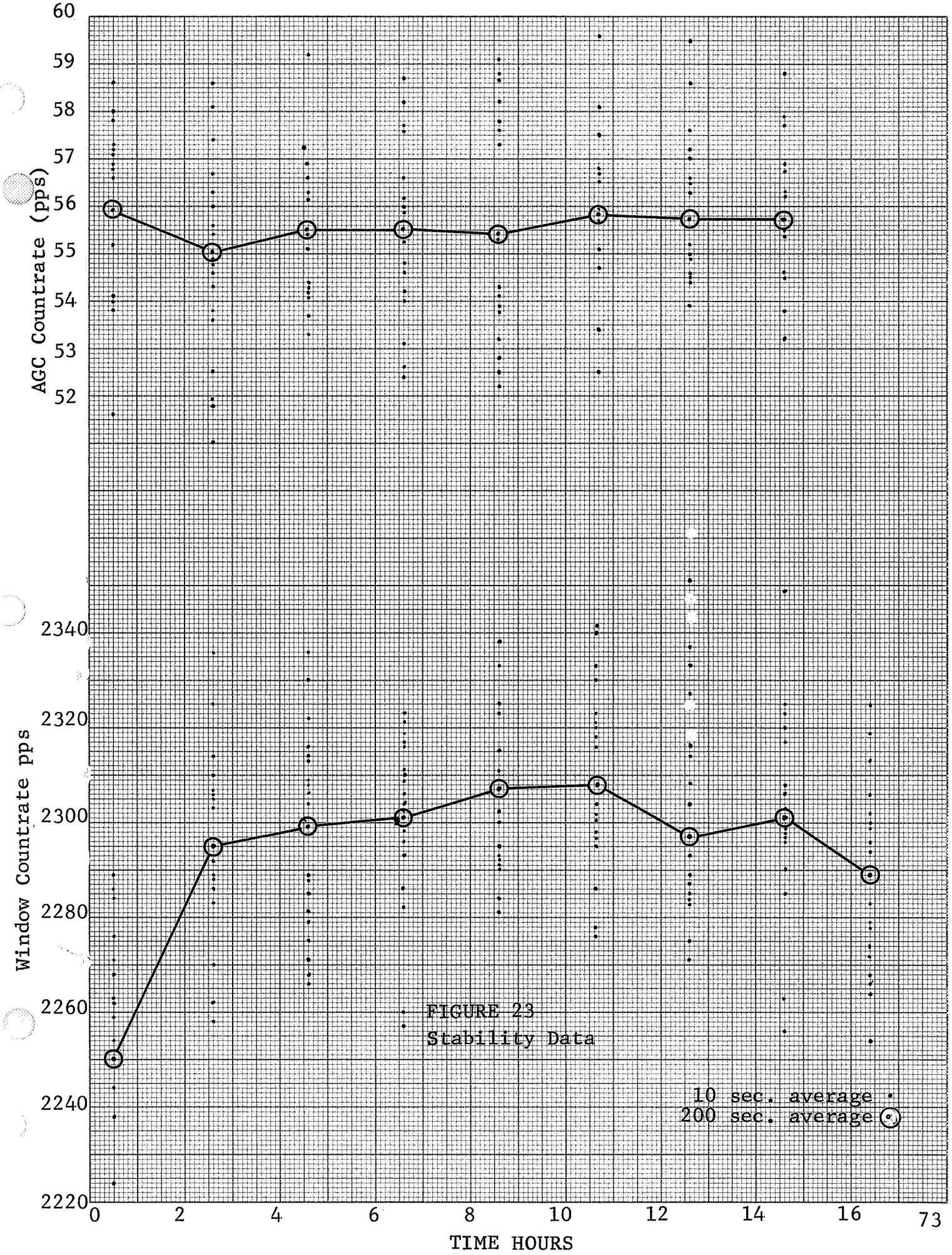

FIGURE 23
Stability Data

RECOMMENDATIONS RESULTING FROM PHASE I DEVELOPMENT AND TESTING

This section describes areas requiring further development identified in the Phase I effort. The primary elements to be considered are the photomultiplier tube high voltage power supply packaging, and methods of automatic gain control. Failures of the detector assembly in the vacuum chamber demonstration testing have indicated a high voltage breakdown problem in the high voltage power supply. As a result, some development in the area of high voltage power supply packaging is required. Methods to consider are a more adequate encapsulation material, better process control, or complete hermetic seal of the package.

The method of automatic gain control must also be investigated. The purpose of this investigation is to optimize the AGC technique in order to reduce the background signal, increase AGC source strength for better control, and provide more stable electronics. A review of the various methods of automatic gain control previously investigated indicates that Americium alphas provide a better reference for automatic gain control. The fact that the alphas and gammas do not track as a function of temperature can be taken care of by temperature compensation of the sensor. A composite crystal will improve the tracking abilities.

Experimentation with a composite CsI(Tl) and NaI(Tl) crystal with AM 241 sealed into the CsI has shown promise. This crystal combination provides the following advantages:

1. Alpha particles are used as the reference and do not create any background in the gamma region. The alphas considered are approximately 5 Mev in energy which, when detected in a scintillation crystal, is equivalent to 2 Mev gamma. This is adequate separation from the 100 Kev backscatter gammas such that Americium alphas will not disturb the background count rate and no 100 Kev backscatter gammas will disturb the AGC circuitry.

2. The 60 Kev gammas from the Americium source when detected in the cesium iodide crystal will appear approximately the same height as the equivalent of 30 Kev gammas as detected in the sodium iodide crystals. Thus the 60 Kev Am 241 gammas appearing as 30 Kev gammas are sufficiently low in amplitude so as not to contribute noise in the 100 Kev region of interest.

By using a NaI(Tl) crystal rather than a CsI(Na) crystal as was done in this present program, some consideration must be given to the thermal and mechanical environments that might be imposed on this crystal assembly. In previous programs, it has been demonstrated that a properly packaged sodium iodide crystal will withstand mechanical environments of shock and vibration. Some consideration must be given to the temperature shock that may be imposed upon the crystal.

Secondary areas which require further development are simplification of the electronics, minor modifications to the source mechanism, and proof testing of the design through an environmental test program.

The purpose of the electronics simplification is to reduce the size and power of the electronics. This can easily be accomplished by removal of the extraneous digital output electronics and the use of regulated power only for referenced voltage levels. The modification of the source mechanism being considered is the increase in unit length to allow an adequate spring for closing the source mechanism in the event of a launch pad explosion or fire. In the present design there is not adequate room for a spring which will retain its spring rate at high temperature.

A second modification to the source mechanism is to provide a more positive method of retaining the source in this mechanism.

A third minor addition to the source is the identification marks such that the source can be gripped for installation in the proper direction, minimizing wasted time during the source installation procedure.

A third effort is to prove the design through environmental testing. These tests should include the effects of temperature, shock, vibration, vacuum, thermal shock and sterilization. These above areas are recommended, for inclusion in the Phase II effort of this program. The program will include updating the design through further breadboard testing, modification of the working mode, environmental testing of the working model, further development of an adequate PM tube high voltage power supply/detector assembly, and investigation of methods of AGC. Upon completion of these studies and tests, the resultant design modifications will be incorporated into two engineering prototype atmospheric density sensors. These sensors will then be demonstrated in the altitude chamber and delivered for evaluation by NASA - LRC.

CONCLUSIONS OF PHASE I DEVELOPMENT

The following conclusions have been reached as a result of the Phase I program.

1. An atmospheric air density sensor can be designed within the size, weight, and power constraints of 100 cubic inches, 5 pounds, and 5 watts.

2. The sensor design can incorporate sterilizable components to a high percentage.

3. Adequate detector design for operation in a vacuum is yet to be proven.

4. Composition effects are yet to be determined via argon tests.

5. A clean 100 Kev gamma source is available in the form of Gadolinium 153.

6. Improvements in the automatic gain control design are needed to improve temperature stability and sensor repeatability.

A Phase II program is recommended to complete development in the areas still needing improvement and provide engineering prototypes which will meet all the requirements of this program.

PHASE II - DESIGN

As a result of the development and testing on the Phase I hardware, Phase II design was incorporated to improve the system in the areas that were found lacking during the test. The initial program set forth in Phase II was to provide a new system and rerun tests in the 60-foot sphere at the NASA Langley Research facilities. Due to the numerous problems throughout the program, lack of funds, and lack of availability of the test chamber, the program was not completed. The hardware was developed and the course set forth for the development and lab tests were made, but the testing in the 60-foot sphere was eliminated from the program.

Figure 24 illustrates in block diagram form the source, detector, and signal conditioning electronics which comprise the atmospheric density sensor.

The Gd-153 source is mounted in a shield mechanism which performs the following functions. With the shield mechanism closed, the gamma radiation is attenuated such that the dose rate at 1 meter is less than 2.0 millirem per hour. The shield and source may then be installed in a vehicle without undue hazard. Upon external command (through the vehicle umbilical), the shield mechanism can be opened and latched, exposing the source. In case of an aborted mission, the shield mechanism can be unlatched and closed on external command. After launch, the shield mechanism remains open and there is no way in which it can be closed and latched. When in flight, the shield mechanism can be momentarily closed on command through a radio command link.

When in the exposed configuration, enough shielding is interposed between the source and detector to attenuate direct transmission to a negligible level (less than one pulse per second).

With the shield mechanism in the open position, the source radiation pattern is loosely collimated to reduce the possibility of air scatter close to the vehicle surface and resultant errors due to shock layer effects.

The source is located approximately one meter from the detector. As gamma photons impinge upon the detector crystal, light scintillations are produced which are sensed and amplified by the pulses whose amplitude is approximately proportional to the impinging photon energy and whose rate is equal to the rate of impingement.

These pulses are further amplified in the signal condition electronics and pass to an upper level (UL) and lower level (LL) discriminator. The upper level discriminator passes all pulses

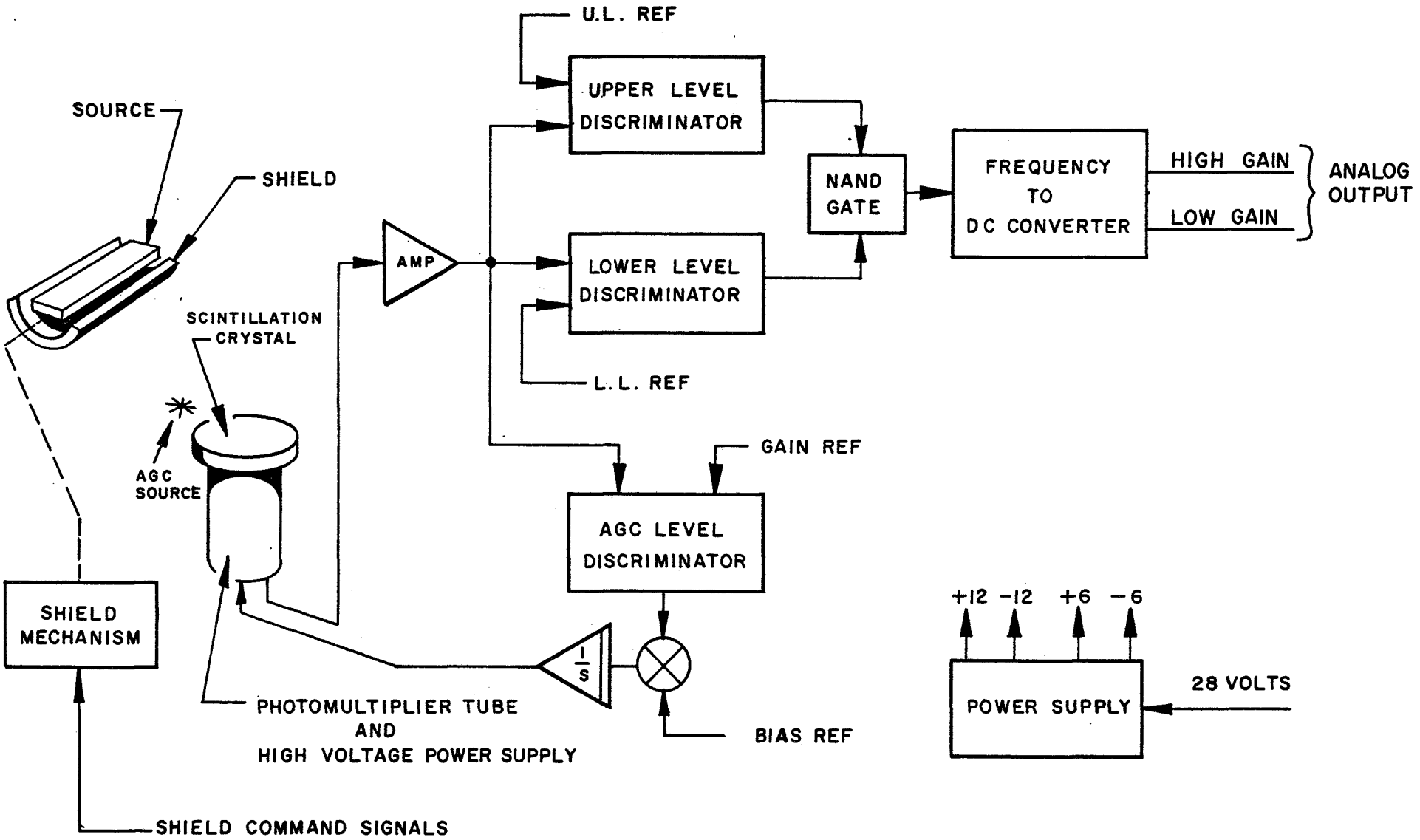

FIGURE 24 - BLOCK DIAGRAM, ATMOSPHERE DENSITY SENSOR

of amplitude greater than the UL reference. The lower level discriminator passes all pulses of amplitude greater than the LL reference. These two discriminator outputs pass to a NAND gate such that only those pulses of amplitude between the UL and LL reference produce output pulses. Thus, an energy "window" in established which is set to accept only the scattered 100 Kev photons and reject most other noise and background pulses.

The pulse output is converted to a 0 to 4 volt output signal by the pulse to dc converter. The dc output level is directly proportional to the pulse rate. Automatic scaling is performed by providing a two-slope output: high sensitivity output from 0 to 4 volt output, lower sensitivity output from 0 to 4 volt output for 0 to 40,000 Hz. These dc outputs can be telemetered directly.

Since photomultiplier tubes do not exhibit good stability over time and temperature, an automatic gain control (AGC) is employed. A reference gamma source of 2 Mev from an Am-241 is introduced into the detector crystal. This provides a reference output from the detector which is examined by the AGC electronics. If the pulse height of the reference output is not correct, the gain of the photomultiplier tubes adjusted by varying its high voltage until the reference pulse height is brought back to the proper level. The pulse height is measured by the AGC level discriminator. Some of the reference pulses will fall below this reference level and some above. Those that fall above pass through the discriminator and the pulse rate compared with a bias integrator which lowers the photomultiplier tube gain. This reduces the output pulse height reducing the number of AGC pulses passing through the AGC discriminator. In this way, a constant AGC count rate and reference pulse height is maintained.

Source Assembly

During design evaluation and testing of the source holder, two potential problem areas were uncovered. In the spring mechanism, it will be possible at high temperatures, as in the case of an explosion on the launch pad, that the tension would be destroyed by heat. The second problem existed on the pivot mechanism, where increased heat could cause expansion to the point where the shutter would not close. These problems were eliminated by redesign of the pivot mechanism so that adequate clearances would be available under all temperature conditions, and the springs were made of different tempered steel which would allow the tension to be maintained under all expected temperature conditions.

Detector Assembly

During the testing of the 60-foot sphere on the Phase I hardware, both photomultiplier tube and high voltage power supply failed. Both units were returned to the original manufacturer, EMR, for evaluation and repair. After many months of evaluation, EMR concluded that the problems associated with the high voltage

power supply during tests were a result of the potting technique that was used in encapsulating the high voltage section. Conrac had anticipated this type of problem and had set forth a program to redesign the high voltage power supply using a different technique. After EMR had completed the test and repair of one unit, it was returned to Conrac and then subjected to vibration and shock tests, The shock tests indicated no problem areas with respect to design, but the vibration test pointed out an area in the housing which had a high resonance and would have caused a complete failure over sustained operation at this frequency.

Conrac's evaluation of the high voltage power supply problem covered three areas of design. The first was to be a continuation of the design in the Phase I hardware with whatever improvements were requires as a result of EMR's evaluation ahd Conrac's environmental testing. The second was to have a power supply redesigned by Pulse Engineering Corporation of San Jose, California. Pulse Engineering had previously designed and built a high voltage power supply/photomultiplier tube combination for Conrac on the Apollo program. These units had been very successful throughout the environmental tests which had been run on this program. The third approach was to use the basic EMR design, but to change the housing so that it would be evacuated and sealed. EMR's evaluation of the failures and the cause of the failure were not adequate in Conrac's opinion to continue with this type assembly. The costs quoted by Pulse Engineering were prohibitive of the program. Conrac therefore completed the design of the detector using the basic high voltage power supply from EMR and a completely sealed assembly. The vibration problems that were present in the original design were eliminated during the basic redesign. The Conrac designed detector is the same as shown in Figure 7. The entire unit, including the crystals, photomultiplier tube, high voltage power supply were assembled and tested. During the assembly, the photomultiplier tube was preloaded with a spring and shims so that a constant pressure existed between the photomultiplier tube and the window. After assembly was completed, the detector housing and the electrical header were welded using the electron beam process. The unit was then evacuated and filled with a trace of helium prior to sealing so that adequate leak tests could be performed after sealing. The final results of this process during the temperature and bench tests at Conrac proved to be satisfactory.

The testing of the Phase I detector had some instabilities due to the electronics and the automatic gain control techniques. A Barium 133 source was used with a sodium activated cesium iodide crystal. Part of the gamma spectrum from the Barium source and part of the Gd 153 gamma overlapped the detector and caused an instability in the AGC. The Phase II design used a NaI(Tl) detector crystal and a cesium iodide (na) AGC crystal with an Americium 241 alpha source. During the initial testing of this combination, the AGC signal was found to be too great in

amplitude and could not be handled adequately by electronics. This problem was solved by a series of optical filters which essentially reduced the pulse height of the AGC signal out of the photomultiplier tube. Additional problems of the spectrum smearing were also present in this design and were solved by providing a quartz crystal with the proper coefficient transmission.

Electronics

The major problems associated with the electronics in Phase I were in the area of automatic gain control and the stability over temperature environment. Figure 25 is a schematic diagram of Phase II electronics. A considerable amount of time was spent in the development and testing of the electronics for the AGC. The basic integrated circuits were finally changed from 709s to 741s which provided the system with more stability over the temperature range and additional circuitry was added to compensate the AGC network along with the optical filters that were added into the detector. The entire system was tested over the temperature range from -15°C to +50°C with input count rates from approximately 300 to 30,000 counts. The results of these tests are shown on Tables XI and XII. Results of these tests indicate that the system operates within error band of ±2% of the entire frequency temperature range. The checkout, calibration and test plan for the system are described in Appendix D.

CONCLUSIONS OF PHASE II

The basic aims of the Phase II program was directed toward accomplishing design improvements as a result of the Phase I design, and the fabrication and testing of two engineering prototype Gamma Backscatter Atmospheric Density Sensors. The Phase I and Phase II programs have proven the basic design of the Gamma Backscatter Atmospheric Density Sensor for use in atmospheric studies. The results of the programs are summarized as follows:

1. An engineering model of the system has proven over the temperature and frequency range that the system is accurate to within ±2%.

2. The unit can be packaged into a 100 cubic inch size and use less than 5 watts of power. The weight of the engineering model slightly exceeded the 5 pound limit, but several areas of weight reduction can be accomplished with continued design effort.

3. Final testing of the system in a large test chamber was not accomplished because of the availability of the chamber.

The use of a 100 Kev gamma source in the form of Gd 153 will probably prove out to be one of the most significant results of this program. This source has shown that it can provide a high energy gamma source that can be easily shielded and has a clean spectrum which probably will be used in many other fields of radiation study.

REFERENCES

1. Gebbie, N.W.: Final Report - More Probe/Lander Density Sensing System. NASA CR-66094, February 1966.

2. Hakewessell, D.B.: Feasibility Study for an X-Ray Back-scatter Free Air Density Sensor. NASA CR-66148, September 1966.

3. Whitaker, D.B.; and Gardner, R.P.: Mathematical Model Predictions and Optimization Study of Gamma Ray Atmosphere Density Sensor. NASA CR-66676, August 1968.

4. 1973 Voyager Capsule Systems Constraints and Requirements Documents. Table of Mars Model Atmospheres, SE002 BB002-2A21, JPL, January 1967, p. 19.

5. Production Study of Gadolinium -153, Summary of Results March 1967 - December 1967. ORNL Intragency Agreement AEC 40-108-67, MIPR-L-1775.

6. Price: Radiation Shielding.

7. Final Report, Improved Sterilizable Multiplier Phototube, Electro-Mechanical Research, Inc. JPL Contract No. 951555, EMR Report No. 2641-4476.

8. JPL Specification ZPP-2010-SPL-D, Sterilization Parts List for Spacecraft Application, October 1967.

APPENDIX A

Methods of Automatic Gain Control

1.0 INTRODUCTION AND SUMMARY

This appendix describes several techniques for stabilizing the pulse height output of scintillator-photomultiplier tube type gamma radiation detectors. These techniques were considered for use in the Gamma Backscatter Atmosphere Density Sensor being developed for National Aeronautics and Space Administration, Langley Research Center, under Contract NAS1-7791. This sensor measures the amount of 100 Kev gamma radiation scattered from a source to a detector by the atmosphere. The amount of scatter and thus the detector output is directly proportional to the atmospheric density.

The method of stabilization is through the use of automatic gain control (AGC) techniques. A reference radiation source is placed near the detector. The detector output pulse height from this reference source is measured and compared with a reference voltage level. If the pulse height is too large or too small, the gain of the photomultiplier tube is correspondingly adjusted. Thus, variations of the crystal, photomultiplier, and its power supply with time, temperature, or other environment that cause pulse height changes are automatically corrected.

2.0 DESCRIPTION OF VARIOUS AGC METHODS

The important requirements of the optimum AGC approach are listed below:

1. The reference source must have a long half-life.

2. The reference source pulse height must track the signal pulse height.

3. The reference source must not contribute to the background noise level in the signal energy region.

This investigation centered around the use of Americium 241 alphas; Americium 241, 60 Kev gammas; Barium 133, 355 Kev gammas; and Gadolinium 153, 100 Kev gammas as reference sources. The signal source in all cases is backscattered Gd-153, 100 Kev gammas. The detector crystals considered were NaI(Tl), CsI(Tl), and CsI(Na), or combinations thereof. The use of a CsI(Na) crystal is most attractive since it exhibits good gamma detection qualities and is rugged. The following paragraphs describe several AGC methods and their relative advantages.

2.1 CsI (Na) Detector and Am-241 Alpha Reference. The AM-241 alphas provide an excellent pulse reference with good resolution. The Americium can be seeded directly in the crystal material. The alpha contributes negligible countrate in the region of 100 Kev gammas, thus producing no noise. The 60 Kev gammas from the Am-241 may interfere with the 100 Kev gamma backscatter spectrum. The alpha pulse height does not track the gamma pulse height as the crystal temperature is varied.

2.2 NaI(Tl)/CsI(Tl) Crystal Combination and Am-241 Alpha Reference. The pulse height output from a CsI(Tl) crystal is a factor smaller than the NaI(Tl) crystal. By using a main detector crystal of NaI(Tl) and bonding a small CsI(Tl) crystal seeded with Americium 241, a composite crystal is achieved which has the following characteristics.

The alpha pulses provide a good signal for AGC. The 60 gammas introduced by the Am-243 are now much lower in pulse height than the 100 Kev backscatter gammas being detected in the NaI(Tl) portion of the crystal assembly, thus reduced noise. The alpha pulses in the CsI(Tl) crystal and the gamma pulses in the NaI(Tl) crystal track each other better with varying crystal temperature, but still not well enough to be considered a stable detector over wide temperature ranges.

2.3 CsI(Na)/CsI(Tl) Crystal Combination and Am-241 Alpha Reference. The CsI(Tl) crystal has a lower pulse height output than the CsI(Na) crystal. By bonding a small CsI(Tl) crystal seeded with Am-241 to a CsI(Na) crystal, the same results of Paragraph 2.2 can be achieved. The temperature tracking of the alphas in the CsI(Tl) and the backscatter gammas in the CsI(Na) are probably not as good as the combination of 2.2, since both materials are CsI and little compensation would result. This has not been verified by test.

2.4 CsI(Na) Crystal and Am-241 60 Kev Gamma Reference. The use of a gamma reference is considered to eliminate the effect of differing temperature sensitivities of crystals to alphas and gammas. By using a gamma reference of lower energy than the signal, it cannot contribute noise. This technique is difficult to implement because the backscatter signal contributes large and varying count rates in the 60 Kev region which will upset the AGC. Unless a very high AGC count rate, compared with the signal count rate, is used, this method appears impractical. For the present application, there a 40,000 pps signal is expected, the AGC count rate should be at least 100 times greater to achieve stable operation. This is not practical with the pulse width characteristics of the scintillation material.

2.5 CsI(Na) Crystal with Ba-133, 355 Kev Gamma Reference. The 355 Kev Gamma output from the Ba-133 source provides a very good reference. The 80 Kev gamma output can be effectively shielded so that it does not contribute noise. The detector itself however in the scintillation process generates a Compton continuum which introduces some noise in the 100 Kev region. This noise can be minimized by reducing the reference count to as low a rate as possible while still providing enough for good AGC response.

2.6 CsI(Na) Crystal with No Auxiliary Reference Source. The 100 Kev gamma backscatter pulse height can be used directly to control the gain of the detector. The accuracy of this method improves as backscatter countrate increases; however, in the very low density regions, the AGC becomes ineffective. A small Gd-153 source can be added to establish a minimum count rate.

2.7 Shuttering Method. The method described in Paragraphs 2.5 and 2.6 can be improved by shutting the reference source and operating the AGC on a low duty cycle. During periods when backscatter measurements are taken, the reference source is closed and the gain is held, thus no noise contribution. Between successive backscatter measurements, the reference source is opened and AGC electronics activated to provide correction. The mechanical shuttering required degrades the reliability and adds weight to the system making the approach not attractive.

3.0 CONCLUSIONS

Table I summarizes the approaches discussed above. The method chosen for the present program is that defined in Paragraph 2.5. It provides good AGC with little complexity. The shortcoming is the noise introduced. Further study appears warranted on the combination crystal and alpha reference approach. Perhaps by choosing the proper combination of crystals and amount of doping, an assembly in which the gammas and alphas track with temperature can be achieved.

Literature has shown that by changing the amount of doping, a crystal can exhibit either a negative or positive temperature sensitivity. The possibility of accurate compensation therefore seems possible.

Further study of the electronics required to implement approach 2.6 also appears warranted.

TABLE I - COMPARISON OF VARIOUS AGC TECHNIQUES

Para.	Signal Crystal	Ref. Crystal	Ref. Source	Shutter	Advantages	Disadvantages
2.1	CsI(Na)	CsI(Na)	Am-241 Alpha	None	Rugged Simple	Very temperature sensitive. Some noise at 60 Kev
2.2	NaI(Tl)	CsI(Tl)	Am-241 Alpha	None	Simple No noise contribution	Somewhat temperature sensitive. Not rugged. Susceptible to thermal shock.
2.3	CsI(Na)	CsI(Tl)	Am-241 Alpha	None	Simple No noise contribution Rugged	Somewhat temperature sensitive
2.4	CsI(Na)	CsI(Na)	Am-241 Gamma	None	No noise contribution Rugged Not temperature sensitive	Complicated electronics Limited dynamic range (high rate)
2.5	CsI(Na)	CsI(Na)	Ba-133 Gamma	None	Simple Rugged Not temperature sensitive	Small noise contribution
2.6	CsI(Na)	CsI(Na)	Gd-153 Back-scatter Gamma	None	Rugged Not temperature sensitive No noise contribution	Complicated electronics Limited dynamic range (low rate)
2.7	CsI(Na)	CsI(Na)	Ba-133 Gamma	Yes	Rugged Not temperature sensitive No noise contribution	Complicated mechanically Less than 100% duty cycle

APPENDIX B

Reliability Analysis

1.0 SCOPE

The following pages present the Reliability Block Diagram and Math Model, Failure Mode and Effects Analysis, and Failure Rate Analysis for the Engineering Prototype Gamma Backscatter Atmospheric Density Sensor. This sensor is being developed under Contract NAS1-7791 for NASA, Langley Research Center, for eventual applications to planetary atmospheric exploration.

2.0 RELIABILITY BLOCK DIAGRAM

The Reliability Block Diagram illustrates the seven elements that make up the Detector and Electronics portion of the sensor. The radioactive source element has not been considered at this time. The seven elements considered are:

1. Photomultiplier Tube and Circuitry
2. High Voltage Power Supply
3. Pre-amplifier and Window Discriminator
4. Automatic Gain Control
5. Analog Converter
6. Pulse Delay Converter
7. Low Voltage Power Supply

3.0 FAILURE MODE AND EFFECT ANALYSIS

The Failure Mode and Effect Analysis has been limited to general type failures of various sensor elements rather than detail failure analysis to the piece part level. The results of this analysis show that the sensor will fail to achieve its mission if failures of any parts occur. Therefore, the unit reliability is based on a complete parts count assuming no redundancy or partial success.

4.0 FAILURE RATE

The detail failure rate analysis is summarized on the summary page showing a total mission probability of success of 89.61%. This success probability is almost entirely due to failures that could occur during the long transit period where the sensor is in a power-off condition. The major contributor to this failure rate is the High Voltage Power Supply and its large number of semiconductor elements. Some room for improvement is possible in this area by better application of the parts used.

The probability of success during periods of the mission other than transit is better than 99%.

NASA - LRC AIR DENSITY SENSOR (ADS-104)
Contract No. NAS1-7791

RELIABILITY BLOCK DIAGRAM
AND MATH MODEL PART 3060500

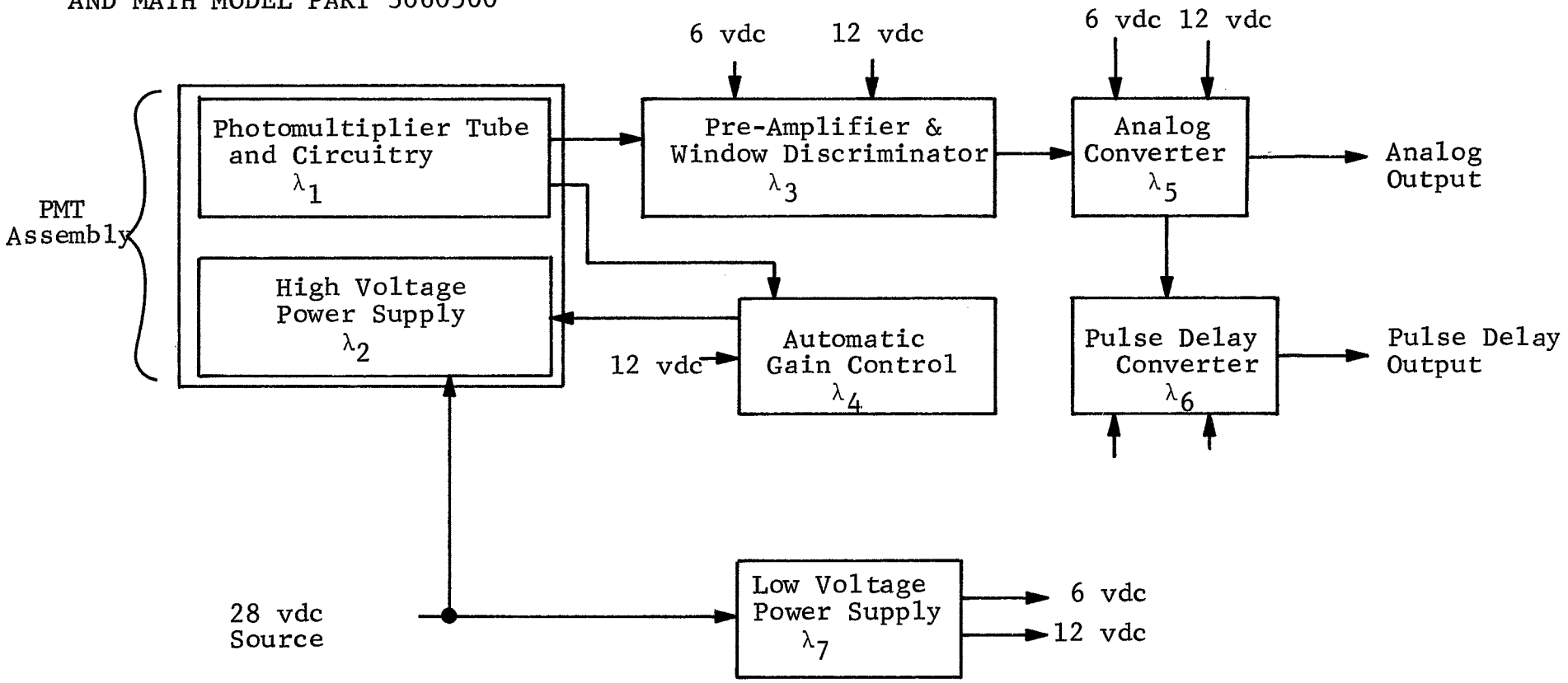

$$R = \lambda_1 + \lambda_2 + \lambda_3 + \lambda_4 + \lambda_5 + \lambda_6 + \lambda_7$$

NASA-LRC AIR DENSITY SENSOR (ADS-104)

Contract No. NAS1-7791

FAILURE MODE AND EFFECT
DRAWING - 3060500

Item	Drawing Number	Function	Failure Type	Failure Effect On the Item	Failure Effect On the Product
PMT Assembly λ_1 and λ_2	3060502	Radiation Detection Signal Conditioning High Voltage Power Supply	a. PM Tube Failure b. HV Breakdown (Low resistance path) c. H.V.Breakdown(High resistance path) d. Loss of high voltage	a. Loss of Signal b. Short circuit in H.V. No signal c. Excessive Noise & high count rate. d_1 No output d_2 Gain shift	a. Actual Failure b. Actual Failure c. Possible Failure d_1 Actual Failure d_2 Possible Failure
Pre-Amp. & Window Discriminator λ_3	3060502	Signal Amplifier Pulse Height Discriminator Anti-coincidence Circuit	a. Pre-amp. Loss b. Pre-amp. Oscillation c. Loss of Upper Window d. Loss of Lower Window e. Anti-coincidence loss	a. Loss of Signal b. Incorrect count Rate c_1 High Signal/Noise c_2 Loss of Signal d_1 Incorrect Count Rate d_2 Loss of Signal e_1 Loss of Signal e_2 (Same as c.)	a. Actual Failure b. Possible Failure c_1 Possible Failure c_2 Actual Failure d_1 Actual Failure d_2 Actual Failure e_1 Actual Failure e_2 (Same as c.)
Auto.Gain Control λ_4	3060502	Control of PM Tube Gain	a. AGC Oscillation b. Signal/Window Shift c. AGC Ckt Failure	a. Count Rate Distortion b. Count Rate Shift c. Loss of Signal	a. Possible Failure b. Possible Failure c. Actual Failure
Analog Converter λ_5	3060502	Digital to Analog Signal Conditioning	a. Circuit Failure b. Transfer Function Shift	a. Constant Output including zero b. Incorrect Signal	a. Actual Failure a. Actual Failure
Pulse Delay Circuit λ_6	3060502	Provides Separate Telemetry Signal Based upon the Analog Converter Signal	a. P.D.Circuit Loss	a_1 Loss P.D.Signal a_2 Constant P.D. Signal	a_1 Possible Failure a_2 Possible Failure
Low Voltage Power Supply λ_7	3060502	Power Source for All Assemblies except PMT Assembly	a. LVPS Component Failure	a_1 Loss of the output Voltages a_2 Shift of the output voltages (Gain increase) a_3 D.C. Ripple.	a_1 Actual Failure a_2 Possible Failure a_3 Possible Failure

TABLE VII - RELIABILITY ANALYSIS SUMMARY

(1)	(2) Subassembly	Failure Rate x 10^{-6} (3) Launch	(4) Transit	(5) Orbit	(6) Descend	(7) Remarks
1 2	PMT Assy. & HVPS	180.75	9.84	27.03	376.75	Actual Part Calculation
3	Amp. & Disc.	20.37	1.72	3.46	27.83	Actual Part Calculation
4	AGC	7.90	1.95	3.59	10.20	Actual Part Calculation
5	Analog Conv.	13.07	2.19	4.23	15.96	Actual Part Calculation
6	Pulse Conv.	18.57	1.47	2.17	23.60	Actual Part Calculation
7	LVPS	40.27	1.47	3.44	86.51	Actual Part Calculation
	Total F.R.	240.93	18.64	43.92	540.85	
	MTBF (Hrs)	4151	53,648	22,769	1,849	
	PROBABILITY OF SUCCESS	99.98%	89.85%	99.78%	99.97%	TOTAL MISSION P_T = 89.61%

Column Description:

(1) Block identification from the reliability block diagram.
(2) Block (Subassembly) Description
(3) (4) (5) (6) Assumed mission regimes

	Launch	Transit	Orbit	Descent
a. Duration (t)	0.5 hr	5/60 hr	50.0 hr	0.5 hr
b. Power Applied	No	No	Yes	Yes
c. Component Temperature (T)	+85°C	+40°C	+85°C	+85°C
d. Application Factor (K_A)	Missile	Orbit	Missile	Missile

(7) Conditions for determining predicted values.

λ_1 PMT and CIRCUITRY and
λ_2 HIGH VOLTAGE POWER SUPPLY Page 1 of 2

NASA-LRC AIR DENSITY SENSOR (ADS-104)
CONTRACT NO. NAS1-7791

Item	Ckt.No. (Ref.)	Component	Value	Description or P/N	MIL-SPEC (ER Level P)	Qualif. Document	At +85°C Stress Rated	At +85°C Stress Applied	Stress Ratio	K_A L	K_A Q	F.R. x 10^{-6} Hours BASE T=+85°C S.R. =.1	BASE S.R. Defined	TOTAL t=.5 Launch	TOTAL T=+40°C t=5760 Transit	TOTAL t=50 Orbit	TOTAL t=.5
1	R1	Res. CC	10 Ω	RCR07G100J	MIL-R-39008	ZZP-2748-5528	188 mw		<.1 .013	8	1	.325	.325	2.6	.170	.325	2.6
2	R2	Res. MF	56 K	RL07GF563J	MIL-R-22684B	5501	188 mw		.065	8	1	.325	.325	2.6	.170	.325	2.6
3	R3	Res. MF	2.1 K	RL07GF222	↑	↑	188 mw		.003	8	1	.325	.325	2.6	.170	.325	2.6
4	R4	Res. MF	510 Ω	RL07GF511			188 mw		.004	8	1	.325	.325	2.6	.170	.325	2.6
5	R5	Res. MF	6.8 K	RL07GF681			188 mw		.004	8	1	.325	.325	2.6	.170	.325	2.6
6	R6	Res. MF	13 K	RL07GF132			188 mw		.12	8	1	.325	.325	2.6	.170	.325	2.6
7	R7	Res. MF	33 K	RL07GF332			188 mw		.05	8	1	.325	.325	2.6	.170	.325	2.6
8	R8	Res. MF	910 Ω	RL07GF991			188 mw		.0005	8	1	.325	.325	2.6	.170	.325	2.6
9	R9	Res. MF	910 Ω	RL07GF911J	MIL-R-22684 B	↓ 5501	188 mw		.0005	8	1	.325	.325	2.6	.170	.325	2.6
10	R10	Res. CC	220 K	RCR07G224J	MIL-R-39008	ZZP-2748-5528	188 mw		.015	8	1	.325	.325	2.6	.170	.325	2.6
11	16 Dynodes	Res. Micronox Film	6-8 M	-		ZZP-2748	188 mw		.001	8	1	.325	.325	41.6	2.72	5.365	41.6
12	AC Load Resistor	Res MF	10 K	RL07GF103J	MIL-R-22684B	-5501	188 mw		.0001	8	1	.325	.325	2.6	.170	.325	2.6
13	R11	Res. MF	100 Ω	RL07GF-101J	↑	↕	188 mw		<.1	8	1	.325	.325	2.6	.170	.325	2.6
14	R13	Res. MF	3.6 K	RL07GF362-J	MIL-R-22684B	ZZP-2748-5501	188 mw		.008	8	1	.325	.325	2.6	.170	.325	2.6
15	R14	Sensistor	150 Ω	TG 1/8	MIL-T-23648A	QPL	145 mw		.005	8	1	.325	.325	2.6	.170	.325	2.6
16	C1	Cap. WT	8.2 µf	109D825x0060C0	(Similar to MIL-C-3965)	QPL	60 v	30 v	.5	25	1	.075	3.8	1.9	.014	3.8	.95
17	C2	Cap. ST	1.0 µf	150D 105x0050A0	(Similar to MIL-C-26655)	ZZP-2744-2501	50 v	30 v	.5 with 510 in series	50	1	.019	.23	.95	.0077	.23	11.5
18	C3	Cap. C	.01 µf	CK30CW103K	MIL-C-11015	ZZP-2744-2502	200 v	30 v	.1	15	1	.0032	.0032	.048	.0020	.0032	.048
19	C4	Cap. C	1000 Pf	CK20CW102K	MIL-C-11015	ZZP-2744-2502	200 v	5 v	.1	15	1	.0032	.0032	.048	.0020	.0032	.048
20	C5	Cap. C	.001 µf	MKW102K30	(Similar to MIL-C-25)	-	3000 v	500 v	.25	20	1	.015	.16	.3	.0062	.16	3.2
21	C6	Cap. C	.001 µf	MKW102K30	(Similar to MIL-C-25)	-	3000 v	1000 v	.5	20	1	.015	.68	.3	.0062	.68	13.6
22	C7	Cap. C	.002 µf	MKW202K30	(Similar to MIL-C-25)	-	3000 v	1000 v	.5	20	1	.015	.68	.3	.0062	.68	13.6
23	C8	Cap. C	.002 µf	MKW202K30	(Similar to MIL-C-25)	-	3000 v	1000 v	.5	20	1	.015	.68	.3	.0062	.68	13.6
24	15 Dynode	Cap. (rated G 500 v)	100 pf	CYFM10C101J	MIL-C-5	ZZP-2744-2534	500 v	-	.4	60	1	.015	.34	.9	.0062	.34	20/4
25	HV Coupling Cap.	Cap. M	.001 pf	MKW102K50	(Similar to MIL-C-25)	-	5000 v	-	.6	20	1	.015	1.2	.3	.0062	1.2	24
26	T1	Transformer	-	TF6QX40ZZ	MIL-T-27	QPL	-	-	.060	50	1	.7	.7	.7	.21	.7	3.5
27	V1	PMT	-		MIL-E-1	-	-	-	-	1.0	1	1.0	1.0	1.0	1.0	1.0	1.0
28	Q1	Transistor		2N2605	MIL-S-19500	ZZP-2061-PPL-J	400	5 mw	T_n	25	1.5	.780	.780	19.5	.46	1.2	19.5
29	Q2	Transistor		2N718A	MIL-S-19500	QPL	500 mw	45 mw	Used	25	1.5	.290	.365	7.3	.29	.55	9.1

λ_1 PMT and CIRCUITRY and
λ_2 HIGH VOLTAGE POWER SUPPLY **Page 2 of 2**

NASA-LRC AIR DENSITY SENSOR (ADS-104)

CONTRACT NO. NAS1-7791

Item	Ckt.No. (Ref.)	Component	Value	Description or P/N	MIL-SPEC (ER Level P)	Qualif. Document	At +85°C Stress Rated	At +85°C Stress Applied	Stress Ratio	K_A L	K_A Q	F.R. x 10^{-6} Hours BASE T=+35°C S.R. =.1	BASE S.R. Defined	TOTAL t=.5 Launch	TOTAL t=5760 T=+40°C Transit	TOTAL t=50 Orbit	TOTAL t=.5
30	Q3	Transistor		2N2605	MIL-S-19500	ZZP-2061 PPL-U	400	15 mw	T_n Used	25	1.5	.780	.780	19.5	.46	1.2	19.5
31	Q4	Transistor		2N2297	↕	QPL	800 mw	111 mw	↕	25	1.5	.290	.410	7.3	.33	.62	10.3
32	Q5	Transistor		2N 718A		QPL	500 mw	1 mw		25	1.5	.290	.290	7.3	.21	.44	7.3
33	Q6	Transistor		2N718A		QPL	500 mw	1 mw		25	1.5	.290	.290	7.3	.21	.44	7.3
34	CR1	Diode		1N916	MIL-S-19500	ZPP-2745-3001	80 mw	3 mw	T_n Used	10	1.5	.290	.325	2.9	.248	.49	3.25
35	CR2	Diode		1N3284	MIL-S-19500	QPL	250 mw	5 mw		10	1.5	.410	.410	4.1	.210	.615	4.1
36	CR3	Diode		1N3284	MIL-S-19500	QPL	250 mw	5 mw	T_n Used	10	1.5	.410	.410	4.1	.210	.615	4.1
37	CR4	Diode		1N3284	↕	↕	250 mw	1 mw	↕	10	1.5	.410	.410	4.1	.210	.615	4.1
38	CR5	Diode		1N3284			250 mw	1 mw		10	1.5	.410	.410	4.1	.210	.615	4.1
39	CR6	Diode		1N3284			250 mw	1 mw		10	1.5	.410	.410	4.1	.210	.615	4.1
40	CR7	Diode		1N3284	MIL-S-19500	QPL	250 mw	1 mw	T_n Used	10	1.5	.410	.410	4.1	.210	.615	4.1
													TOTAL	180.75	9.84	27.03	376.75

λ_3 AMP. & WINDOW DISCRIMINATOR 3060502 Page 1 of 2

NASA-LRC AIR DENSITY SENSOR (ADS-104)
CONTRACT NO. NAS1-7791

Item	Ckt.No. (Ref.)	Component	Value	Description or P/N	MIL-SPEC (ER Level P)	Qualif. Document	At +85°C Stress Rated	At +85°C Stress Applied	Stress Ratio	K_A L	K_A O	F.R. x 10^{-6} Hours BASE T=+85°C S.R. =.1	BASE S.R. Defined	TOTAL T=+40°C t=.5 Launch	TOTAL T=+40°C t=5760 Transit	TOTAL t=50 Orbit	TOTAL t=.5
1	R1	Res. CC	51. Ω	RCR07	MIL-R-39008	ZPP-2748-5528	188 mv	<1 mw	<.1	50	1	.01	.01	.5	.0035	.01	.5
2	R2	MF	2. K	RNR60	MIL-R-55182	-5555	215	<1	<.1	1.5	1	.29	.29	.435	.19	.29	.435
3	R3	CC	51. Ω	RCR07	MIL-R-39008	-5528	215	<1	<.1	50.3	1	.01	.01	.5	.0035	.01	.5
4	R4	CC	200 Ω	RCR07	MIL-R-39008	-5528	188	<1	<.1	50	1	.01	.01	.5	.0035	.01	.5
5	R5	MF	3.3 K	RNR60	MIL-R-55182	-5555	215	<1	<.1	1.5	1	.29	.29	.435	.19	.29	.435
6	R6	MF	10 K	RNR60	MIL-R-55182	-5555	215	<1	<.1	1.5	1	.29	.29	.435	.19	.29	.435
7	R7	CC	1 K	RCR07	MIL-R-39008	-5528	188	<1	<.1	50	1	.01	.01	.5	.0035	.01	.5
8	R8	CC	910 Ω	RCR07	MIL-R-39008	-5528	188	36	.2	50	1	.01	.016	.5	.0035	.016	.8
9	R9	CC	51 Ω	RCR07	MIL-R-39008	-5528	188	<1	<.1	50	1	.01	.01	.5	.0035	.01	.5
10	R11	MF	150 Ω	RNR60	MIL-R-55182	-5555	215	170	.8	1.5	1	.29	.47	.435	.19	.47	.705
11	R10	MF	Select	RNR60	MIL-R-55182	-5555	215	30	.1	1.5	1	.29	.29	.435	.19	.29	.435
12	R12	CC	510 Ω	RCR07	MIL-R-39008	-5528	188	<1	<.1	50	1	.01	.01	.5	.0035	.01	.5
13	R14	MF	150 Ω	RNR60	MIL-R-55182	-5555	215	170	.8	1.5	1	.29	.47	.435	.19	.47	.705
14	R13	MF	Select	RNR60	MIL-R-55182	-5555	215	30	.2	1.5	1	.29	.32	.435	.19	.32	.480
15	R15	CC	510 Ω	RCR07	MIL-R-39008	-5528	188	<1	<.1	50	1	.01	.01	.5	.0035	.01	.5
16	R16	CC	24 K	RCR07	MIL-R-39008	-5528	188	6	<.1	50	1	.01	.01	.5	.0035	.01	.5
17	R17	CC	24 K	RCR07	MIL-R-39008	-5528	188	6	<.1	50	1	.01	.01	.5	.0035	.01	.5
18	R18	CC	510 Ω	RCR07	MIL-R-39008	-5528	188	<1	<.1	50	1	.01	.01	.5	.0035	.01	.5
19	R19	CC	510 Ω	RCR07	MIL-R-39008	-5528	188	<1	<.1	50	1	.01	.01	.5	.0035	.01	.5
20	R20	CC	510 Ω	RCR07	MIL-R-39008	-5528	188	<1	<.1	50	1	.01	.01	.5	.0035	.01	.5
21	R21	CC	510 Ω	RCR07	MIL-R-39008	-5528	188	72	.4	50	1	.01	.039	1.950	.0035	.01	1.950
22	R94	Res. CC	510 Ω	RCR07	MIL-R-39008	-5528	188	<1	<.1	50	1	.01	.01	.5	.0035	.01	.5
23																	
24	C1	Cap. S.T.	139 µf	CSR	MIL-C-39003	ZPP-2744-2501	15 v	6 v	.4	50	1	.017	.054	.85	.0069	.054	2.700
25	C2	CER	510 pf	CKR	MIL-C-39003	-2502	200	<1 v	<.1	15	1	.0033	.0033	.05	.0019	.0033	.050
26	C3	CER	56 pf	CKR	MIL-C-39014	-2502	200	<1 v	<.1	15	1	.0033	.0033	.05	.0019	.0033	.050
27	C4	CER	0.1	CKR	MIL-C-39014	-2503	100	6 v	<.1	15	1	.0033	.0033	.05	.0019	.0033	.550
28	C5	CER	1500 pf		MIL-C-39014	-2502	200	<1 v	<.1	15	1	.0033	.0033	.05	.0019	.0033	.050
29	C6	CER	0.1µf	CKR	MIL-C-39014	-2503	100	12 v	.10	15	1	.0033	.0033	.05	.0019	.0033	.050
30	C7	CER	0.1µf	CKR	MIL-C-39014	-2503	100	6 v	<.1	15	1	.0033	.0033	.05	.0019	.0033	.050
31	C8	CER	0.1µf	CKR	MIL-C-39014	-2503	100	6 v	<.1	15	1	.0033	.0033	.05	.0019	.0033	.050
32	C9	CER	0.1µf	CKR	MIL-C-39014	-2503	100	12 v	.10	15	1	.0033	.0052	.05	.0019	.0033	.050
33	C10	CER	0.1µf	CKR	MIL-C-39014	-2503	100	12 v	.2	15	1	.0033	.0052	.05	.0019	.0052	.078
34	C11	CER	47 µf	CKR	MIL-C-39014	-2502	200	6 v	<.1	15	1	.0033	.0033	.05	.0019	.0033	.050
35	C12	CER	22 µf	CKR	MIL-C-39014	ZPP-2744-2502	200	6 v	<.1	15	1	.0033	.0033	.05	.0019	.0033	.050
													SUB TOTAL	13.330	1.597	2.948	16.093

λ_3 AMP. & WINDOW DISCRIMINATOR 3060502 Page 2 of 2

NASA-LRC AIR DENSITY SENSOR (ADS-104)

CONTRACT NO. NAS1-7791

Item	Ckt. No. (Ref.)	Component Title	Description or P/N	MIL-SPEC (ER Level P)	Qualif. Document	At +85°C Stress Rated	At +85°C Stress Applied	Stress Ratio	π_A L	π_A C	F.R. $\times 10^{-6}$ Hours B A S E T=+40°C S.R. =.1	B A S E T=+40°C S.R. Defined	T O T A L t=.5 Launch	T O T A L t=5760 Transit	T O T A L t=50 Orbit	T O T A L t=.5
36	~~ER-1~~	~~Diodes~~	~~Rect.~~ ~~1N916~~	Deleted	MIL-S-19500	ZPP-2746-3001	~~80 mw~~	~~<1 mw~~	$*T_n$=.4 +0	10	1	.033	.033	.330	.014	.033	.330
37	~~ER-2~~	~~Rect.~~	~~1N916~~	Deleted	MIL-S-19500	~~3001~~	~~80 mw~~	~~<1 mw~~	$*T_n$=.4 +0	10	1	.033	.033	.330	.014	.033	.330
38	Q1	Xsters S1 NPN	2N2222A	175°		ZPP-2751-7041	500 mw	66 mw	$*T_n$=.4 +33	25	1	.033	.066	.825	.014	.066	1.65
39	Z-1	IC	µA702	15°		-2750-6009	300 mw	100 mw	$*T_n$=.48+.3	25	1	.041	.073	1.025	.014	.073	1.825
40	Z-2		µA710	150°		-6010	300 mw	100 mw	$*T_n$=.48+.3	25	1	.041	.073	1.025	.014	.073	1.825
41	Z-3		µA710	150°		-6010	300 mw	100 mw	$*T_n$=.48+.3	25	1	.041	.073	1.025	.014	.073	1.825
42	Z-4		SE160G	175°		-6020	150 mw	45 mw	$*T_n$=.4+.3	25	1	.033	.061	.825	.014	.061	1.525
43	Z-5		SE160G	175°		-6020	150 mw	45 mw	$*T_n$=.4+.3	25	1	.033	.061	.825	.014	.061	1.525
44	Z-6	IC	SE101G	175°	MIL-S-19500	-6012	40 mw	7 mw	$*T_n$=.4+.02	25	1	.033	.036	.825	.014	.036	.900
														7.035	.126	.509	11.735
												SUB TOTAL Page 1		13.330	1.597	2.948	16.093
												λ_3 TOTAL		20.365	1.723	3.457	27.828

* Except for Transit

λ_4 AGC 3060502

NASA-LRC AIR DENSITY SENSOR (ADS-104)
CONTRACT NO. NAS1-7791

Item	Ckt.No. (Ref.)	Component	Value	Description or P/N	MIL-SPEC (ER Level P)	Qualif. Document	At +85°C Stress Rated	At +85°C Stress Applied	Stress Ratio	K_A L	K_A O	F.R. x 10^{-6} Hours B A S E T=+85°C S.R. =.1	S.R. Defined	t=.5 Launch	T O T A L T=+40°C t=5760 Transit	t=50 Orbit	t=.5
1	R23	Res.	M.F.	11 K	RNR 60 Deleted	MIL-R-55182	ZPP-2748-5555	215 mw	<1 mw	<.1	1.5	1	.29	.29	.435	.19	.01	.435
2	R24	Res.	M.F.	2.2 K	RNR 60 Deleted	MIL-R-55182	-5555	215 mw	<5 mw	<.1	1.5	1	.29	.29	.435	.19	.01	.435
3	R25		CC	100 Ω	RCR 07 Deleted	MIL-R-39008	-5528	188	6	<.1	50	1	.01	.01	.500	.0035	.01	.5
4	R26		CC	1 K	RCR 07 Deleted	MIL-R-39008	-5528	188	36	.2	50	1	.01	.016	.500	.0035	.016	.8
5	R27		MF	1 K	RNR 60	MIL-R-55182	-5555	215	<1	<.1	1.5	1	.29	.29	.435	.19	.29	.435
6	R28		MF	200 Ω	RNR 60	MIL-R-55182	-5555	215	5	<.1	1.5	1	.29	.29	.435	.19	.29	.435
7	R29		MF	200 K	RNR 60	MIL-R-55182	-5555	215	25	.1	1.5	1	.29	.29	.435	.19	.29	.435
8	R30		MF	18.22 K	RNR 60	MIL-R-55182	-5555	215	2	<.1	1.5	1	.29	.29	.435	.19	.29	.435
9	R31		CC	510 Ω	RCR07 Deleted	MIL-R-39008	-5528	188	70	.4	50	1	.01	.039	.500	.0035	.039	1.950
10	R32		MF	61.9Ω	RNR 60	MIL-R-55182	-5555	215	<1	<.1	1.5	1	.29	.29	.435	.19	.29	.435
11	R33		MF	24.3 K	RNR 60	MIL-R-55182	-5555	215	<1	<.1	1.5	1	.29	.29	.435	.19	.29	.435
12	R35		CC	24.3 K	RCR 07	MIL-R-39008	-5528	188	<1	<.1	1.5	1	.01	.01	.500	.0035	.01	.5
13	R36		CC	5.1 K	RCR 07	MIL-R-39008	-5528	188	<1	<.1	1.5	1	.29	.29	.435	.19	.29	.435
14	R37		CC	13 K	RCR 07	MIL-R-39008	-5528	188	<1	<.1	1.5	1	.29	.29	.435	.19	.29	.435
15	R38		CC	8.2 K	RCR 07	MIL-R-39008	-5528	188	<1	<.1	1.5	1	.29	.29	.435	.19	.29	.435
16	R106	Res.	CC	200 Ω	RCR 07	MIL-R-39008	-5528	188	<1	<.1	1.5	1	.29	.29	.435	.19	.29	.435
17	C-13	Cap.	CER	0.1 µf	CKR Deleted	MIL-C-39014	ZPP-2744-2593	200 v	<1 v	<.1	15	1	.0033	.0033	.050	.0019	.0033	.050
18	C-14		CER	0.1 µf	CKR Deleted	MIL-C-39014	-2503	200 v	<1	<.1	15	1	.0033	.0033	.050	.0019	.0033	.050
19	C 15		PC	3000 pf		MIL-C-(27287)	P64437	50 v	6 v	.12	25	1	.0015	.0015	.038	.0010	.0015	.038
20	C-16		M	1 µf	CIM (Non-ER) Deleted	MIL-C-27287	ZPP-2744-2515	75 v	<1 v	<.1	25	1	.0015	.0015	.038	.0010	.0015	.038
21	C 17		M	5 µf	CIM (Non-ER)	MIL-C-27287		75 v	4 v	<.1	25	1	.0015	.0015	.038	.001	.0015	.038
22	C 18		CER	680 µf	CKR	MIL-C-39014	-2503	200 v	<1 v	<.1	15	1	.0033	.0033	.050	.0019	.0033	.050
23	C 19	Cap.	CER	100 pf	CKR	MIL-C-39014	-2503	200 v	<1 v	<.1	15	1	.0033	.0033	.050	.0019	.0033	.050
24	Deleted																	
25	Deleted																	
26	Q-2	Xster	Si	NPN	2N2222A- Deleted	MIL-S-19500	ZPP-2751-7041	500 mw	66 mw	*T_n=.4+.33	25	1	.033	.066	.825	.014	.066	1.650
27	Z-9	IC			µA710	MIL-S-19500	ZPP-2750-6010	300 mw	100 mw	*T_n=.48+.3	25	1	.041	.073	1.025	.014	.073	1.825
28	Z-10	IC			SE160G	MIL-S-19500	ZPP-2750-6020	150 mw	45 mw	*T_n=.4+.3	25	1	.033	.061	.825	.014	.061	1.525
29	Z-11	IC			µA709	MIL-S-19500	APP-2750-6009	300 mw	85 mw	*T_n=.48+.3	25	1	.041	.073	1.025	.014	.073	1.825
													λ_4	TOTAL	7.901	1.952	3.588	10.201

* Except for Transit

λ 5 ANALOG CONVERTER
3060502

NASA-LRC AIR DENSITY SENSOR (ADS-104)
CONTRACT NO. NAS1-7791

Item	Ckt.No. (Ref.)	Component	Value	Description or P/N	MIL-SPEC (ER Level P)	Qualif. Document	At +85°C Stress Rated	At +85°C Stress Applied	Stress Ratio	K_A L	K_A Q	F.R. x 10^{-6} Hours BASE T=+85°C S.R. =.1	BASE S.R. Defined	TOTAL t=.5 Launch	TOTAL T=+40°C t=5760 Transit	TOTAL t=50 Orbit	TOTAL t=.5
1	R39	Res. CC	510 Ω	RCR07 Deleted	MIL-R-39008	ZPP-2748-5528	100 mw	70 mw	.4	50	1	.01	.039	.500	.0035	.039	1.950
2	R40	MF	4.99 K	RNR60	MIL-R-55182	-5555	215	<1	<.1	1.5	1	.29	.29	.435	.19	.29	.435
3	R41	MF	5.11 K	RNR60	MIL-R-55182	-5555	215	<1	<.1	1.5	1	.29	.29	.435	.19	.29	.435
4	R42	MF	22.1 K	RNR60	MIL-R-55182	-5555	215	<1	<.1	1.5	1	.29	.29	.435	.19	.29	.435
5	R43	CC	5.1 K	RCR07	MIL-R-39008	-5528	188	<1	<.1	50	1	.01	.01	.500	.0035	.01	.5
6	R44	MF	2.49 K	RNR60	MIL-R-55182	-5555	215	3	<.1	1.5	1	.29	.29	.435	.19	.32	.435
7	R45	MF	2.8 K	RNR60-	MIL-R-55182	-5555	215	<1	<.1	1.5	1	.29	.29	.435	.19	.32	.435
8	R46	MF	30.1 K	RNR60	MIL-R-55182	-5555	215	3	<.1	1.5	1	.29	.29	.435	.19	.29	.435
9	R47	MF	20 K	RNR60	MIL-R-55182	-5555	215	3	<.1	1.5	1	.29	.29	.435	.19	.29	.435
10	R48	MF	5.9 K	RNR60	MIL-R-55182	-5555	215	5	<.1	1.5	1	.29	.29	.435	.19	.29	.435
11	R49	MF	165 Ω	RNR60	MIL-R-55182	-5555	215	<1	<.1	1.5	1	.29	.29	.435	.19	.29	.435
12	R50	CC	1.45K	RCR07	MIL-R-39008	-5528	188	<1	<.1	50	1	.01	.01	.500	.0035	.01	.5
13	R51	CC	5.1 K	RCR07	MIL-R-39008	-5528	188	<1	<.1	50	1	.01	.01	.500	.0035	.01	.5
14	R67	Res. CC	5.1 K	RCR07	MIL-R-39008	-5528	188	<1	<.1	50	1	.01	.01	.500	.0035	.01	.5
15	C54	Cap. PC	Select		MIL-C-(27287)	P-64437	50 v	6 v	.12	25	1	.0015	.0015	.0375	.0250	.0015	.0375
16	C23	M	2 µf	CTM (Non ER)	MIL-C-27287	ZPP-2744-2515	100 v	1 v	<.1	25	1	.0015	.0015	.038	.0010	.0015	.038
17	C24	CER	680 pf	CKR	MIL-C-39014	-2503	200 v	<1 v	<.1	15	1	.0033	.0033	.050	.0019	.0033	.050
18	C25	CER	100 pf	CKR	MIL-C-39014	-2503	200 v	<1 v	<.1	15	1	.0033	.0033	.050	.0019	.0033	.050
19	C26	CER	680 pf	CKR	MIL-C-39014	-2503	200 v	6 v	<.1	15	1	.0033	.0033	.050	.0019	.0033	.050
20	C27	CER	100 pf	CKR	MIL-C-39014	-2503	200 v	6 v	<.1	15	1	.0033	.0033	.050	.0019	.0033	.050
21	C28	CER	680 pf	CKR	MIL-C-39014	-2503	200 v	<1 v	<.1	15	1	.0033	.0033	.050	.0019	.0033	.050
22	C29	Cap. CER	100 pf	CKR	MIL-C-39014	-2503	200 v	6 v	<.1	15	1	.0033	.0033	.050	.0019	.0033	.050
23	CR-3	Diode	Rect.	1N916	MIL-S-19500	ZPP-2746-3001	80 mw	13 mw	T_n=.4 +.2	10	1	.033	.051	.330	.014	.051	.330
24	Z12	IC		SE 160G	MIL-S-19500	ZPP-2750-6020	150 mw	45 mw	T_n=.4+.3	25	1	.033	.061	.825	.014	.061	1.525
25	Z13			µA 709	MIL-S-19500	ZPP-2750-6010	300 mw	112 mw	T_n=.48+.3	25	1	.041	.079	1.025	.014	.079	1.975
36	Z14			µA 709	MIL-S-19500	ZPP-2750-6010	300 mw	80 mw	T_n=.48+.27	25	1	.041	.066	1.025	.014	.066	1.650
27	Z15	IC		µA 709	MIL-S-19500	ZPP-2750-6010	300 mw	100 mw	T_n=.48+.3	25	1	.041	.073	1.025	.014	.073	1.825
28	R95	Res. MF	237 Ω	RNR 60	MIL-R-55182	ZPP-2748-5555	215 mw	5 mw	<.1	1.5	1	.29	.29	.435	.19	.29	.433
29	R96	MF	91 K	RNR 60	MIL-R-55182	-5555	215 mw	10 mw	<.1	1.5	1	.29	.29	.435	.19	.29	.435
30	R97	CC	1.5 K	RCR-8	MIL-R-39008	-5528	188 mw	<1 mw	<.1	50	1	.01	.01	.500	.0035	.01	.5
31	R98	CC	1 K	RCR07	MIL-R-39008	-5528	188 mw	<1 mw	<.1	50	1	.01	.01	.500	.0035	.01	.5
32	R99	Res. CC	10 K	RCR07	MIL-R-39008	ZPP-2748-5528	188 mw	<1 mw	<.1	50	1	.01	.01	.500	.0035	.01	.5
													TOTAL	13.068	2.19	4.230	15.966

λ.6 PULSE DELAY CONVERTER 3060502 — Page 1 of 2

NASA-LRC AIR DENSITY SENSOR (ADS-104)
CONTRACT NO. NAS1-7791

Item	Ckt.No. (Ref.)	Component	Value	Description or P/N	MIL-SPEC (CR Level P)	Qualif. Document	At +85°C Stress Rated	At +85°C Stress Applied	Stress Ratio	K_A L	K_A Q	F.R. x 10^{-6} Hours BASE T=+85°C S.R. =.1	BASE S.R. Defined	TOTAL t=.5 Launch	TOTAL T=+40°C t=5760 Transit	TOTAL t=50 Orbit	TOTAL t=.5
1	R53	Res. CC	51 K	RCR07	MIL-R-39008	ZPP-2748-5528	188	<1 mw	<.1	50	1	.01	.01	.5	.0035	.01	.5
2	R55	CC	510 Ω	RCR07		-5528	188	2	<.1	50	1	.01	.01	.5	.0035	.01	.5
3	R57	CC	33 K	RCR07		-5528	188	<1	<.1	50	1	.01	.01	.5	.0035	.01	.5
4	R60	CC	69.8 K	RCR07		-5528	188	<1	<.1	50	1	.01	.01	.5	.0035	.01	.5
5	R59	CC	4.22 Ω	RCR07		-5528	188	<1	<.1	50	1	.01	.01	.5	.0035	.01	.5
6	R61	CC	102 Ω	RCR07	MIL-R-39008	-5528	188	<1	<.1	50	1	.01	.01	.5	.0035	.01	.5
7	R62	MF	23.2 K	RNR60	MIL-R-55182	-5528	215	<1	<.1	1.5	1	.29	.29	.435	.19	.29	.435
8	R63	MF	10 K	RNR60	MIL-R-55182	-5528	215	25	<.1	1.5	1	.29	.29	.435	.19	.29	.435
9	R64	CC	5.1 K	RCR07	MIL-R-39008	-5528	188	5	<.1	50	1	.01	.01	.5	.0035	.01	.5
10	R65	CC	5.1 K	RCR07	MIL-R-39008	-5528	188	5	<.1	50	1	.01	.01	.5	.0035	.01	.5
11	R66	CC	10 K	RCR07		-5528	188	<1	<.1	50	1	.01	.01	.5	.0035	.01	.5
12	R69	CC	5.1 K	RCR07		-5528	188	<1	<.1	50	1	.01	.01	.5	.0035	.01	.5
13	R70	CC	5.1 K	RCR07		-5528	188	<1	<.1	50	1	.01	.01	.5	.0035	.01	.5
14	R100	CC	20 K	RCR07		-5528	188	30	.2	50	1	.01	.016	.8	.0035	.016	.8
15	R101	CC	62 K	RCR07		-5528	188	<1	<.1	50	1	.01	.01	.5	.0035	.01	.5
16	R102	CC	10 K	RCR07		-5528	188	1	<.1	50	1	.01	.01	.5	.0035	.01	.5
17	R103	CC	100 K	RCR07		-5528	188	6	<.1	50	1	.01	.01	.5	.0035	.01	.5
18	R104	Res. CC	10 K	RCR07		-5528	188	<1	<.1	50	1	.01	.01	.5	.0035	.01	.5
19	C31	Cap. CER	680 pf	CKR	MIL-C-39014	ZPP-2744-2502	200 v	<1 v	<.1	15	1	.0033	.0033	.05	.0019	.033	.050
20	C32	CER	100 pf	CKR	MIL-C-39014	-2502	200 v	6 v	<.1	15	1	.0033	.0033	.05	.0019	.0019	.050
21	C33	M	2 uf	CTM	MIL-C-27278		50 v	12 v	.2	25	1	.0015	.0019	.038	.0010	.0019	.048
22	C34	CER	680 pf	CKR	MIL-C-39014	-2502	200 v	<1 v	<.1	15	1	.0033	.0033	.05	.05	.0019	.050
23	C35	CER	100 pf	CKR		-2502	200 v	6 v	<.1	15	1	.0033	.0033	.05	.05	.0019	.050
24	C36	CER	680 pf	CKR		-2502	200 v	<1 v	<.1	15	1	.0033	.0033	.05	.05	.0019	.050
25	C37	CER	100 pf	CKR		-2502	200 v	6 v	<.1	15	1	.0033	.0033	.05	.05	.0019	.050
26	C38	CER	.1 µf	CKR		-2502	200 v	5 v	<.1	15	1	.0033	.0033	.05	.05	.0019	.050
27	C52	CER	.1 µf	CKR	MIL-C-39014	-2502	100 v	6 v	<.1	15	1	.0033	.0033	.05	.05	.0019	.050
28	C53	Cap. S.T.	3.3 µf	CSR	MIL-C-39003	-2502	50 v	6 v	.1	50	1	.019	.019	.950	.0077	.019	.950
													SUB TOTAL	10.263	1.308	1.653	10.373

NASA-LRC AIR DENSITY SENSOR (ADS-104)

CONTRACT NO. NAS1-7791

Item	Ckt.No. (Ref.)	Component	Value	Description or P/N	MIL-SPEC (ER Level P)	Qualif. Document	At +85°C Stress Rated	At +85°C Stress Applied	Stress Ratio	K_A L	K_A O	F.R. x 10^{-6} Hours BASE T=+35°C S.R. =.1	BASE S.R. Defined	TOTAL T=+40°C t=.5 Launch	TOTAL T=+40°C t=5760 Transit	TOTAL t=50 Orbit	TOTAL t=.5
29	CR4	Diode	RECT	1N916	MIL-S-19500	ZPP-2746-3001	80 mw	2.5 mw	T_n=.4 +0	10	1	.033	.033	.330	.014	.033	.330
30	CR5	↕	RECT	1N916	↕	-3001	80 mw	<1	T_n=.4 +4	10	1	.033	.033	.330	.014	.033	.330
31	CR6	↕	RECT	1N916	↕	-3001	80 mw	<1	T_n=.4 +0	10	1	.033	.033	.330	.014	.033	.330
32	CR7	↕	RECT	1N916	↕	-3001	80 mw	<1	T_n=.4 +0	10	1	.033	.033	.330	.014	.033	.330
33	CR16	Diode	RECT	1N916	↕	-3001	80 mw	<1	T_n=.4 +0	10	1	.033	.033	.330	.014	.033	.330
34	Z17	Int.Ckts	-	µa709	↕	ZPP-2750-6009	300 mw	80 mw	T_n=.48+.27	25	1	.041	.066	1.025	.014	.066	1.650
35	Z18	↕	-	µa709	↕	↕	300 mw	80 mw	T_n=.48+.27	25	1	.041	.066	1.025	.014	.066	1.650
36	Z19	Int.Ckts	-	µa709	MIL-S-19500	ZPP-2750-6009	300 mw	80 mw	T_n=.48+.27	25	1	.041	.066	1.025	.014	.066	1.650
37	Q11	Transistor	-	2N1132	MIL-S-19500/177	QPL	600 mw	20 mw	T_n=.4+.033	25	1	.092	.107	2.30	.031	.107	5.350
38	Q12	Transistor	-	MEM550 (3049623)	-	-	112 mw	1 mw	T_n=.6+.009	25	1	.051	.051	1.28	.017	.051	1.28
													TOTAL	18.568	1.468	2.174	23.603

λ_7 LOW VOLTAGE POWER SUPPLY **Page 1 of 2**

NASA-LRC AIR DENSITY SENSOR (ADS-104)
CONTRACT NO. NAS1-7791

Item	Ckt.No. (Ref.)	Component	Value	Description or P/N	MIL-SPEC (ER Level P)	Qualif. Document	At +85°C Stress Rated	At +85°C Stress Applied	Stress Ratio	K_A L	K_A C	F.R. x 10^{-6} Hours BASE T=+85°C S.R. =.1	BASE S.R. Defined	TOTAL t=.5 Launch	TOTAL T=+40°C t=5760 Transit	TOTAL t=50 Orbit	TOTAL t=.5
1	R75	Resistor CC	22 Ω	RCR07G240JP	MIL-R-39008	2PP-2748-5528	188 mw	106 mw	.56	50	1	.01	.088	.5	.0035	.088	4.4
2	R76	CC	8.2 K	RCR07G822JP		-5528	188 mw	96 mw	.51	50	1	.01	.056	.5	.0035	.056	2.8
3	R77	CC	68 Ω	RCR07G680JP		-5528	188 mw	10 mw	<.1	50	1	.01	.01	.5	.0035	.01	.5
4	R78	CC	68 Ω	RCR07G680JP	MIL-R-39008	-5528	188 mw	106 mw	.56	50	1	.01	.088	.5	.0035	.088	4.8
5	R79	MF	*7.5 K	RNR69C7501FP	MIL-R-55182	-5555	215	18 mw	<.1	1.5	1	.29	.29	.435	.19	.29	.435
6	R80	CC	3 K	RCR07G302JP	MIL-R-39008	-5528	188	3 mw	<.1	50	1	.01	.01	.5	.0035	.01	.5
7	R81	CC	5.1 K	RCR07G512JP	MIL-R-39008	-5528	188	5 mw	<.1	50	1	.01	.01	.5	.0035	.01	.5
8	R82	MF	4.99K	RNR69C4991FP	MIL-R-55182	-5555	215	7 mw	<.1	1.5	1	.29	.29	.435	.19	.29	.435
9	R83	CC	1.5 K	RCR076152JP	MIL-R-39008	-5528	188	24 mw	.13	50	1	.01	.01	.5	.0035	.01	.5
10	R84	CC	10 Ω	RCR20G100JP	MIL-R-39008	-5528	375	100 mw	.38	50	1	.01	.039	.5	.0035	.039	.2
11	R85	CC	10 K	RCR07G103JP	MIL-R-39008	-5528	188	4 mw	<.1	50	1	.01	.01	.5	.0035	.01	.5
12	R86	MF	10 K	RNR60C1002FP	MIL-R-55182	-5555	215	4 mw	<.1	1.5	1	.29	.29	.435	.19	.29	.435
13	R87	CC	5.1 K	RCR07G512JP	MIL-R-39008	-5528	188	3 mw	<.1	50	1	.01	.01	.5	.0035	.01	.5
14	R88	CC	5.1 K	RCR07G512JP	MIL-R-39008	-5528	188	5 mw	<.1	50	1	.01	.01	.5	.0035	.01	.5
15	R89	MF	10 K	RNR60C1002FP	MIL-R-55182	-5555	215	4 mw	<.1	1.5	1	.29	.29	.435	.19	.29	.435
16	R90	CC	1.5 K	RCR07G152JP	MIL-R-39008	-5528	188	24 mw	.13	50	1	.01	.01	.5	.0035	.01	.5
17	R90	CC	20 Ω	RCR20G200JP	MIL-R-39008	-5528	375	40 mw	.11	50	1	.01	.01	.5	.0035	.01	.5
18	R92	CC	10 K	RCR07G103JP	MIL-R-39008	-5528	188	4 mw	<.1	50	1	.01	.01	.5	.0035	.01	.5
19	R107	Resistor MF	511 Ω	RNR60C5110FP	MIL-R-55182	-5555	215	25 mw	.12	1.5	1	.29	.29	.435	.19	.29	.435
20	C40	Cap. S.T.	15 µf	CSR13H156KP	MIL-C-39003	-2501	75 v	32 v	.43	50	1	.017	.054	.85	.0069	.054	2.7
21	C41	P	.039 µf	127P3939R5S4	MIL-C-14157 (non ER)	-2508	50 v	28 v	.56	-	1	.005	.023	.005	.005	.023	.023
22	C42	P	.0022µf	127P22291S4	MIL-C-14157 (non ER)	-2508	100 v	64 v	.64	-	1	.005	.023	.005	.005	.023	.023
23	C43	P	.039µf	127P3939R5S4	MIL-C-14157 (non ER)	-2508	50 v	28 v	.56	-	1	.005	.023	.005	.005	.023	.023
24	C44	ST	100 µf	CSRk3E107KP	MIL-C-39003	-2501	20 v	12 v	.6	50	1	.017	.21	.85	.0069	.21	10.50
25	C45	ST	100 µf	CSR13E107KP	MIL-C-39003	-2501	20 v	12 v	.6	50	1	.017	.21	.85	.0069	.21	10.50
26	C46	(VK1)C	680 pf	(VK01 CKR05CW681KP	MIL-C-39014	-2502	200 v	4 v	<.1	15	1	.0074	.0074	.111	.005	.0074	.111
27	C47	C	100 pf	CKR05CW101KP		-2502	200 v	6 v	<.1	15	1	.0074	.0074	.111	.005	.0074	.111
28	C48	C	680 Pf	CKR05CW681KP		-2502	200 v	4 v	<.1	15	1	.0074	.0074	.111	.005	.0074	.111
29	C49	(VK1)C	100 pf	CKR05CW101KP	MIL-C-39014	-2502	200 v	6 v	<.1	15	1	.0074	.0074	.111	.005	.0074	.111
30	C50	ST	100 µf	CSR13E107KP	MIL-C-39003	-2508	20 v	6 v	.3	50	1	.017	.035	.85	.0069	.035	1.75
31	C51	Cap. ST	100 µf	CSR13E107KP	MIL-C-39003	ZPP-2744 -2508	20 v	6 v	.3	50	1	.017	.035	.85	.0069	.035	1.75

* To be selected during calibration-value shown is nominal.

NASA-LRC AIR DENSITY SENSOR (ADS-104)

CONTRACT NO. NAS1-7791

Item	Ckt.No. (Ref.)	Component	Value	Description or P/N	MIL-SPEC (ER Level P)	Qualif. Document	At +85°C Stress Rated	At +85°C Stress Applied	Stress Ratio	L	C	F.R. x 10^{-6} Hours BASE T=+85°C S.R.	BASE S.R. Defined	GO t=.5 Launch	GO T=+40°C t=5760 Transit	GO t=50 Orbit	GO t=.5
32	CR10	Diode Rec.		Jan-TX-1N4942	MIL-S-19500/359	QPL	800 ma	83 ma	Tn=A+.104	10	1	.033	.041	.330	Tn=.20 .0195	.041	.410
33	CR11	Diode Rec.		Jan-TX-1N4946			800 ma	162 ma	.4+.203	10	1	.033	.051	.330	Tn=.30 .0255	.051	.510
34	CR12	Rec.		Jan-TX-1N4946			800 ma	162 ma	.203	10	1	.033	.051	.330	Tn=.30 .0255	.051	.510
35	CR13	Rec.		Jan-TX-1N4946			800 ma	20 ma	.4+.02	10	1	.033	.033	.330	Tn=.12 .0140	.0325	.330
36	CR14	Rec.		Jan-TX-1N4946	MIL-S-19500/359	OPL	800 ma	20 ma	.4+.02	10	1	.033	.033	.330	Tn=.12 .0140	.0325	.330
37	CR15	Diode Zener	9.3 v	1N2623A		ZPP-2746-3017	750 mw	15 mw	Tn=.4+.02	10	1	.098	.098	.980	Tn=.12 .0140	.098	.980
38	Q6	Transistor P.Sw		2N2893	MIL-S-19500/181	ZPP-2751-7052	30 w	80 mw	Tn=.343 +0.03	75	1	.058	.065	4.35	Tn=.11 .028	.065	4.875
39	Q7	Transistor P.Sw		2N2893		-7052	30 w	80 mw	.343 +0.03	75	1	.058	.065	4.35	Tn=.11 .028	.065	4.875
40	Q8	Reg.		Jan-TX-2N2893	MIL-S-19500/181	ZPP=2751-7052	30 w	588 mw	Tn=.343 +.020	75	1	.058	.058	4.35	Tn=.11 .028	.058	4.875
41	Q13	Transistor Reg.		Jan 2N2893	MIL-S-19500/181	OPL	30 w	342 mw	Tn=.4 +.57	75	1	.058	.058	4.35	Tn=.11 .028	.058	4.875
42	Z20	I.C. OpAmp NPN Si		µA709	(DS #6009)	ZPP-2750-6009	300 mw	100 mw	Tn=.343 +.333	25	1	.0290	.0610	.0290	Tn=.433 .0365	.0610	1.525
43	Z21	I.C. OpAmp NPN Si		µA709	(DS #6009)	ZPP-2750-6009	300 mw	100 mw	Tn=.343 +.333	25	1	.0290	.0610	.0290	Tn=.433 .0365	.0610	1.525
44	Q9	Amp.		Jan-2N1132	MIL-S-19500/177	QPL	600 mw	20 mw	Tn=.4+.033 +.	25	1	.092	.107	2.30	Tn=.086 .031	.107	5.350
45	T1	Transformer			MIL-T-27	QPL	130°C	85°C	-	50	1	.2	.2	10.0	.2	.2	10.
													TOTAL	46.272	1.469	3.436	86.51

APPENDIX C

Test Data

Curve Fit Data - Density Run #1

5-Curie Source

TERM	COEFFICIENT
0	1082.87
1	2.15633E+07
2	-2.34408E+09

Density Actual gm/cm^3	Count Rate Actual pps	Count Rate Calculated	Difference	Percent Difference
1.26140E-04	24598.3	24553.1	45.1894	.184048
.001018	20547.8	20605.1	-57.3064	-.278118
7.69380E-04	16271	16285.7	-14.6908	-9.02065E-02
5.14860E-04	11515	11563.6	-48.59	-.420198
2.57790E-04	6589.8	6485.9	103.901	1.60196
1.71230E-04	4769	4706.43	62.5732	1.32953
1.36450E-04	4056	3981.54	74.4614	1.87017
1.32800E-04	3868.5	3905.14	-36.6361	-.938152
1.00790E-04	3195.7	3232.42	-36.7212	-1.13603
6.70910E-05	2514.4	2519.02	-4.62008	-.183408
3.32790E-05	1805.6	1797.88	7.724	.429618
2.47870E-05	1559.89	1615.92	-56.0261	-3.46714
1.64510E-05	1449.8	1436.97	12.83	.892852
8.18540E-06	1240.7	1259.21	-18.5135	-1.47024
1.63310E-06	1084.5	1118.07	-33.5749	-3.00292

TERM	COEFFICIENT
0	1110.71
1	1.94420E+07
2	-657711333

Density Actual gm/cm^3	Count Rate Actual pps	Count Rate Calculated	Difference	Percent Difference
1.63310E-06	1084.5	1142.46	-57.9564	-5.07296
5.75830E-06	1172.2	1222.64	-50.4384	-4.12537
8.00520E-06	1227.5	1266.3	-38.8022	-3.06421
1.61030E-05	1541.5	1423.61	117.889	8.28098
4.90200E-05	2098.4	2062.17	36.2271	1.75675
1.14070E-04	3315	3319.9	-4.89603	-1.47475
3.57830E-04	7997.3	7983.42	13.8836	.173905
5.98560E-04	12492.9	12512.3	-19.3584	-.154715
1.21650E-04	23792	23788.5	3.45197	.014511

Curve Fit Data - Density Run #2

1-Curie Source

TERM	COEFFICIENT
0	419.772
1	3.87270E+06
2	- 2.59474E+08

Density Actual gm/cm^3	Count Rate Actual pps	Count Rate Calculated	Difference	Percent Difference
.001239	4839	4819.72	19.2794	.400011
1.01240E-03	4056.1	4074.54	-18.4425	-.452628
7.68460E-04	3220.2	3242.56	-22.3582	-.689522
5.16640E-04	2351	2351.3	-.304817	-1.29637E-02
2.59160E-04	1431.4	1405.99	25.4067	1.80703
.00017	1097.9	1070.63	27.268	2.54691
8.24820E-05	752.5	737.435	15.0653	2.04293
3.33280E-05	544.57	548.553	-3.98321	-.726129
8.74000E-06	434.3	453.6	-19.2997	-4.25479
1.69380E-06	403.7	426.331	-22.631	-5.30831

TERM	COEFFICIENT
0	474.312
1	3.92553E+06
2	-8.45965E+07

Density Actual gm/cm^3	Count Rate Actual pps	Count Rate Calculated	Difference	Percent Difference
1.69380E-06	403.7	480.961	-77.2607	-16.0638
7.41680E-06	535.9	503.422	32.4779	6.45143
.000021	573.5	556.711	16.7893	3.0158
5.93900E-05	720.9	707.151	13.7491	1.9443
1.24630E-04	983.7	962.237	21.463	2.23053
3.73320E-04	1927.4	1928.	-.601776	-3.12124E-02
6.49870E-04	2989	2989.67	-.670208	-2.24175E-02
9.75290E-04	4208	4222.38	-14.3775	-.340506
1.27250E-03	5341	5332.57	8.43091	.158102

APPENDIX D

CHECK-OUT CALIBRATION AND TEST PLAN SUMMARY

1.0 SUMMARY

This appendix describes the test setup for calibrating and testing the ADS-104 System. The system as shipped will be calibrated for use with 50 foot cable between the electronics and detector, and a Gd 153 gamma source. Details of handling and calibrating with high strength sources are also contained in this appendix.

2.0 TEST BOX

The test box provides the electrical interface between the sensor and test equipment as is illustrated in the Interconnection Block Diagram, Figure 1. Figure 2 shows the wiring of the PM/HVPS. The unit is powered from a 28-volt source and the input voltage and current are monitored in the test box. The primary outputs of the sensor are the 0 to 4 volt dc which is measured with a digital voltmeter. Switches are also provided to energize the shield solenoids for opening and closing the source mechanism.

Secondary output from the sensor can also be monitored as a check on sensor performance. These outputs are shown as dashed lines on Figure 1. Pulses out of the UL discriminator, LL discriminator, and NAND Gate can be monitored. The AGE high voltage power supply control voltage is monitored to insure in-limit control.

The test box schematic is shown in Figure 3.

3.0 CALIBRATION

This section describes the calibration procedures and presents calibration data taken on the Atmosphere Density Sensor (ADS-104). Calibration adjustments are performed on the unit to set up the AGC, set the UL and LL of the output window, set up the slopes and end points on the pulse to dc converter.

3.1 Gain. The pulse height spectrum as measured at TP7 has the Am 241 AGC peak and the Gd 153 calibration source direct transmission peak at 100 Kev. The Am 241 source strength is selected to produce approximately 200 pulses per second in the AGC spectrum. R28 is selected so that the AGC discriminator level (Gain reference) is set at 4.0 volts. The gain bias (R32) is then selected so that the AGC spectrum peak falls at 4 volts and the AGC discriminator output count rate is 100 pulses per second.

3.2 Window. The sensor air backscatter pulse height spectrum as measured is shown in Figure 4. The optimum upper and lower discriminator levels are seen to be 0.9 volt and 1.5 volts. R10 adjusts the low level and R13 adjusts the upper level to these values.

3.3 Pulse to DC Converter. Selection of resistors R42B, R46A, R46B, R49, and R95 is necessary to provide the desired slopes, breakpoint, and end points of the pulse to dc converter. The calibration data are summarized in Table I.

4.0 DEMONSTRATION TEST PLAN

The following tests shall be performed at NASA, Langley Research Center, to demonstrate the performance of the Atmosphere Density Sensor after a brief confidence check period.

4.1 Installation and Check-out. The sensor shall be placed near the floor of the 60-foot diameter altitude sphere, facing upward. Cable interconnection shall be made between the sensor and its test equipment via a 100-foot cable. The sensor shall be turned on and background and AGC measurements recorded. This data shall be compared with previously recorded data to verify proper sensor operation. If desired, the altitude sphere may be closed and evacuated while the sensor is in this configuration, and stability of sensor output monitored. The data format is shown in Table II.

4.2 One-Curie Calibration. The sensor shall be placed near the floor of the 60-foot diameter altitude sphere, facing upward with the unloaded source assembly and detector separated by one meter. A sensor check shall be performed using the Gd 153 calibration source and a background measurement taken. The 1-curie Gd 153 source shall be installed and the source mechanism closed and a second reference measurement taken. The chamber shall be sealed and the source mechanism opened. The chamber shall slowly be evacuated and the measurements in Table III recorded. Pressure shall be measured using the Wallace and Tiernan pressure gage. Temperature shall be measured using the recording thermocouple. Evacuation shall proceed to a pressure of 1 mm hg. Data shall be taken both during evacuation and refill. When back to atmospheric pressure, the source mechanism shall be closed and a reference reading recorded. The source shall then be removed and background readings recorded. The calibration source shall be replaced and reference readings recorded.

4.3 Five-Curie Calibration. The 5-curie Gd 153 calibration run shall follow the same procedure as the 1-curie calibration of paragraph 4.2.

TABLE I

CALIBRATION DATA SUMMARY

(Reference Figure 1)

	DESIRED	ACTUAL
GAIN		
AGC Source Spectrum (volts) TP4	+4.5	
AGC Gain Reference (volts) TPF	1.5	
R28 (ohms)		402
R29 (ohms)		49.9
AGC Disc Output (Hz) TP7	750	
WINDOW		
UL Disc. Ref. (volts)	---	1.25
LL Disc. Ref. (volts)	---	.850
R10 (ohms)		604
R13 (ohms)		1.18K
Background (Hz)	0	25
PULSE TO DC CONVERTER		
25 pps Output (volts)	0	±.025
TPE at 4 KHz Output (volts) H Gain	4.0V	0
Breakpoint Output (volts)	2.5	2.56
TPD at 40,000 Hz Output (volts) L Gain	4	
R46A (ohms)		2.8K
R47B (ohms)		7.5K
R53 (ohms)		110K
R56 (ohms)		4.7K
R58 (ohms)		19.6K
R108B (ohms)		110K

TABLE II

INSTALLATION AND CHECK-OUT DATA

	Ref.	Cor.	1	2	3	4	5
Date							
Half Life Factor							
BACKGROUND							
UL pps							
LL pps							
Window pps							
Averaging Time							
DC Output L Gain							
DC Output H Gain							
AGC pps							
AGC Output							
CALIBRATION SOURCE							
UL pps							
LL pps							
Window pps							
Averaging Time							
DC Output L Gain							
DC Output H Gain							
AGC pps							
AGC Output							

TABLE III

ONE-CURIE CALIBRATION

	25 μCi Ref.	Cor.	Back-ground	25 μCi Ref.	1 C Ref.	1	2
Date							
Half Life Factor							
UL pps							
LL pps							
Window pps							
Averaging Time							
DC Output L Gain							
DC Output H Gain							
AGC pps							
AGC Output							
Pressure							
Time							

	n-1	n	1 C Ref.	Back-ground	25 μCi Ref.	1	2
Date							
Half Life Factor							
UL pps							
LL pps							
Window pps							
Averaging Time							
DC Output L Gain							
DC Output H Gain							
AGC pps							
AGC Output							
Pressure							
Temperature							
Time							

4.4 Composition Sensitivity. Based upon previous test results, the 1-curie or 5-curie source shall be selected to perform the test. Background and reference measurements shall be recorded as in paragraph 4.2. Data shall be recorded as the chamber is evacuated to a pressure of 1.0 mm hg. Argon gas shall be slowly introduced to a pressure of 100 mm hg and data recorded. The chamber shall then be evacuated to 1 mm hg and data recorded. The chamber shall be slowly returned to 1 atmosphere and data recorded. Final background and reference measurements shall be recorded as in paragraph 4.2.

4.5 Separation Sensitivity. Based upon previous test results, the 1-curie or 5-curie source shall be selected for this test. Background and reference measurements shall be recorded as in paragraph 4.2, except the source to detector separation shall be 50 cm in lieu of 100 cm. Data shall be recorded as the chamber is evacuated to 1 mm hg and returned to 1 atmosphere. Final background and reference measurements shall be recorded as in paragraph 4.2.

5.0 SOURCE HANDLING

The source handling and safety procedures are described in this section. The 5-curie Gd 153 source will be used as reference. The source characteristics are listed below.

Material - Gadolinium 153

Strength - 5 curies

Half Life - 242 days

Gamma Energy - 70 Kev	97 Kev	103 Kev
Percent Yield - 3.1%	30%	22%

Form - Sealed Source,
Welded S.S. Capsule

Dose Rate Constant (Computed) 0.24 $\frac{r - cm^2}{mc - hr}$

Dose Rate Constant (Measured) 0.22 $\frac{r - cm^2}{mc - hr}$

The measured dose rate constant is lower than the computed since effects of self-absorption and capsule wall absorption have not been considered. For the dose rate calculations, the more conservative dose rate constant of 0.24 $\frac{r - cm^2}{mc - hr}$ will be used.

The sequence of source installation is outlined below.

1. Open cask and remove source from shielded container using 5-foot handling tongs.

2. Place source on floor and regrasp source in proper orientation for installation.

3. Install source in source assembly and actuate mechanism to the closed position.

4. Tighten screws securing the source. (Source is shielded in this operation.)

The sequence of source removal is outlined below.

5. Loosen screw securing source. (Source is shielded in this operation.)

6. Actuate mechanism to the open position and grasp source using 5-foot handling tongs.

7. Remove source and place in shielded container.

The total dose rate during this operation is tabulated below.

Operation Number	Time (hr)	Calculated Dose (mr)
1	.002	1.0
2	.003	1.5
3	.003	1.5
4		
5		
6	.003	1.5
7	.002	1.0
TOTAL	.013	6.5

The computed dose per installation and removal cycle is 6.5 mr. This cycle can be repeated fifteen times per week without exceeding a 100 mr per week limit.

The test plan calls for 6 source installation removals, thus allowing for reasonable contingency.

The maximum dose rate on the outside surface of the sphere, assuming 5-foot minimum distance and the attenuation afforded by the 1/4-inch thick steel walls, is computed as 1.0 mr per hour.

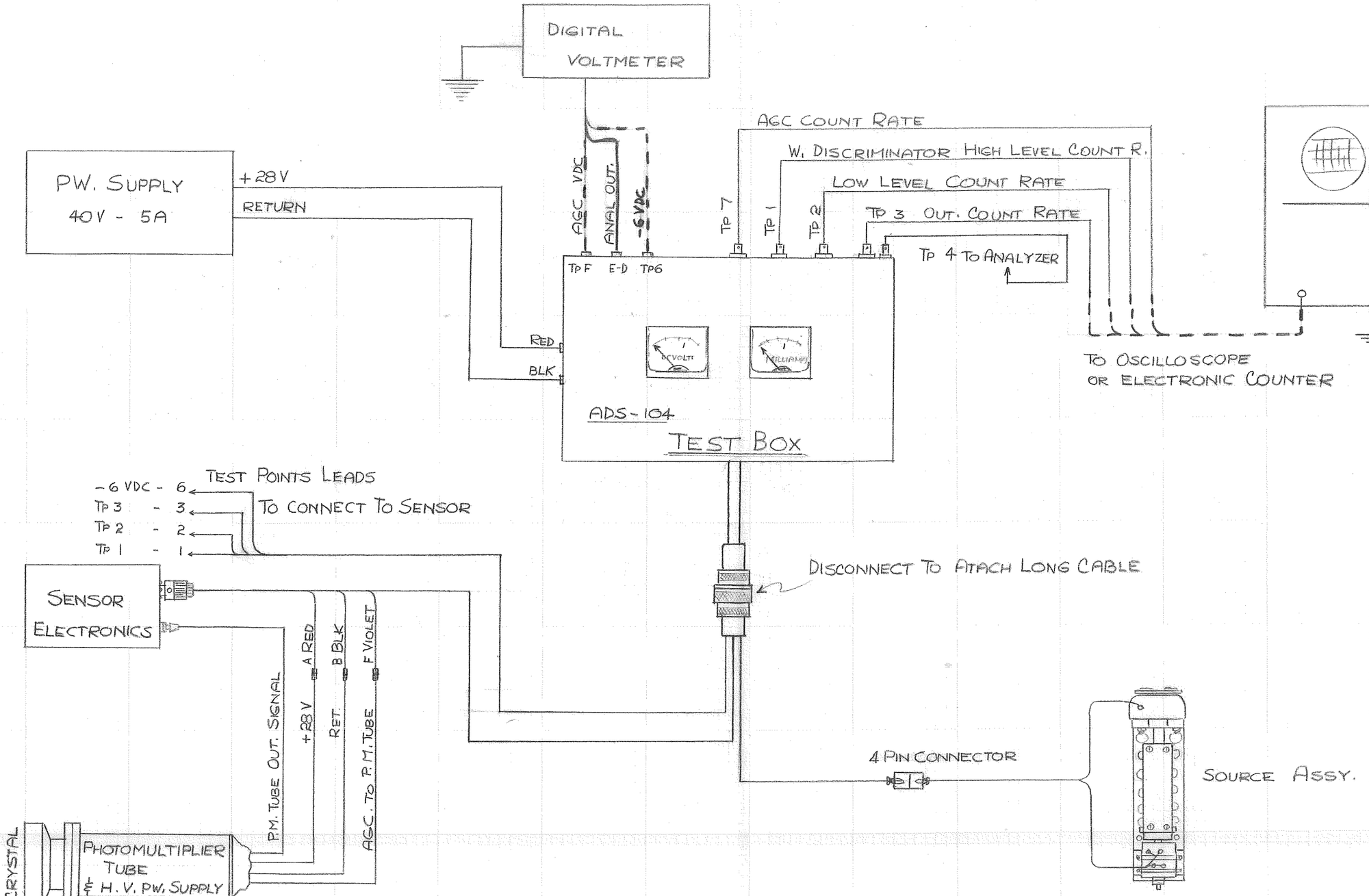

ADS-104

INTERCONNECTING DIAGRAM Figure 1

NOTE: 1) SOURCE HOLDER NORMALY OPENED
TO OPERATE SOURCE HOLDER DEPRESS SWITCH
MARKED "CLOSE" & "OPEN"
BOTH SWITCHES LOCATED ON ADS-104 TEST BOX.

2) TP E - HIGH GAIN ANALOG OUT.
TP D - LOW GAIN ANALOG OUT.

NASA

ADS-104

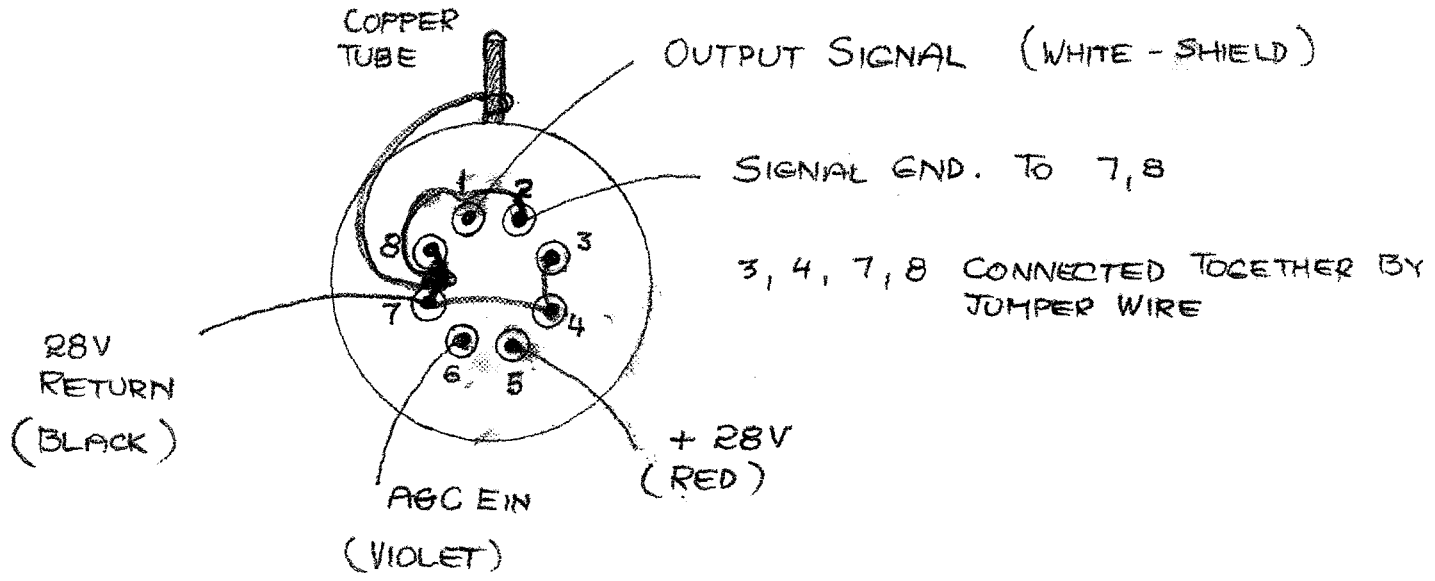

OUTSIDE VIEW OF P.M. TUBE CONNECTIONS

FIGURE 2

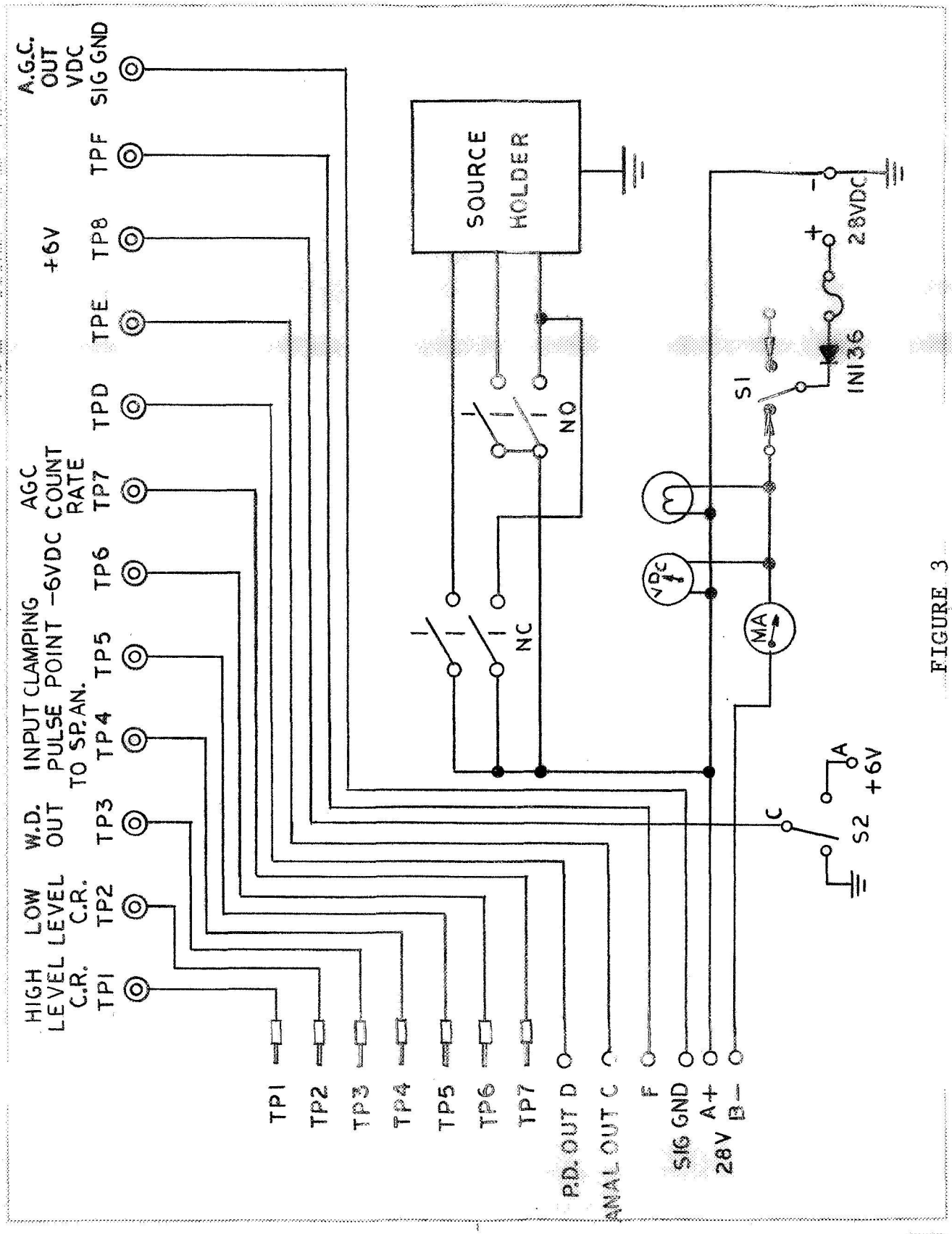
A.G.C. OUT VDC
SIG GND
TPF
+6V
TP8
TPE
TPD
AGC COUNT RATE
TP7
INPUT CLAMPING PULSE POINT -6VDC TO SP.AN.
TP6
TP5
W.D. OUT
TP4
TP3
LOW LEVEL C.R.
TP2
HIGH LEVEL C.R.
TP1
SOURCE HOLDER
NO
NC
S1
1N136
28VDC
VDC
MA
A
+6V
S2
C
TP1
TP2
TP3
TP4
TP5
TP6
TP7
P.D. OUT D
ANAL OUT C
F
SIG GND
28V A+
B-

FIGURE 3

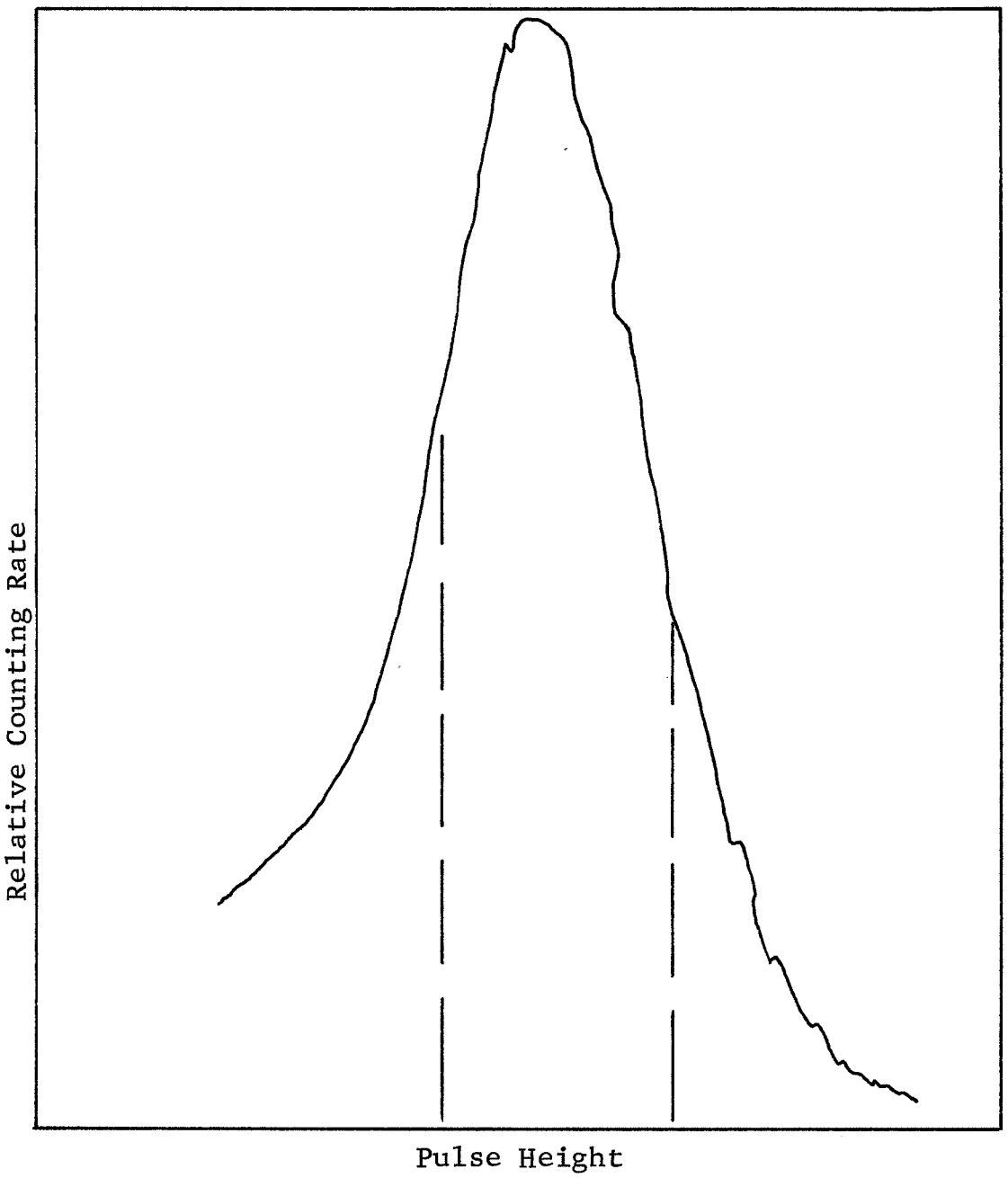

FIGURE 4 - Backscatter Pulse Height Spectrum